JAERI-M
86-131

PROGRESS REPORT ON SAFETY RESEARCH OF HIGH-LEVEL WASTE MANAGEMENT FOR THE PERIOD APRIL 1985 TO MARCH 1986

September 1986

(Eds.) Haruto NAKAMURA and Shingo TASHIRO

日本原子力研究所
Japan Atomic Energy Research Institute

JAERI-M レポートは，日本原子力研究所が不定期に公刊している研究報告書です。
入手の問合わせは，日本原子力研究所技術情報部情報資料課（〒319—11 茨城県那珂郡東海村）あて，お申しこしください。なお，このほかに財団法人原子力弘済会資料センター（〒319-11 茨城県那珂郡東海村日本原子力研究所内）で複写による実費頒布をおこなっております。

JAERI-M reports are issued irregularly.
Inquiries about availability of the reports should be addressed to Information Division, Department of Technical Information, Japan Atomic Energy Research Institute, Tokai-mura, Naka-gun, Ibaraki-ken 319-11, Japan.

編集兼発行　日本原子力研究所
印　　刷　山田軽印刷所

JAERI-M 86-131

Progress Report on Safety Research of High-Level Waste Management for the Period April 1985 to March 1986

(Eds) Haruto NAKAMURA and Shingo TASHIRO

Department of Environmental Safety Research
Tokai Research Establishment,
Japan Atomic Energy Research Institute
Tokai-mura, Naka-gun, Ibaraki-ken

(Received August 12, 1986)

Researches on high level waste management in fiscal year of 1985 is reviewed.

Topics are as follows;

1) Glass waste form was examined with emphasis on the leaching mechanisms under various conditions to predict the long-term leach rates.
Leaching rate was examined in synthesized groundwater and a leaching model was developed.
Cooperation between Japan and Australia on development of SYNROC has started.

2) Heating experiments with a real size simulated canister and migration tests using non-sorbing tracer has been carried out in a near surface granite rock mass.
2D-SEEP, the coupled computer code of heat and groundwater flow, has been developed.

3) Japanese group participated the ESOPE project of OECD/NEA SWG.
Small particles of an organic phase was found in sediment as a material to have significant influence on technetium fixation.

4) Alpha radiation stability of vitrified forms under beta and gamma irradiation have newly started in WASTEF.

Keywords: High Level Radioactive Waste, WASTEF, Leaching Mechanism, Field Test in Granite, Seabed Disposal, SYNROC

1985年4月より1986年3月までの高レベル廃棄物処理処分の安全性研究に関する研究報告

日本原子力研究所東海研究所環境安全研究部
（編）中村　治人・田代　晋吾

（1986年8月12日受理）

高レベル廃棄物処理処分に関する1985年度の研究内容をまとめた。

主な点は次の事項である。

1）ガラス固化体の長期浸出率を予測するため，種々の条件での浸出機構に力点をおいた実験を行った。合成地下水中での浸出率の測定を行うとともに，浸出モデルの開発を行った。

また，SYNROC固化法に関する日豪協力研究を開始した。

2）花崗岩岩盤中でのフィールド実験では，実物大の廃棄物を模擬したヒータによる加熱実験と非吸着性イオンを使った元素移行実験を行った。

熱伝達と地下水流の複合現象を評価する計算コード2D−SEEPを開発した。

3）日本チームとして，OECD/NEAの海洋底下処分ワーキンググループ（SWG）の国際共同実験（ESOPE）に参加し，堆積物中にT_cを固定するに効果的な有機性の小粒子が存在することを見出した。

4）WASTEFにおいて新たに，$\beta-\gamma$存在下でのα加速実験を開始した。

東海研究所：〒319−11　茨城県那珂郡東海村白方字白根2−4

Contents

目　　次

Introduction

Research activities in the fiscal year of 1985 on high level waste management are reviewed following the progress reports (JAERI-M 82-145, 83-076, 84-133, 85-090). Safety studies and development of new technologies were conducted on national program.

The performances of waste forms and other engineered barrier materials were studied to assess the barriers against radionuclide release to environment from repository in deep underground.

SYNROC was studied as one of new waste forms.

Mechanism of retardation of nuclide migration in rock mass and sediment were studied.

Calculation codes to assess the safety of geological disposal were developed.

The effect of alpha radiation on the stability of vitrified waste were examined.

1. Waste Forms Examination

T. Banba

Glass waste form was examined with emphasis on the leaching mechanisms under various conditions to predict the long-term leach rates. In the past year, leaching of simulated waste glass was examined in synthesized groundwater by the MCC-4 dynamic leach test method. And we set about developing the leaching model for the long-term prediction of leach rates.

SYNROC waste form is one of the most feasible alternatives because of its stability assurance for a long time. Cooperation between Japan and Australia on development of SYNROC waste forms has started and the SYNROC fabrication process by utilizing the hydroxide-route precursor was examined to estimate the applicability of the fabrication in a hot run. Also irradiation tests of SYNROC waste form were carried out by using the argon ions beam of a Van de Graaff accelerator.

1.1 Leaching Behavior of Simulated High-Level Waste Glass in Flowing Synthesized Groundwater

Hiroshi Kamizono

Disposal sites suitable for the isolation of high-level waste (HLW) glass may be constructed in geological formations more than several hundred meters below the surface. The contact of groundwater with HLW glass placed in the disposal sites will be the primary cause of waste radionuclides escaping into the biosphere. Therefore, much attention has been paid to the leaching behavior of HLW glass under geologic disposal conditions. In the present study, leaching of simulated HLW glass was examined in synthesized groundwater and deionized water by the MCC-4 dynamic leach test method and the MCC-1 static leach test method [1].

Experimental

The simulated high-level waste glass used for the present study was borosilicate glass containing 11.7 wt% of simulated high-level waste (JW-D). The glass specimens of 1 x 1 x 1 cm in size were subjected to both dynamic and static leach tests at 70°C for up to 28 days. The synthesized groundwater used here contains the kations of Na^+, Ca^{2+} and Mg^{2+}, and the anions of HCO_3^- and SO_4^{2-} (Table 1). The pH value of this water was adjusted by the use of tris(hydroxymethyl)aminomethane, $NH_2C(CH_2OH)_3$. The procedure for

synthesis is described elsewhere [2]. In the MCC-4 method, the flow rate was controlled at about 0.1, 0.01 and 0.001 ml/min.

Results

Figures 1 and 2 show the relationship between normalized elemental mass losses (NL) for boron and leach time in days. Both figures indicate that the values of NL increase with increasing flow rate. In the case of deionized water (Fig.1), the values of NL obtained by the MCC-1 method tend to be larger than those by the MCC-4 method with the slowest flow rate of 0.001 ml/min. (tendency A). In the case of synthesized groundwater (Fig.2), however, this tendency cannot be clearly seen, and the values of NL by the MCC-1 method are almost equal to those by the MCC-4 method at 0.001 ml/min.

Figure 3(a) shows that in the case of synthesized groundwater the pH values do not change markedly during either the dynamic or the static type leach test. However in Fig.3(b), one can easily see that in the case of deionized water the pH values are dependent on the type of leach tests; the values level off at more than 9 in the MCC-1 method, and they do not increase by more than 6 in the MCC-4 method.

The results described above imply that in leachants such as deionized water, which does not have buffer capacity, the pH value can be easily increased by alkaline elements leached from the glass thereby helping it to dissolve progressively and result in tendency A.

References

1. Materials Characterization Center, "Nuclear Waste Materials Handbook", DOE/TIC-11400, Pacific Northwest Laboratory, Richland, Washington (1981).
2. H. Kamizono, "Leaching Behavior of Simulated High-Level Waste Glass in Groundwater", J. Nucl. Mater. 127 (1985) 242-246.

Table 1 Value of pH and composition of synthesized groundwater

pH	7.7
Na	13 (in mg/liter)
Ca	60
Mg	54
HCO_3^-	Nearly saturated
SO_4^{2-}	190

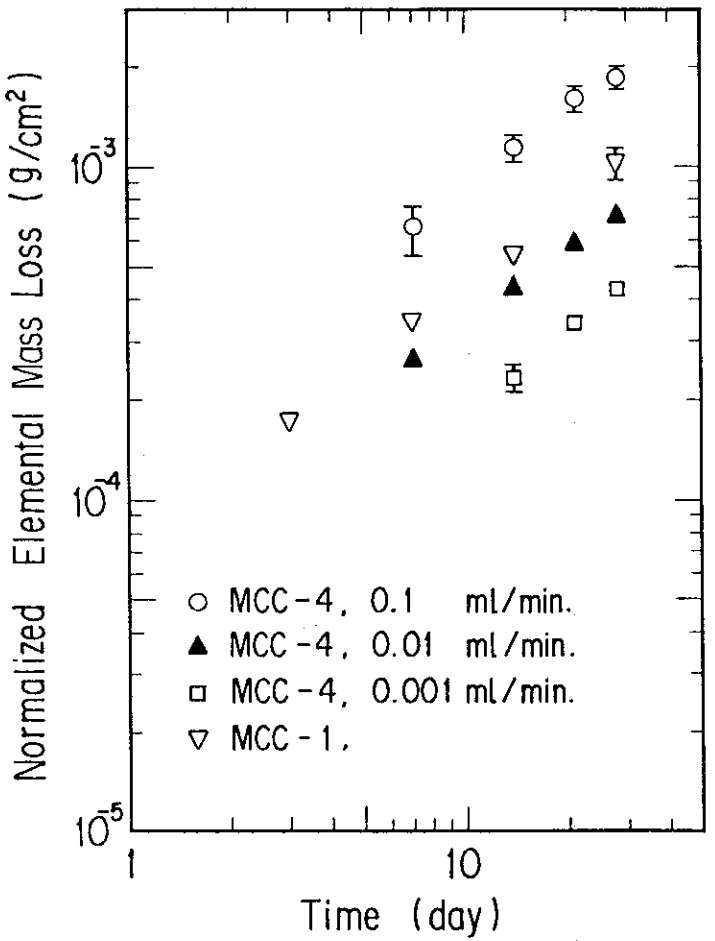

Fig. 1 Relationship between NL for boron and leach time in days in the case of deionized water.

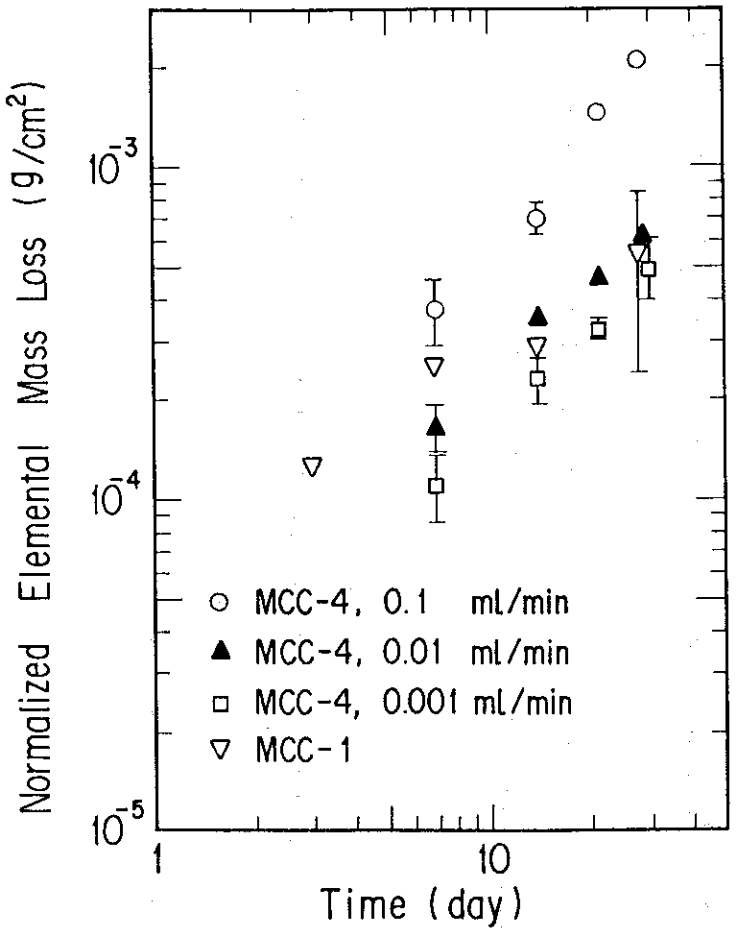

Fig. 2 Relationship between NL for boron and leach time in days in the case of synthesized groundwater.

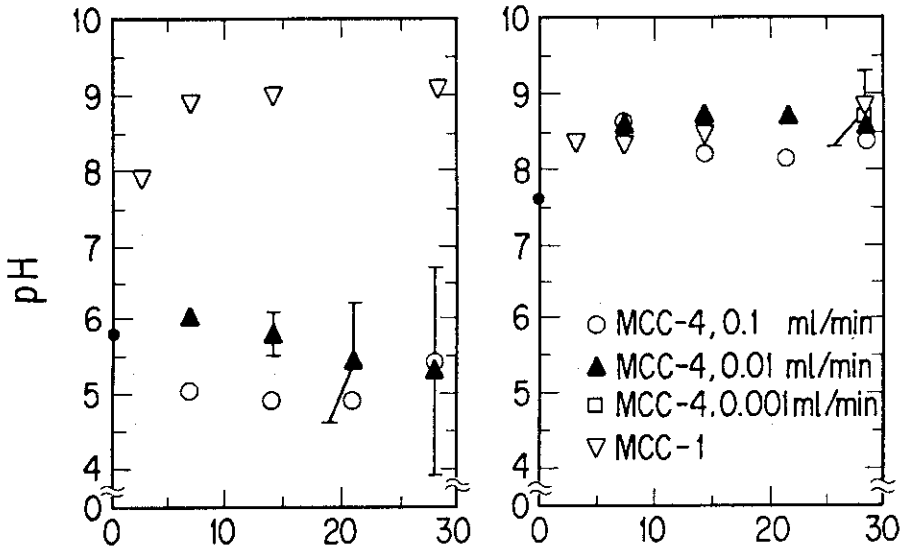

(a) Deionized water (b) Synthesized groundwater

Fig. 3 Change of pH during leach tests.

1.2 MOVING BOUNDARY MODEL FOR LEACHING OF NUCLEAR WASTE GLASS

T. Banba

The surface layers formed on glass surface during leaching play an important role in the leaching mechanisms of glass waste forms[1,2]. We have carried out Soxhlet type leach test and proposed the leaching mechanisms based on the characteristics of the surface layers and the leach rates of elements[3,4]. In the present paper, we describe the mathematical leaching model which uses one-dimensional diffusion. The model can treat the growth of surface layers as a moving boundary, and also treat chemical reaction in surface layers.

The concept of the model is shown in Fig. 1 schematically. Any given substance diffuses in accordance with Fick's law in bulk glass and in surface layers which grow with time during leaching. In the surface layers, some substances participate in the formation of sheet silicate[3](i.e. chemical reaction) and become immobile. The other diffusing substances go out into the solution.

The model adopts the following assumptions: 1) The leaching system is restricted in one-dimensional geometry. 2) The velocity of the moving boundary between the bulk glass and the surface layers depends on time alone. 3) Chemical reaction in the surface layers is considered as an irreversible first-order reaction. 4) A fictitious film exists at the solution-surface layers interface.

With these assumptions, the following equations are obtained.

$$\frac{\partial c_A}{\partial t} = D_{A1}\frac{\partial^2 c_A}{\partial x^2} - R_A c_A \qquad (0 \leq x \leq X)$$

$$\frac{\partial c_A}{\partial t} = D_{A2}\frac{\partial^2 c_A}{\partial x^2} \qquad (x \geq X)$$

$$X = f(t).$$

The initial condition is

$$c_A = c_{A0}. \qquad x \geq 0, \quad t = 0$$

The boundary conditions are

$$-D_{A1}\left.\frac{\partial c_A}{\partial x}\right|_{x=0} = K_A(c_A|_{x=0} - c_{As}), \qquad x = 0$$

$$D_{A1}\left.\frac{\partial c_A}{\partial x}\right|_{x=X-0} = D_{A2}\left.\frac{\partial c_A}{\partial x}\right|_{x=X+0}, \qquad x = X$$

$$c_A = c_{A0}. \qquad x = \infty$$

Where c_A is the concentration of diffusing substance A, D_{A1} and D_{A2} are the diffusion coefficients of A in the surface layers and the bulk glass, respectively, R_A is the reaction rate in the layers, t is the time, x is the space coordinate, X is the position of the moving boundary, c_{A0} is the initial concentration of A, c_{As} is the concentration of A in the solution and K_A is the film mass transfer coefficient of A.

The above equations were solved by using the Crank-Nicolson implicit method. As for the treatment of the moving boundary, we used the method proposed by Crank[5] who gave special finite-difference formulae based on Lagrangian interpolation.

Calculations based on the proposed model was carried out utilizing the experimental data obtained by Soxhlet type leach test for the simulated waste glass[4]. The calculating procedure was as follows. First, the velocity of moving boundary was determined by a trial-and-error method using the leach data of Na which did not participate in the chemical reaction and was depleted from the surface layers. Second, the diffusion coefficient, the reaction rate and the film mass transfer coefficient were calculated using a trial-and-error method so that the calculated leach rates were fitted to the experimental ones.

The calculated results revealed that the position of moving boundary from the solution-surface layers interface was represented by $X = f(t) = 8.83 \times 10^{-2}\{1 - (0.7)^{(t-2)/30}\}$ [cm] and the values of D_{A1}, D_{A2}, R_A and K_A were obtained as shown in Table 1. Doremus[6] gave the value of about 10^{-13} cm^2/s for the diffusion coefficient of Na in soda-lime glasses at 100°C, which was in good agreement with our value of 8.1×10^{-13}. Very small mass transfer coefficients of Ca and Sr might result from low solubility of them because chemical processes such as solubility occurred at the solution- surface layers interface, namely, in the fictitious film which was assumed in order to simplify the mass transfer process.

With the values in Table 1, we can reasonably explain leaching mechanisms of Na, Cs, Ca and Sr. Namely, Na and Cs diffuse much more rapidly in the surface layers than in the bulk glass and leached out into the solution. Calcium and Sr participated in the chemical reaction in the surface layers and remain there. This study shows that the model is valid for calculation of the leach rates of the waste glasses when surface layers grow during leaching, and this study also implies which variables should be measured experimentally to predict the leach rates.

References

1. D.E. Clark, et al., Nucl. Technol., 56, 212 (1982).
2. G. Malow, Scientific Basis for Nuclear Waste Management V, p.25, W. Lutze, Ed., North-Holland, New York (1982).
3. T. Murakami and T. Banba, Nucl. Technol., 67, 419 (1984).
4. T. Banba and T. Murakami, Nucl. Technol., 70, 243 (1985).
5. J. Crank, Q. Jl. Mech. appl. Math., 10, 220 (1957).
6. R.H. Doremus, Glass Science, p.162, John Wiley, New York (1973).

Table 1 The values of D_{A1}, D_{A2}, R_A and K_A for some elements.

element	D_{A1}[cm^2/s]	D_{A2}[cm^2/s]	R_A[s^{-1}]	K_A[cm/s]
Na	4.1×10^{-10}	8.1×10^{-13}	0	4.1×10^{-3}
Cs	9.3×10^{-10}	4.6×10^{-13}	0	9.3×10^{-2}
Ca	2.9×10^{-10}	5.8×10^{-13}	1.0×10^{-2}	2.9×10^{-6}
Sr	4.6×10^{-10}	9.3×10^{-13}	1.5×10^{-2}	4.6×10^{-7}

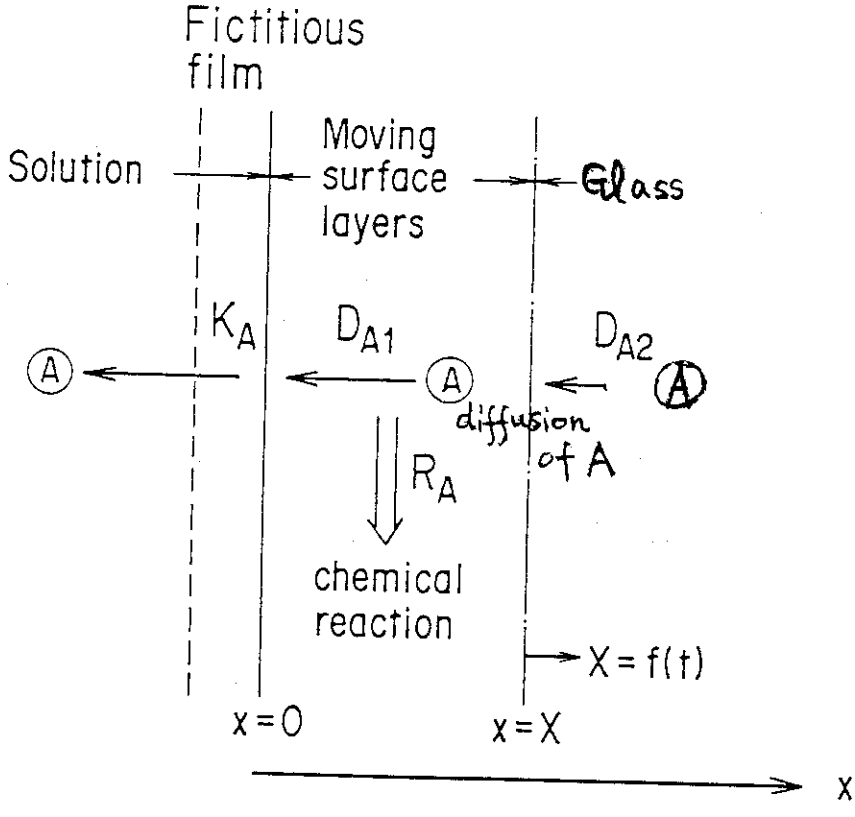

Fig. 1 Schematic diagram of the leaching model.

1.3 Fabrication and leach test of hydroxide-route SYNROC

T. Amaya, T. Murakami and H. Mitamura

Introduction

SYNROC was chosen to be an alternative wasteform to borosilicate glass for the immobilization of high-level waste because of its stability assurance for a long time. As the high-level waste can be incorporated in the crystal lattices of coexisting phases in SYNROC, it is important to mix the waste homogeneously with SYNROC precursors.

Some processes have been developed to yield fine and homogeneous precursors. Dosh and others[1] have developed a Sandia-route process to obtain a finer and more homogeneous precursor. More recently, Kesson and Ringwood[2] have developed an alternative to the Sandia-route process. This alternative process is a more simple process and is named hydroxide-route. Likewise, we are making SYNROC by utilizing the hydroxide-route precursor in our cold experiments to estimate the applicability of the fabrication in a hot run.

Experimental

We make SYNROC in the following way (Fig. 1).

[1] High-level waste is mixed with the precursor at pH=9 with ammonium hydroxide solution.

[2] The slurry is dried and calcined under mixing conditions. We made a calciner to simplify these two processes into one process to avoid complication.

[3] Ti-metal powder is mixed with the calcine. Ti-metal is an oxygen getter at HUP stage.

[4] The mixture is hot-pressed in a graphite die for 2 hours at 1200^{o}C and 300kg/cm^{2} in a stream of nitrogen. We made a induction-heating uniaxial hot pressing (I-HUP) apparatus for this purpose.

After the fabrication of SYNROC, we measured its density by archimedes method and then carried out leach test by MCC-1 method at 90 ^{o}C for 7 days.

Table 1 shows the composition of the precursor and used reagents. The precursor consists of more than 70 wt% of TiO_2. Table 2 shows the composition of the simulated high-level waste called JW-A at JAERI containing 16.52 wt% of sodium and 5.07 wt% of caesium.

The new calciner (Fig. 2) can dry and calcine the SYNROC slurry in the same pot. Its component are mainly the pot, the heater, the motor, and the controller. A thermocouple is placed at the bottom of the propeller shaft to be able to recognize the end of drying and to measure the precise temperature of the slurry. Ar-4%H_2 gas is used to calcine under reducing conditions.

After the calcination, Ti-metal powder is mixed. The mixture is then hot-pressed. Figure 3 shows a I-HUP apparatus. Its component are mainly graphite die, press and press controller, heater and heater controller. An induction-heater was applied to simplify the heating part compared with the resistance heater. The new I-HUP apparatus can heat up to 1300^{o}C and press up to 300kg/cm^{2} for a cylindrical SYNROC sample of 4 cm in diameter. Nitrogen gas is flowed into the graphite die to keep the reducing conditions and to prevent damage to the

graphite die.

Results and discussion

Figure 4 indicates the X-ray diffraction patterns of calcines and SYNROCs made by a resistance-heating uniaxial hot pressing (R-HUP). The calcine C-A is made by our conventional method in which drying and calcination are carried out in separate apparatuses. The calcine C-B is made with the present new calciner. The SYNROCs S-A and S-B are made from the calcines C-A and C-B, respectively. The two patterns of the calcines resemble each other. The two pattern of the SYNROCs also resemble each other. It can be said that the same crystalline phases were formed in the calcines and the SYNROCs, respectively. Peaks of hollandite have already occured in the calcines. This crystalline phase incorporates caesium into the lattice. This implies that a part of caesium is possibly immoblized in the hollandite during calcination. The X-ray pattern of the SYNROC made by I-HUP is the same as that of the sample made by R-HUP.

Table 3 compares the result of the leach rate of the hydroxide-route SYNROC with those of the other SYNROC and glass. As compared with PNL 76-68 glass, the leach rate of the hydroxide-route SYNROC is less than 1/50 of Ca and Cs, 1/100 of Na. As compared with the other SYNROCs, the leach rate of the hydroxide-route SYNROC is about 1/4 of Ca, 1/3 of Cs. Thus it can be said that the leach rate of the hydroxide-route SYNROC is superior to those of the other route SYNROCs.

Table 4 shows the comparison of the leach rates of the hydroxide

route SYNROCs by three processes. The leach rates of SYNROCs made by each process are almost the same, so we can say that the new calciner and the I-HUP apparatus are applicable to hot laboratory operations.

References

(1) R. G. DOSCH, T. J. HEADLEY, and P. HLAVA, "Crystalline titanate ceramic nuclear waste forms: processing and microstructure," J. Amer. Ceram. Soc. 67(5), pp. 354-361 (1984).

(2) S. E. KESSON and A. E. RINGWOOD, private communication (1984).

(*1) K. D. REEVE, D. M. LEVINS, J. L. WOOLFREY, and E. J. RAMM, "Immobilization of high-level radioactive waste in Synroc," Nuclear Waste Management (Advances in Ceramics, Vol. 8), pp. 200-208, G. G. WICKS and W. A. ROSS, Eds., American Ceramic Society, New York (1984).

(*2) D. M. STRACHAN, "Results from long-term use of the MCC-1 static leach test method," Nucl. Chem. Waste Manage., 4, pp. 177-188 (1983).

Table 1 Composition of SYNROC precursor

Component	Content (wt %)	Reagent
TiO_2	71.3	$Ti(C_3H_7O)_4$
CaO	11.1	$Ca(OH)_2$
ZrO_2	6.8	$Zr(C_4H_9O)_4$
BaO	5.5	$Ba(OH)_2 \cdot 8H_2O$
Al_2O_3	5.4	$Al(C_4H_9O)_3$
Total	100.1	

Table 2 Composition of HLW (JW-A)

Component	Content (wt %)
Na_2O	16.52
Fe_2O_3	13.83
MoO_3	9.00
Nd_2O_3	8.56
ZrO_2	8.53
CeO_2	7.03
Cs_2O	5.07
Others	31.46
Total	100.00

Table 3 Leach rates ($g.m^{-2}.d^{-1}$) of SYNROC and waste glass under MCC-1 condition at 90 °C for 7 days in deionized water

	SYNROC			Waste Glass
	Hydroxide-	Sandia-*1	Oxide-*1	PNL 76-68*2
Element	Route	Route	Route	
Ca	5.1×10^{-3}	2.1×10^{-2}	2.6×10^{-2}	4.3×10^{-1}
Cs	3.5×10^{-2}	1.0×10^{-1}	2.5×10^{-1}	2.1×10^{0}
Na	1.4×10^{-2}	—	—	1.9×10^{0}

*1: K. D. Reeve et al. (1984).

*2: D. M. Strachan (1983).

Table 4 Leach rates ($g.m^{-2}.d^{-1}$) of hydroxide-route SYNROCs under MCC-1 condition at 90 °C for 7 days in deionized water

	A (Calciner;	B (Calciner;	C (Crucible;
Element	I-HUP)	R-HUP)	R-HUP)
Ca	7.6×10^{-3}	5.1×10^{-3}	5.9×10^{-3}
Cs	4.2×10^{-2}	3.5×10^{-2}	5.1×10^{-2}
Na	1.3×10^{-2}	1.4×10^{-2}	2.2×10^{-2}
Density	4.22 ($g.cm^{-3}$)	4.14 ($g.cm^{-3}$)	4.18 ($g.cm^{-3}$)

I-HUP: Induction-heating uniaxial pressing.

R-HUP: Resistance-heating uniaxial pressing.

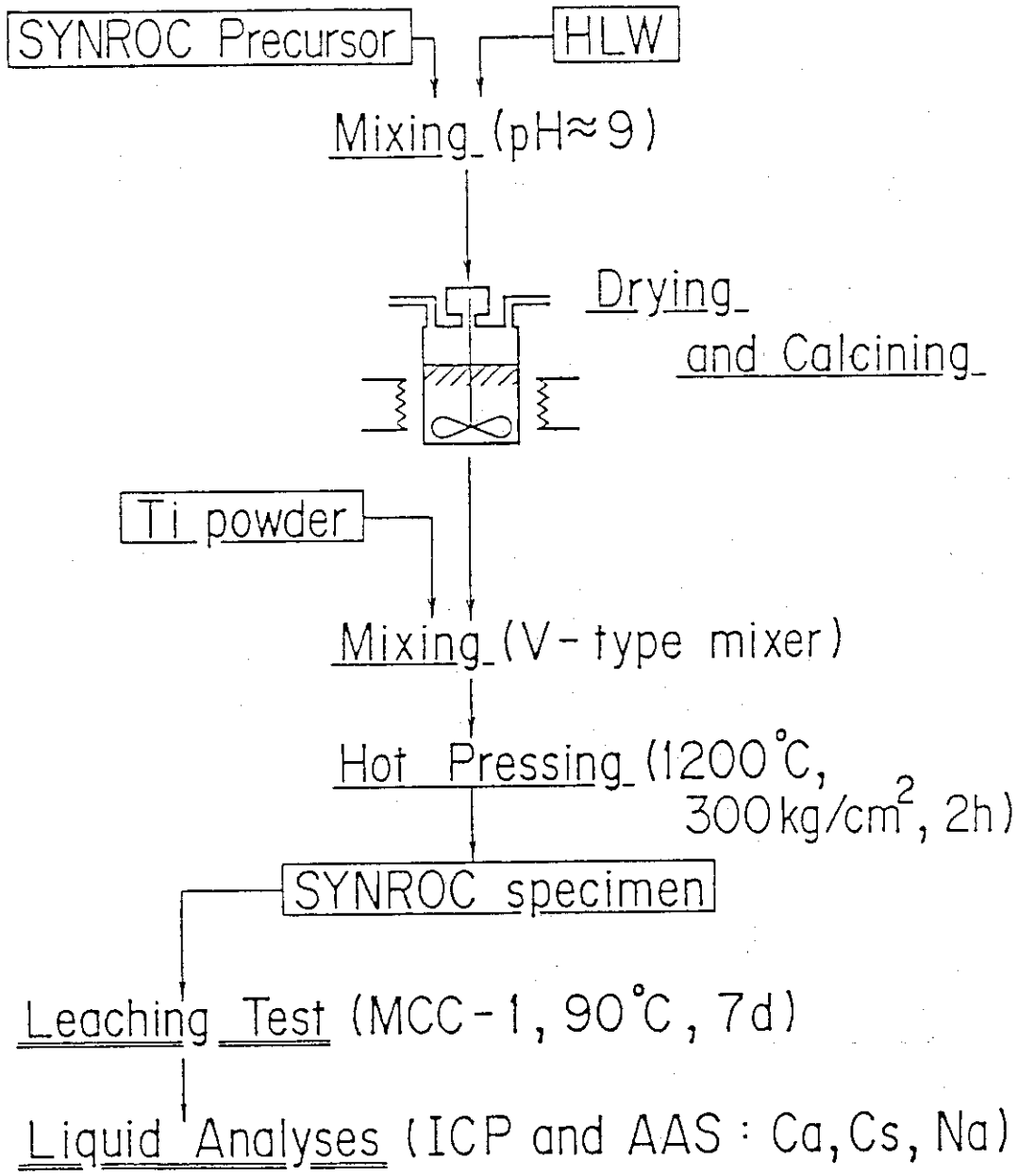

Fig. 1. Flow sheet for prepartion and leach test of SYNROC.

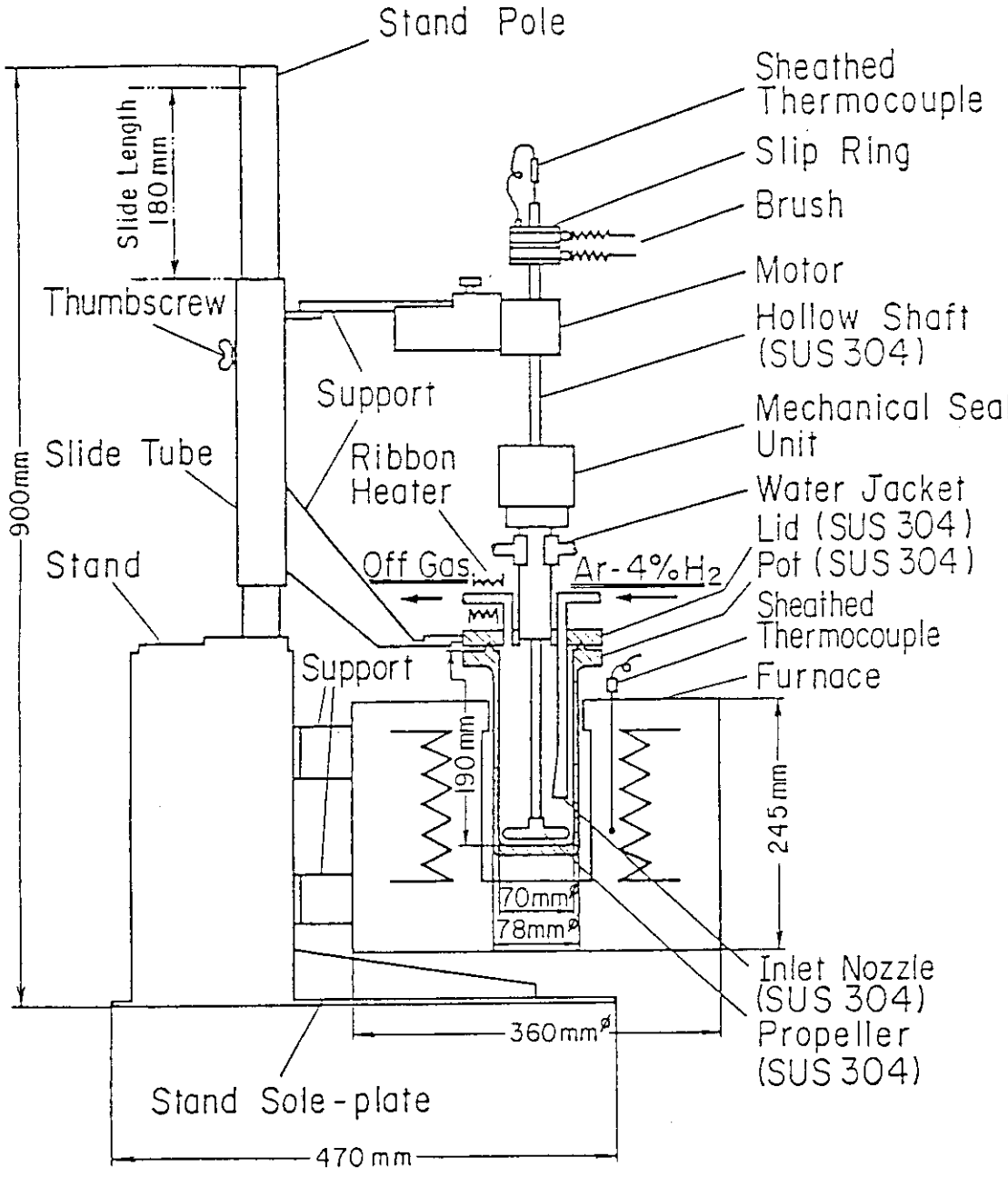

Fig. 2 General view of calciner.

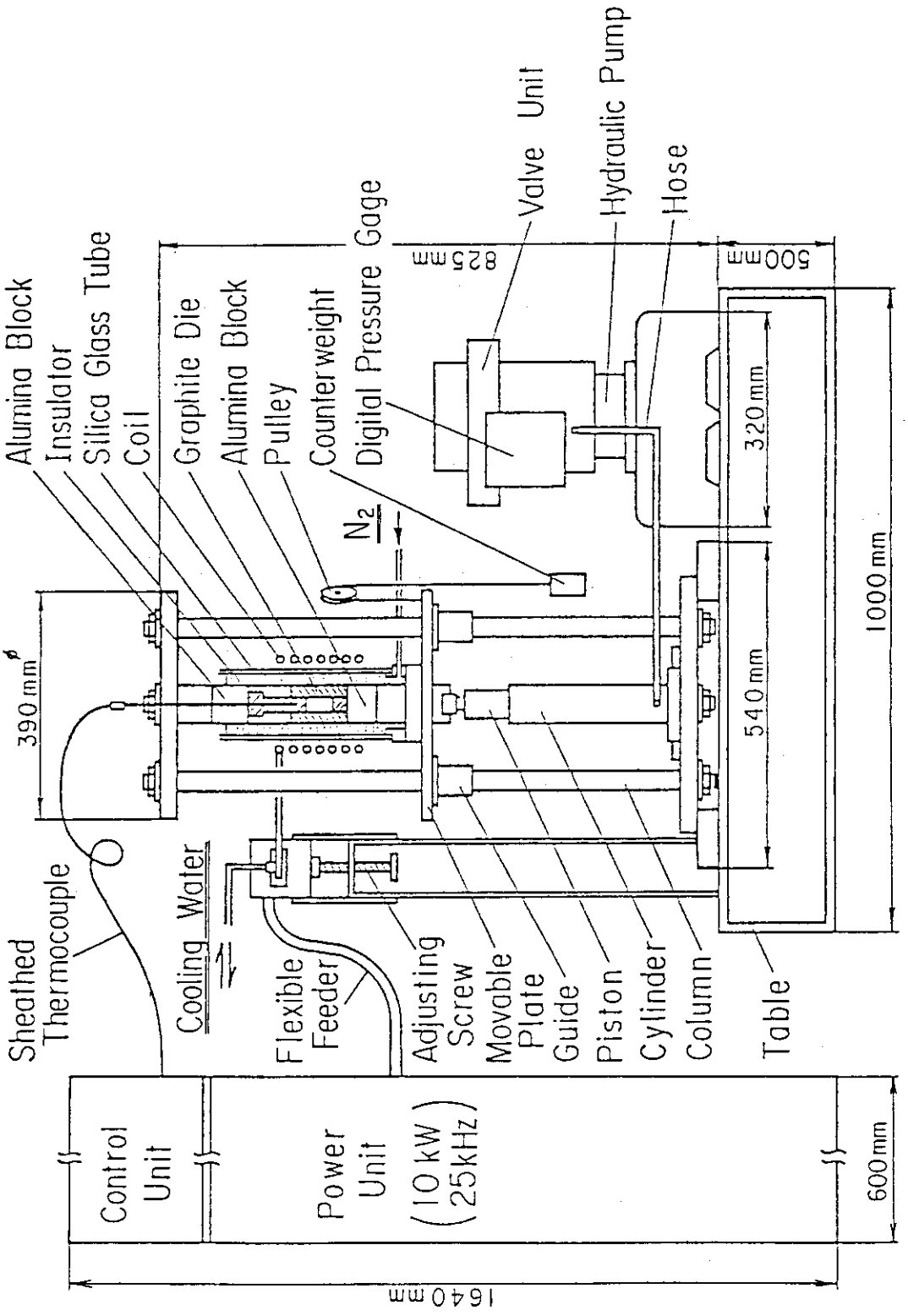

Fig. 3 Induction-heating uniaxial pressing apparatus.

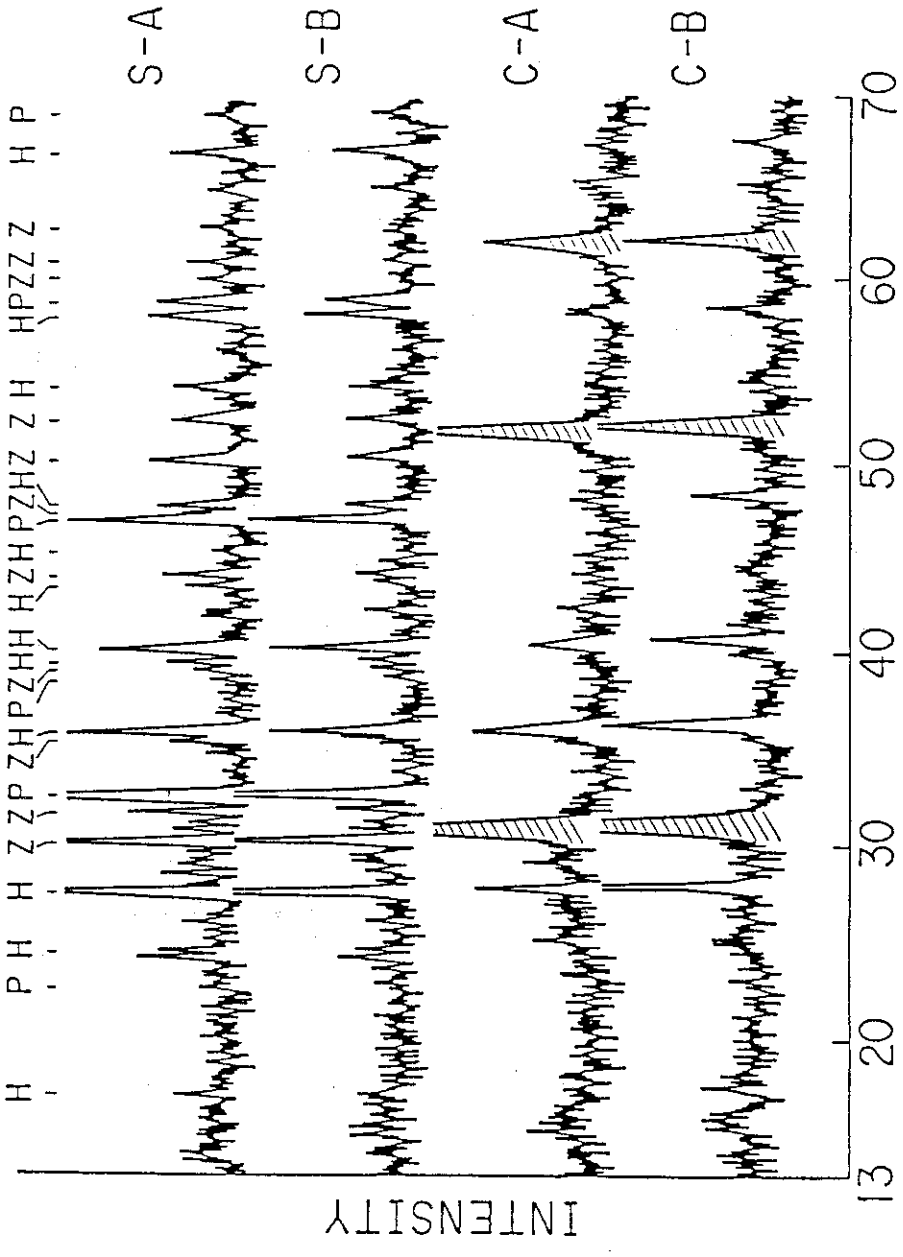

Fig. 4 Powder diffraction patterns. C-B and C-A represent the calcines made with a clciner and a crucible, respectively. S-B and S-A indicate the SYNROCs made from the former and the latter calcines, respectively. H is hollandite, P is perovskite and Z is zirconolite. Shaded unidentified peaks reveal the formation of intermediate products.

1.4 Irradiation tests of SYNROC specimens containing a simulated high level waste

H. Mitamura, T. Murakami and T. Amaya

Introduction

Alpha decays in high level wastes are mostly due to Am, Cm and Pu. The energies of alpha particles are about 5 MeV. The estimated total number of the alpha decays in the SYNROC which contains 10 wt% of a high level waste is 1.1×10^{19} (alpha decays/cm^3).

Maximum range of the 5 MeV alpha particle is about 10 μm in the SYNROC. Consider a plane in a SYNROC. The alpha particles which are generated within 10 μm layers on both sides of this plane are supposed to penetrate the plane. Assuming that one half of these particles pass through the unit cross section of the plane, the dose of the alpha particles is obtained as follows:

$(1/2) \times 1.1 \times 10^{19}$ (α/cm^3) x 20 (μm) x 10^{-4} (cm/μm) = 1.1×10^{16} (α/cm^2).

Since most of irradiating He^+ only passed through thin SYNROC specimens without any influence in our previous test (400 keV helium ion up to a dose of 5.7×10^{16} He^+/cm^2), we used Ar^+ instead of He^+ in the present study. Figure 1 shows an relation between the calculated values of displacement per atom (DPA) in a SYNROC sample due to Ar^+, O^+ and He^+, and the depth from the surface of the sample. The thickness of specimens which we can observe with 200 kV transmission electron microscope is usually thinner than 0.1 μm. Figure 1 depicts that the DPA value due to Ar^+ is $\sim$ 300 times more than that due to He^+ in the 0.1 μm depth of the SYNROC sample.

In the present study, much higher DPA values on the SYNROC specimen are chosen to observe firmly change of the SYNROC specimen owing to irradiation. About twenty times and a hundred times higher values of the dose than 1.1 x 10^{16} (α/cm^2) above mentioned:

1.1 x 10^{16} (ions/cm^2) x $\sim$ 20 = 2 x 10^{17} (ions/cm^2);

1.1 x 10^{16} (ions/cm^2) x$\sim$100 = 1 x 10^{18} (ions/cm^2),

were adopted as the total doses for the thin specimens of the SYNROC in the present irradiation test.

Experimental

A Van de Graaff accelerator[1] was used to generate 400 keV argon ions. The beam of the argon ions is bended with magnets and led to the target room. The beam is finally collimated with a slit of 6 mm in diameter just before irradiation of the specimen. The specimens before and after irradiation were observed with transmission electron microscope (H-800).

(Irradiation condition)

Accelerator: 2 MeV Van de Graaff accelerator.

Irradiating ion: argon ion (Ar^+).

Accelerated voltage: 400 kV.

Irradiated sample: thin sections of ANU-D SYNROC prepared in JAERI;
density 4.22 (g/cm^3);
waste loading 10 wt%.

Ion milling: 6 kV argon ion;
total current of double ion beams (< 1 mA).

	Specimen 1	Specimen 2
total dose	2.25 x 10^{17} (Ar^+/cm^2)	1.05 x 10^{18} (Ar^+/cm^2)
dose intensity	3.96 x 10^{13} ($Ar^+/cm^2 \cdot s$)	3.31 x 10^{13} ($Ar^+/cm^2 \cdot s$)

Results

Photographs 1A, and 2A,B, respectively, show transmission electron micrographs of the hydroxide-route SYNROC specimens before irradiation. Photographs 1B,C,D, and 2C,D,E, respectively, display transmission electron micrographs of the specimens after irradiation with 400 keV argon ion up to doses of 2.25 x 10^{17} and 1.05 x 10^{18} (Ar^+/cm^2). In these photographs, we can no more observe grain boundaries of each crystalline pahse which were present before irradiation. Photographs 1E and 2F, respectively, show electron diffraction patterns of the selected area in the photos. 1D and 2E. In these photographs, amorphous halos alone are observed. Since this amorphousness, however, seems to be caused by melting of the thin specimen, another dose intensity of the ion will be applied in the near future.

Reference

K. SUZUKI, Y. KATANO, T. ARUGA and K. SHIRAISHI, "Miniaturized target chamber for 2MV Van de Graaff accelerator," JAERI-M 84-181 (1984).

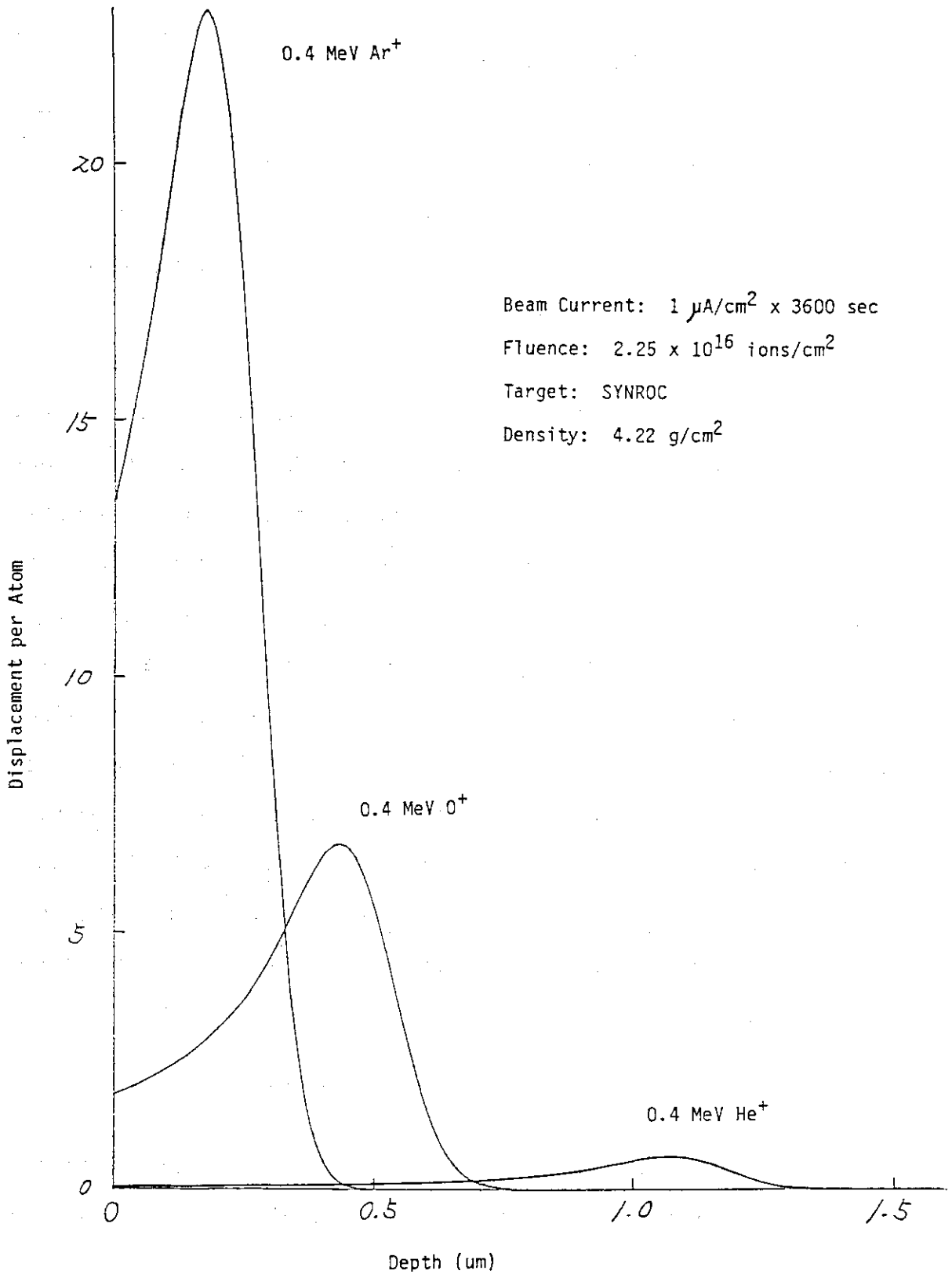

Fig. 1. Profile of displacement per atom against the depth from the surface of the SYNROC sample

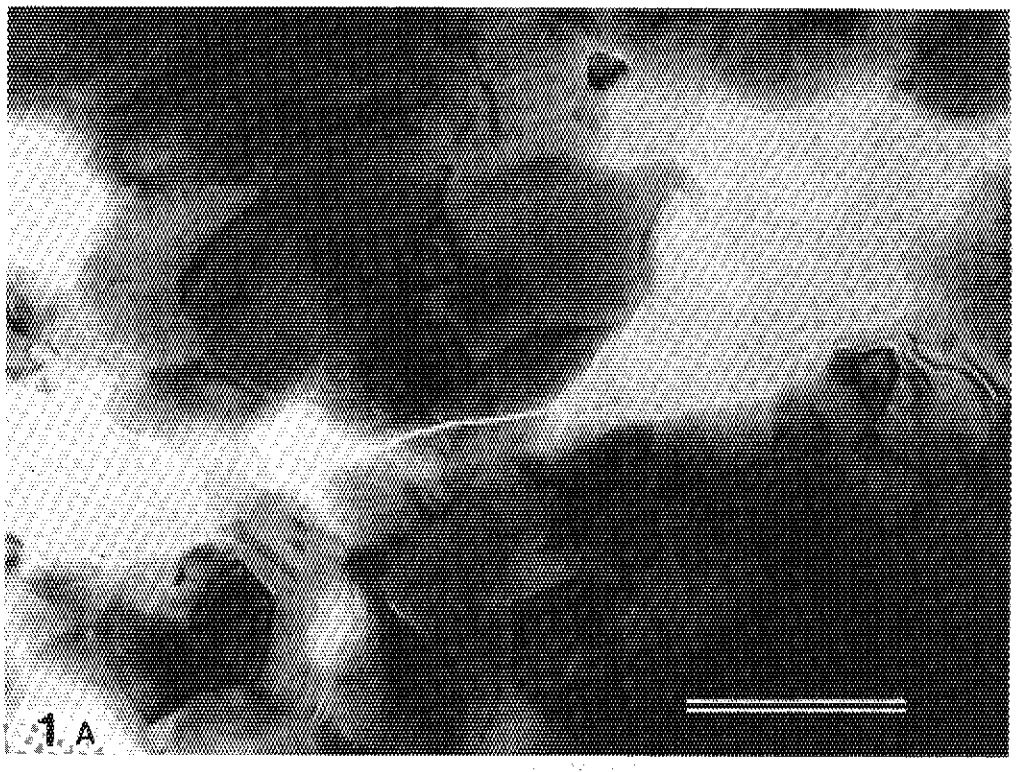

Photo. 1A. Transmission electron micrograph of hydroxide-route SYNROC before irradiation. A black bar is 1 μm.

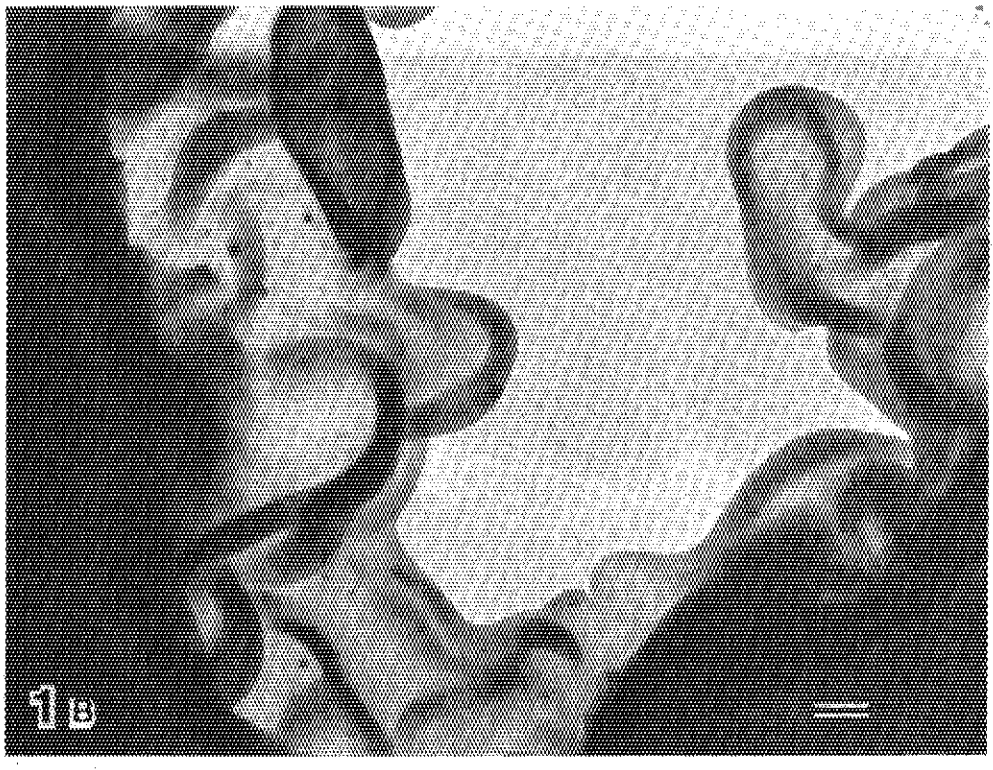

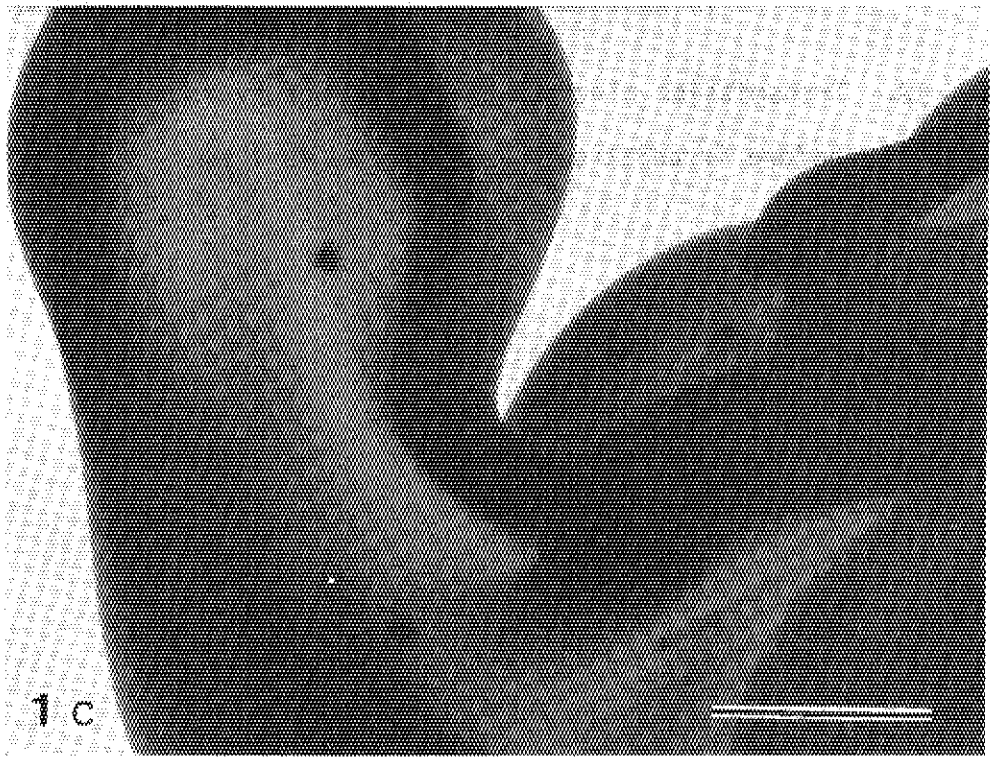

Photo. 1B,C . Transmission electron micrographs of the same samples as that in photo 1A after irradiation with 400 kV argon ion to a dose of 2.25×10^{17} (Ar^{+}/cm^{2}). Each black bar is 1 μm.

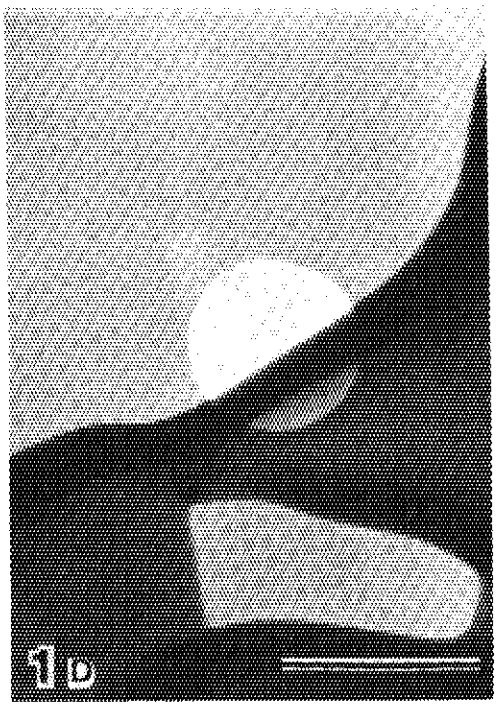

Photo. 1 D. Transmission electron micrographs of the same samples as that in photo 1A after irradiation with 400 kV argon ion to a dose of 2.25×10^{17} (Ar^+/cm^2). Each black bar is 1 μm.

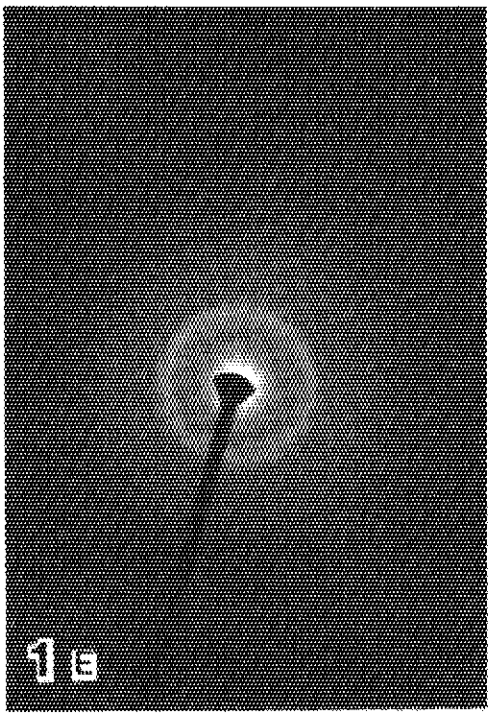

Photo. 1E. Electron diffraction pattern of selected area in the photo. 1D.

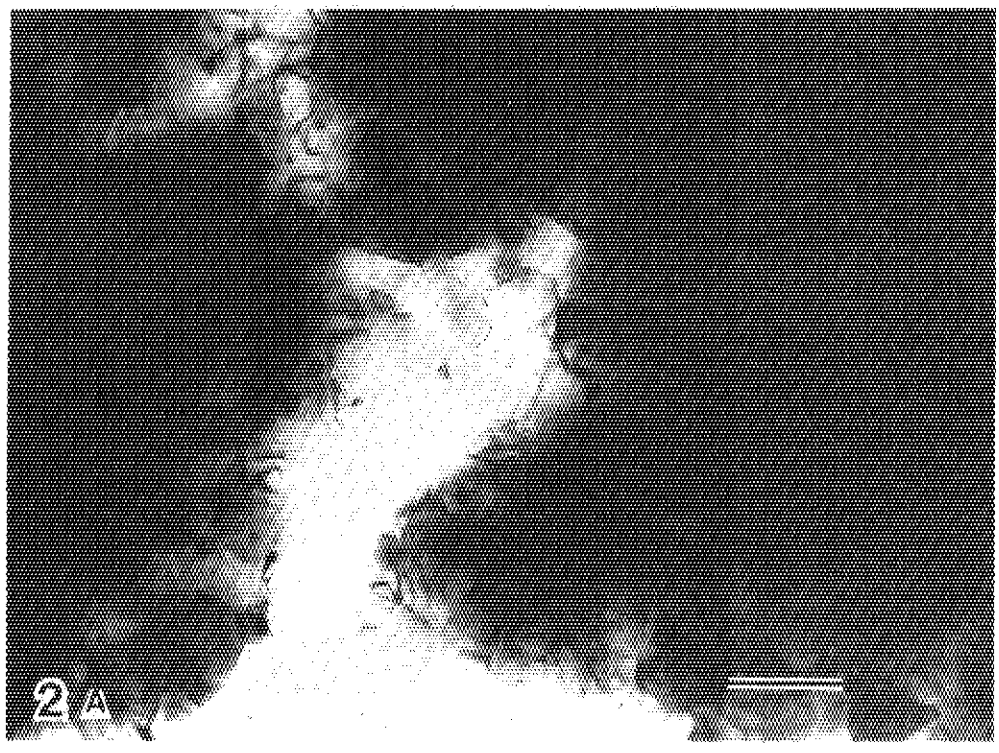

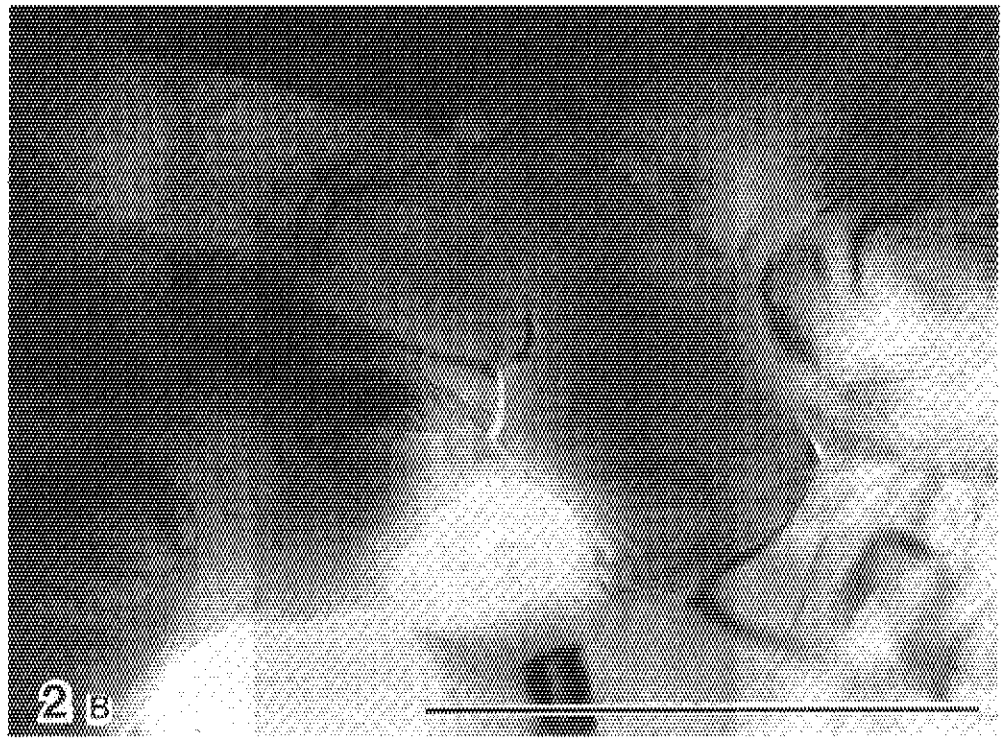

Photo. 2a,B. Transmission electron micrographs of hydroxide-route SYNROC before irradiation. Each black bar is 1 μm.

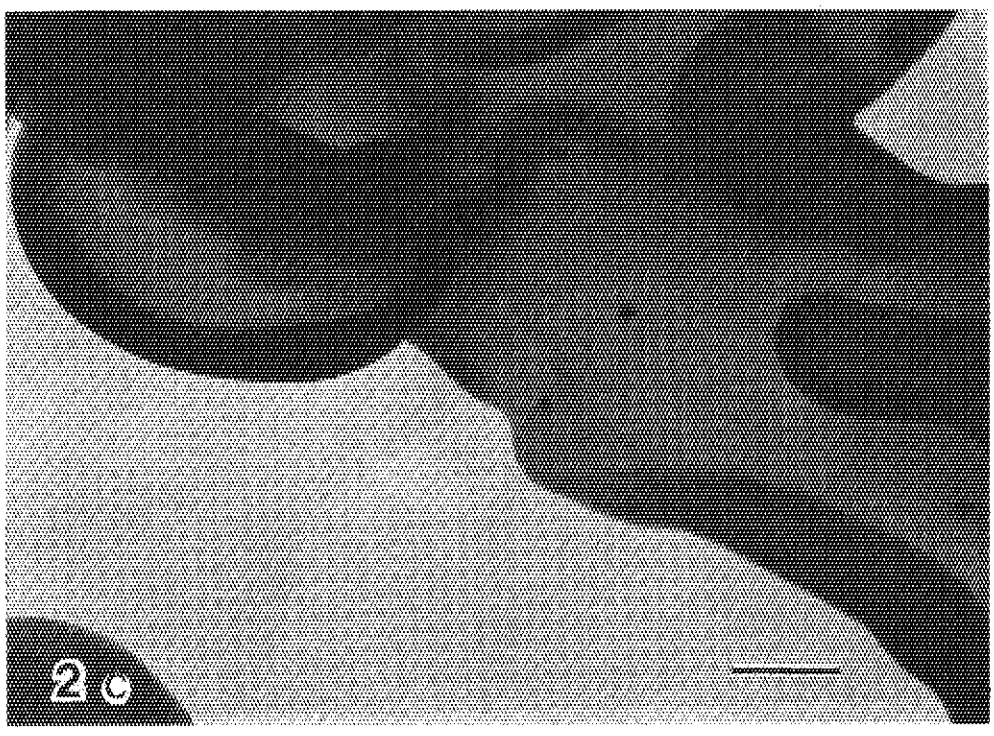

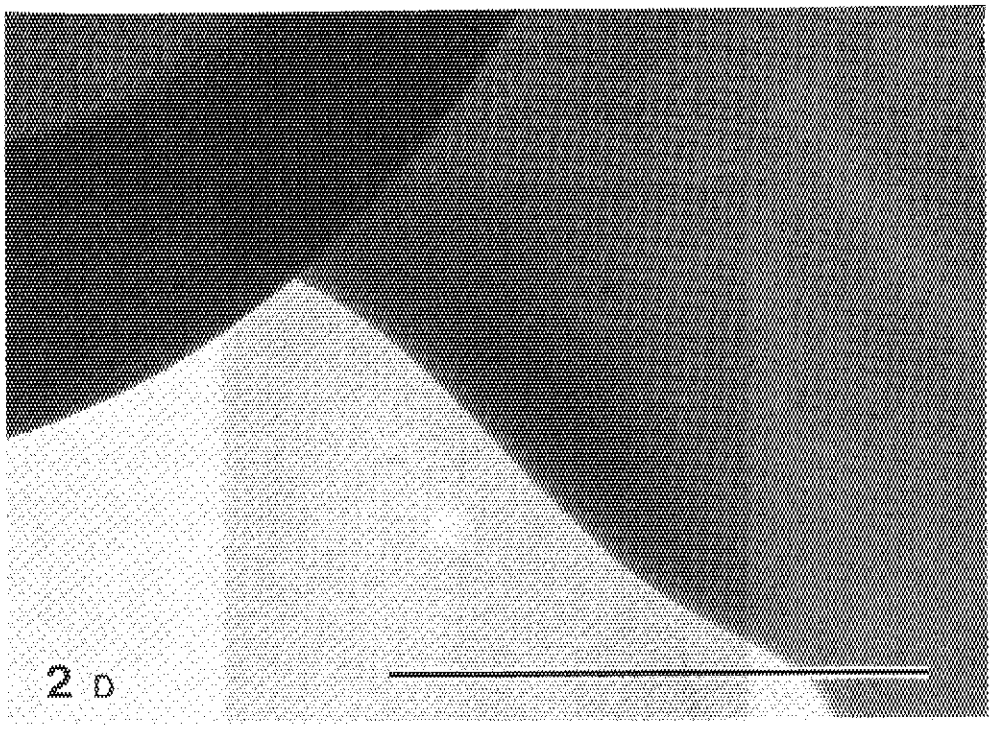

Photo. 2C,D . Transmission electron micrographs of the same sample as that in photo. 2A,B after irradiation with 400 keV argon ion to a dose of 1.05×10^{18} (Ar^{+}/cm^{2}). Each black bar is 1 μm.

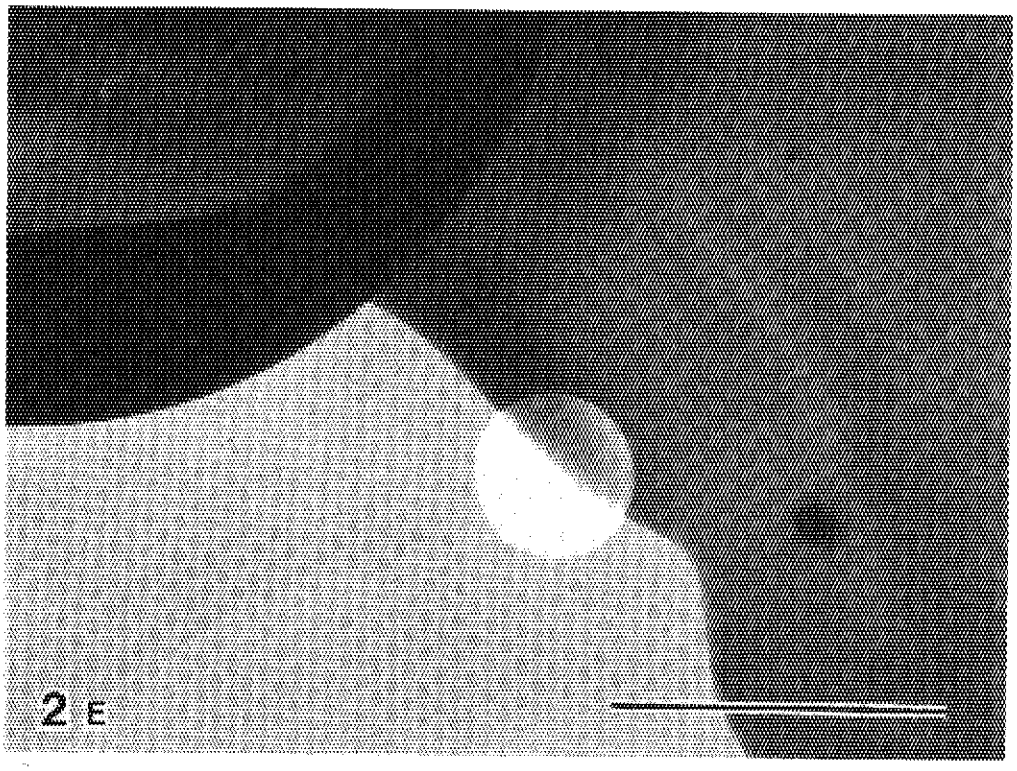

Photo. 2E. Transmission electron micrographs of the same sample as that in photo. 2A,B after irradiation with 400 keV argon ion to a dose of 1.05 x 10^{18} (Ar^{+}/cm^{2}). Each black bar is 1 μm.

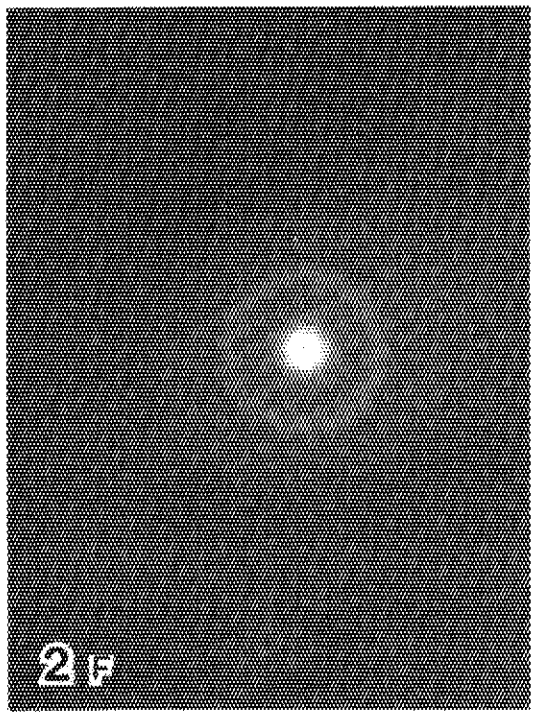

Photo. 2F. Electron diffraction pattern of selected area in the photo. 2E.

2. Safety evaluation for geological disposal

S.Muraoka

Laboratory and field works are carried out to accumulate the data which are indispensable for the safety assessment of geological disposal of high level waste.

This year, we continue the nuclide migration test in granite rock and performance evaluation test of engineered barrier.

As the field experiment, heating experiment with a real size canister and migration test using non-sorbing tracer have been carried out in the granite rock mass.

From this year we have initiated the fundamental feasibility study of subseabed disposal of high level waste.

2D-Seep, the coupled computer code of heat and groundwater flow, has been developed.

2.1 Engineered Barrier

(1) Buffer material test

S. Amagai

Introduction

The aim of this test is to clarify an engineered barrier performance on geological disporsal of high-level radioactive wastes. Thermal conductivity and other characteristics can be studied by using the barrier test equipment. In the first fiscal year, thermal conductivity test has been carried out in some conditions, and it will be continued.

Equipment and experimentals

The testing equipment is shown in Fig. 1. In order to simulate heat generation from HLW, electric heater is set in the center of the equipment. Simulated buffer materials which are the mixtures of bentonite (8 wt%) and zirconia sand (92 wt%), are filled up in a vessel around the heater. The moisture content of buffer materials is 2.82 wt%. The density of the materials is 3.18 g/cm^3. The vessel containing heater and the buffer materials is made of steel, and is set in water tank that is kept at constant temperature.

For thermal conductivity test, 10 thermo-couples can be set up in the buffer materials and can be connected to a data acquision system.

The buffer materials in the vessel were heated at 0.3 KW/h of electric power.

Results and disccusions

After 24 hours of heating, steady state of temperature was obtained. An example of radial temperature distribution after 270 hours of heating is shown in Fig. 2.

In order to calculate the thermal conductivities, this equipment was assumed to be a cylinder of infinite length. Calculated thermal conductivities are shown in Table 1. Thermal conductivities of the inner part were lower than those of outer part.

The difference of the thermal conductivities between inner part and outer part might be caused by the moisture content of buffer materials, as is reported by Radhakrishna [1].

The tests were repeated several times, but similar results were obtained. The variation of moisture content in radial direction in buffer must be investigated.

Reference

[1] H.S. Radhakrishna and K.K. Tsui
Proceedings of the Workshop on near-field phenomena in geologic repositories for radioactive waste. Nuclear Energy Agency, Paris, france. OECD. (1981) p.329-344.

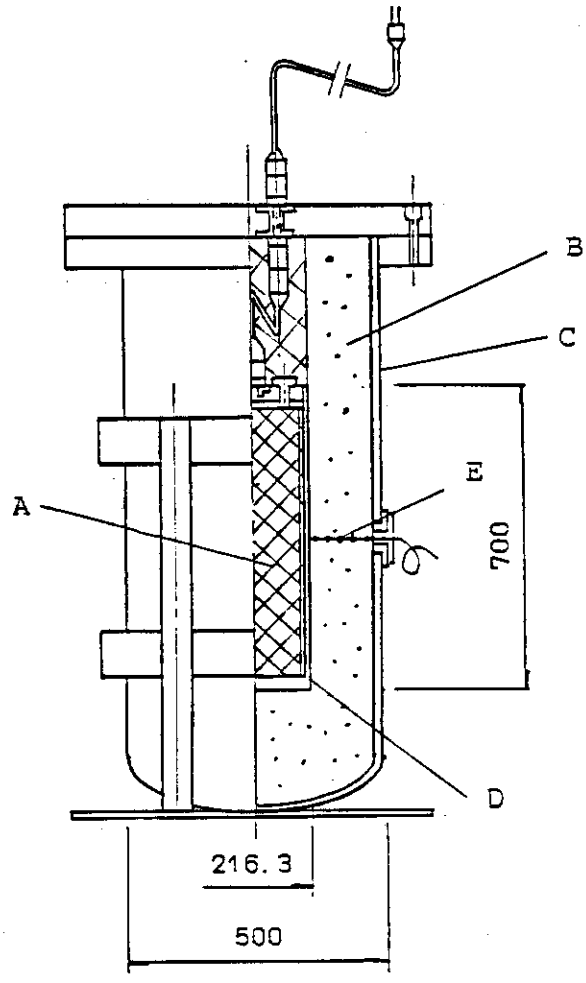

Fig. 1 The equipment of engineered barrier performances test
A; electric heater B; buffer materials
C; outer vessel D; inner vessel E; thermo couples

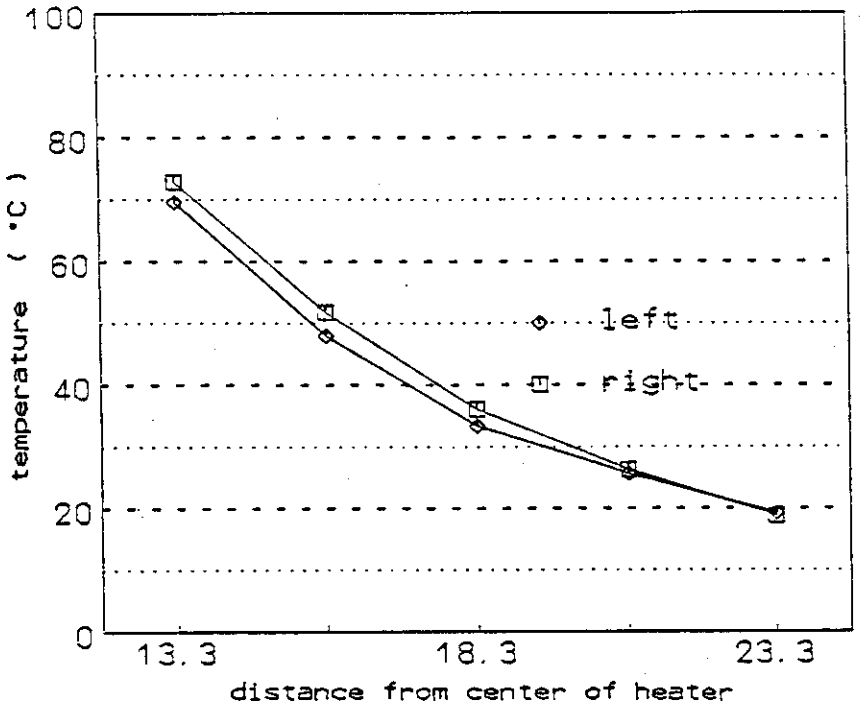

Fig. 2 Thermal distribution

Table 1 Apparant heat conductivity coefficient

Heater 0.3 KW

R(mm)		Kl	Kr	K
133	K	-	-	-
	Temp	69.5	72.9	71.2
158	K	0.604	0.618	0.611
	Temp	47.9	51.8	49.9
183	K	0.762	0.709	0.736
	Temp	33.3	36.1	34.7
208	K	1.244	0.990	1.117
	Temp	25.5	26.3	25.9
233	K	1.344	1.146	1.245
	Temp	19.1	18.8	19.0

R; distance from center of heater
Kl; thermal conductivity in left side (W/m °C)
Kr; thermal conductivity in right side (W/m °C)
K; averaged thermal conductivity (W/m °C)

(2) Effects of gamma-ray irradiation on stress corrosion cracking of candidate high-level waste container materials

M.Kumata

Introduction

A container for a solidified high-level waste glass products (HLW) from the reprocessing of the spent nucler fuel consists of two or more concentric metallic enclosures that act as a barrier against the ingress of groundwater to the waste form and egress of radionuclides to the repository. With a borosilicate glass waste form, the austenitic stainless steels are proposed as the most probable canister materials and low-carbon steels are being considered for use as a overpack[1]. Since high-level gamma-ray emitted from various fission products in HLW might change the environment around the container, the corrosion resistance of these container materials must suit the environment. Although the corrosion resistance of these materials in aqueous environments is well known, there seems to be little work on the influence of high-level gamma-ray irradiation on the corrosion in a repository-relevant environment solution, especially stress corrosion cracking (SCC), of these materials.

In this study, in order to evaluate the corrosion resistance of a candidate austenitic stainless steel, Type 304 ss, for the HLW canister and a low-carbon steel for the HLW overpack under gamma-ray irradiation in groundwater, stress corrosion craking tests were carried out in granite groundwater with gamma-ray irradiation at high temperature (250 $^{\circ}$C).

This study was carried out in corporation at JAERI and Kobe Steel Ltd.

Experimental

1. Materal characteristics

The test materials were commercial Type 304 ss and low-carbon steel, whose chemical compositions are given in Table 1. Specimens were removed from tube material for testing. In order to clear the gamma-ray irradiation effects on SCC, materials were thermally treated as shown in Table 1. The C-ring specimens were made by cutting 1.5-cm-wide rings from the heat-treated, 0.2-cm wall tubing. A 60 segment was then cut from this ring. The C-ring specimens were stressed to 90 % of their room temperature yield strength (0.2 % offset yield strength) and 110 % of the yield strain by thightening a nut on a bolt across the legs of the C. The maximum stresses in the specimens were 3 MPa for 304;1-12 specimens, 3.3 MPa for 304;13-15 specimens, 2.8 MPa for low-carbon steel;1-12 specimens, 3.1 MPa for low-carbon steel;13-15 specimens. The required final outside diameter (OD_f) of the ring to obtain the stresses listed above were calculated from the formula

$$OD_f = OD - \Delta$$

$$\Delta = \frac{f\pi D^2}{4EtZ}$$

where Δ = change of OD giving desired stress, OD = outside diameter, f = desired stress, E = Young's modulus of elasticity, t = wall

thickness of tube, D = mean diameter of tube (OD-t), and Z = correction factor (function of $D/t^{2)}$, Figure 1). The C-ring specimens were bolted using Type 304 ss nuts and bolts. No insulators were used. The specimens were washed in acetone with urtrasonic cleaner, then dried in oven at 70 C one hour.

2. Test Condition

The environmental exposure was conducted in a conventional one-liter autoclave constructed from Type 316 ss. Inner wall of the autoclave was plated with gold. Specimens were placed on a autoclave with ceramic plates prepared for each specimens. About 650 ml of the test solution which was sampled from a tunnel in granitic rock mass pour into the autoclave. Composition of the solution was shown in Table 2. The test-solution-volume to specimen-surface-area ratio was 4.1 ml/cm^2.

Gamma-ray irradiation was carried out in a cabe using a Co-60 source (about 60 kCi) at Takasaki Establishment (JAERI). The autoclave was setted in a gamma-ray irradiation cabe, the solution temperature came up to 250°C, then a Co-60 source was lifted up from a water pule of hausing to in front of the autoclave. With cobalt-glass gamma-ray dosimeter, dose rate in the autoclave was about 1.8×10^5 R/h. The test was run for 30 days and 90 days. The solution temperature was maintained within 2 of 250 °C. A pressure of 4.1 MPa was maintained throughout the test.

SCC tests without irradiation were also carried out as well as with gamma-ray irradiation for comparison. SCC susceptibility of

test specimens with and without gamma-ray irradiation was evaluated with the naked eye.

Results and Discussion

1. Effect of Gamma-ray Irradiation on SCC:

No cracking in the C-ring specimens of both Type 304 ss and low-carbon steel with and without gamma-ray irradiation was observed with the naked eye. The specimens stressed 110 % of the yield strength also showed no cracking. The results are shown in Table 3.

In previous experiment carried out in boiling deionized water with gamma-ray irradiation of 1.1×10^5 R/h for 30 days, double U-bend specimens of sensitized austenitic stainless steels, Type 304 ss, showed susceptibility for intergranular SCC[3]. Though total dose of the C-ring specimens was greater than that of the U-bend specimens, the C-ring specimens showed no cracking. It seems that following several reasons can explain the difference.

(1) the stress of the C-ring type specimen was milder than that of the U-bend type specimen

(2) a crevice of the double U-bend specimen accelerated integranular SCC

2. Solution Analysis :

Using a glass electrode, solution pH and Eh were measured before and after testing. The results are shown in Table 4.

3. Corrosion Products :

Corrosion products observed on the surface of the C-ring specimens of both Type 304 ss and low-carbon steel are now under investigation with X-ray diffraction method.

Refferences

1)NUREG/CR-3427, BMI-2113, vol.4 : "Long-term performance of materials used for high-level waste packaging" (1984)

2)Stress Corrosion Testing, ASTM, STP 425 (1967)

3)Furuya,T. et al.(1984),Proc.ANS Meeting,"Fuel Reprocessing and Waste Management"

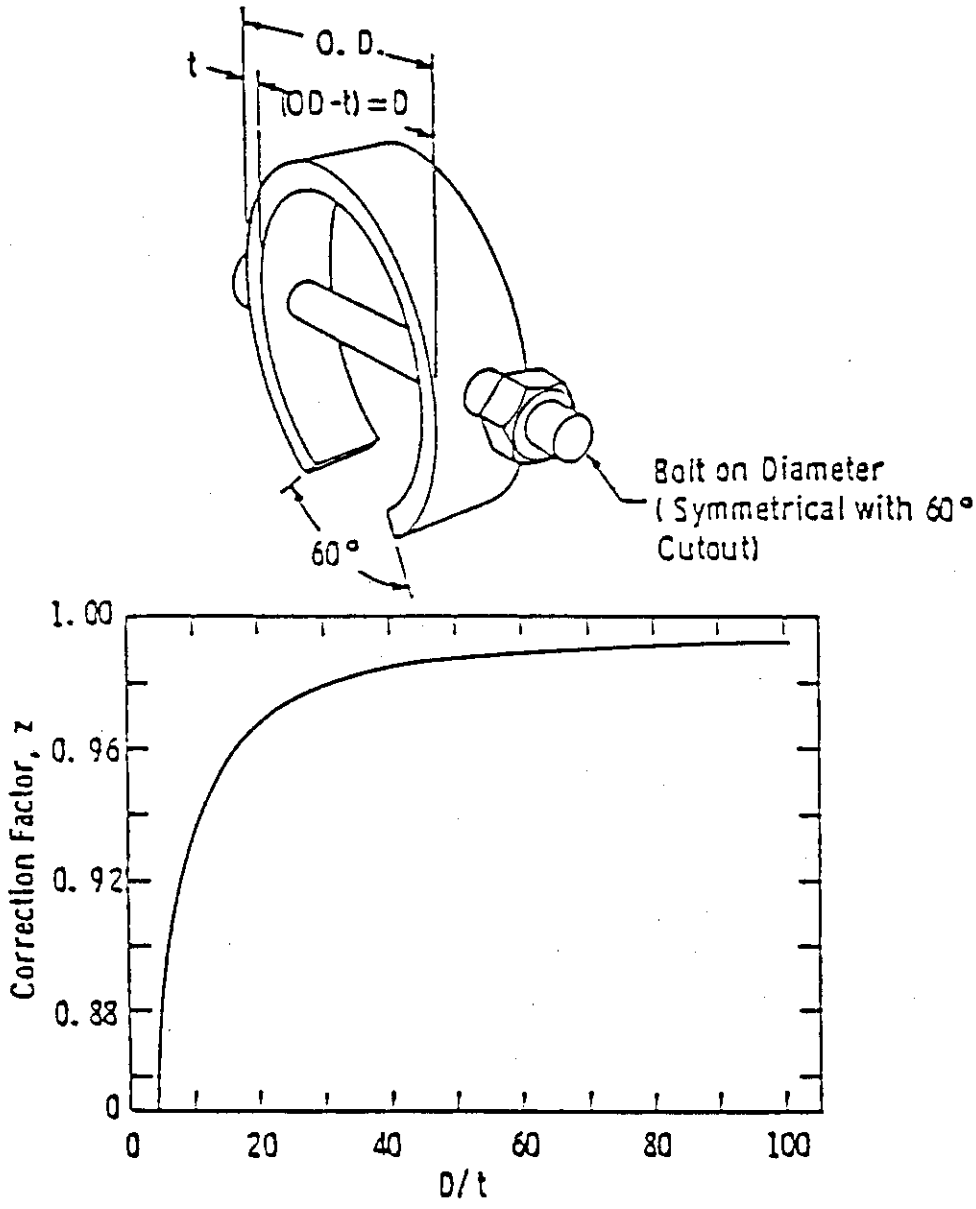

FIGURE 1 — C-ring specimen and correction factor (z) used in calculation of applied stress

Table 1 Chemical composition and heat treatment of test materials

	C	Si	Mn	P	S	Ni	Cr	heat treatment
SUS 304	0.48	0.44	1.30	0.034	0.021	8.55	17.72	700℃x100min→air cooling
Carbon Steel	0.23	0.19	0.46	0.012	0.014	0.03	0.06	→500℃x24h→air cooling

Table 2 Chemical composion of the groundwater (ppm*)

DO	pH	CON.	NH_4	Na	K	Ca	Mg	Fe**	Mn**	Cr**
9.31	8.4	125	<0.1	19.2	0.7	5.5	<0.1	<0.1	<0.1	<0.1

Ni	Al	HCO_3	SO_4	Cl	NO_3	PO_4	Si**	Si***	BOD
<0.1	<0.1	47	8.3	4.7	0.7	<0.5	7.0	6.9	<5

* except pH and CON.(conductivity: μS/cm),

** total,

*** dissolved

Table 3 SCC results for Type 304 ss and low-carbon steel with gamma-ray irradiation in the groundwater

Material	Stress	Dose rate(R/h)	exposure time(h)	dose (R)	SCC*
SUS 304					
(1)~(3)	90%γY	1.8×10^5	684.6	1.2×10^8	0/3
(7)~(9)	90%γY	1.8×10^5	1805.9	3.3×10^8	0/3
(13)~(15)	110%γY	1.4×10^5	709.4	1.0×10^8	0/3
Carbon steel					
(1)~(3)	90%γY	1.8×10^5	684.6	1.2×10^8	0/3
(7)~(9)	90%γY	1.8×10^5	1805.9	3.3×10^8	0/3
(13)~(15)	110%γY	1.4×10^5	709.4	1.0×10^8	0/3

* number of failed specimen/number of total specimen

Table 4 Results of pH and Eh measurements for test solution

run No.	exposure time(h)	pH	Eh(mv)	Temp.*
before testing		7.41	+210	19.7
1	684.6	8.17	−400	68.4
2	1805.9	7.05	−160	49.5
3	709.4	7.31	− 70	57.4

* solution temperature at measurement

2.2 Field test

(1) Heating Experiment with a Real Size Heater of Simulated Canister

K. SHIMOOKA

Heat transfer in a granite rock mass was measured by using a real size of canister, combination of stainless steel package and electric heater, to simulate the burial of actual waste.

Conduction of the heat was predominant in the homogeneous part of the rock mass, however, in the fractured zone heat transfer by groundwater flow was seen.

Experimental method

Based on the results from the small heater test, electric heater was improved to simulate the high-level waste and the canister, 32 heater elements were set in the SUS-304 canister. The size of the heater is 0.4 m in diameter and 1.5 m in length. The testing hole for the heater experiment in the granite rock was 1 m in diameter and 5 m in depth. The canister with heater elements was set in the hole at the depth of 3.75 m and the gap between the outer case of the canister and the wall of the hole was filled up with powdered granite sand.

In order to measure the temperature change, 27 seased thermo-couples were used. 18 thermo-couples were attached to the canister. 3 were burried in the granite sand between the canister and the hole surface. 6 were arranged in the granite rock mass by making boreholes. Arrangement of the heater and the position of the thermo-couples were shown in Fig. 1.

Electric power output for the heater has been adjusted and kept at 4 kW for the period of 1,800 hours by the output controller.

Results and discussion

Temperature distribution at the initial stage around the canister hole is measured. The temperatures at the deeper place of 7 m show the higher values of 13.3-14.3°C compared to those of 11.1-12.6°C at shallow level of 0.5 m in the hole. The temperatures after the heating of 1,800 hours at 4 kW at each depth and those of at each distance from the center

of the canister are listed in Table 1. An isothermal line at each depth around the canister is also shown in Fig. 2.

The isotherm shows a nearly concentric circle for the most part, however, at the depth of 4.75-7.0 m in the direction of 0° the distortion of the isotherm is seen. Testing holes of this direction are crossing the fractured zone where groundwater flow was expected. Therefore, the irregularity along this direction on the isotherm is thought to be caused by the heat transport by groundwater. Nearly concentric circles of the isotherm for the most part show that the heat was transfered by heat conduction in the rock mass.

For the temperature calculation, analytical programs "MARC" and "ADINAT" were used. Actual symmetric model was adopted in this calculation and the grids of finite elements are shown in Fig. 3. Measured temperatures before heating the rock were given to the nodes of the elements as an initial condition. Boundary conditions were set as shown in Fig. 4. Values listed in Table 2 were used for thermal conductivity, specific heat and density.

Both measured and calculated temperatures in the directions of 0° and 120° are shown in Fig. 5 and 6. No difference is seen between calculated and measured temperatures in the direction of 120° where the rock is virtually homogeneous. On the other hand, calculated temperatures do not agree with those of measured in the direction of 0° across the fractured zone. The difference is explained by the heat flow with the groundwater in the fractures. With the exception of the fractured zone, heat transfer in the granite rock mass was definitely explained by the heat conduction. Thus it was made clear that the temperature distribution was predictable by thermal conductivity, specific heat and density of the core sample. However, it was also recognized that the effect of groundwater flow on the heat transfer was not neglisible in the fractured zone.

Table 1 Rock temperatures after the heating of 1,800 hours at 4 kW

(temperature: °C)

Distance (m) \ Depth (m)	0.50	2.75	3.75	4.75	7.00
0.50	44∿47	70∿75	82∿85	51∿56	
0.65		60	72	47	
0.90	32∿36	45∿56	52∿61	34∿44	18∿19
1.30	26∿30	36∿43	36∿45	28∿36	17∿18

Table 2 Values used in the temperature calculation

Value			Unit	Remark
Thermal conductivity	κ	9.177×10^{-1}	cal/m•s•°C	Values of core sample at 20°C (wet condition)
Specific heat	c	1.83×10^{2}	cal/kg•°C	Core sample at 20°C
Density	ρ	2.64×10^{3}	kg/m^3	Core sample at 20°C
Heat transfer rate	H	27.8	cal/m^2•s•°C	AF boundary
Temperature in the room		11.5	°C	

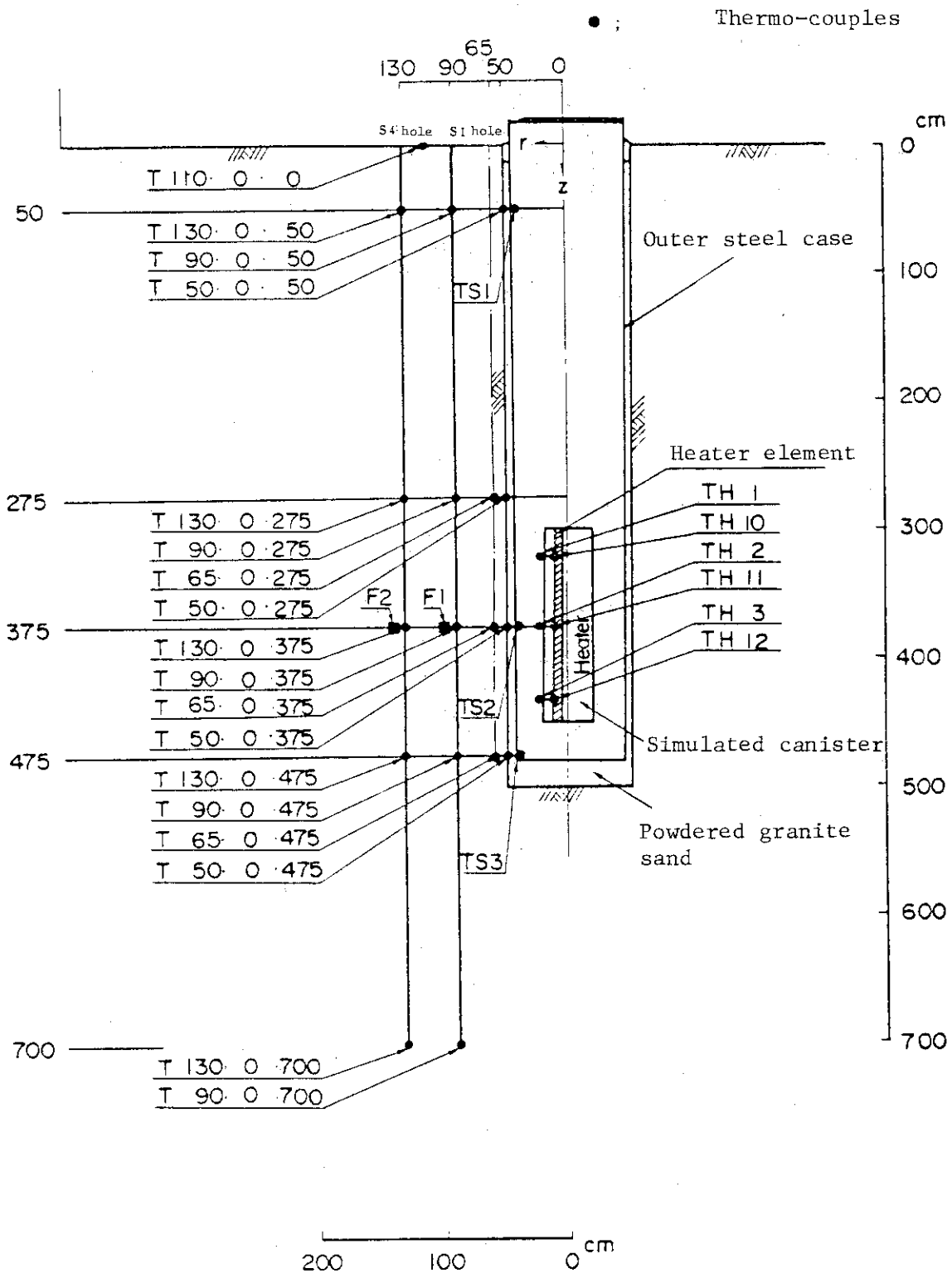

Fig. 1 Arrangement f a heater and position of thermo-couples

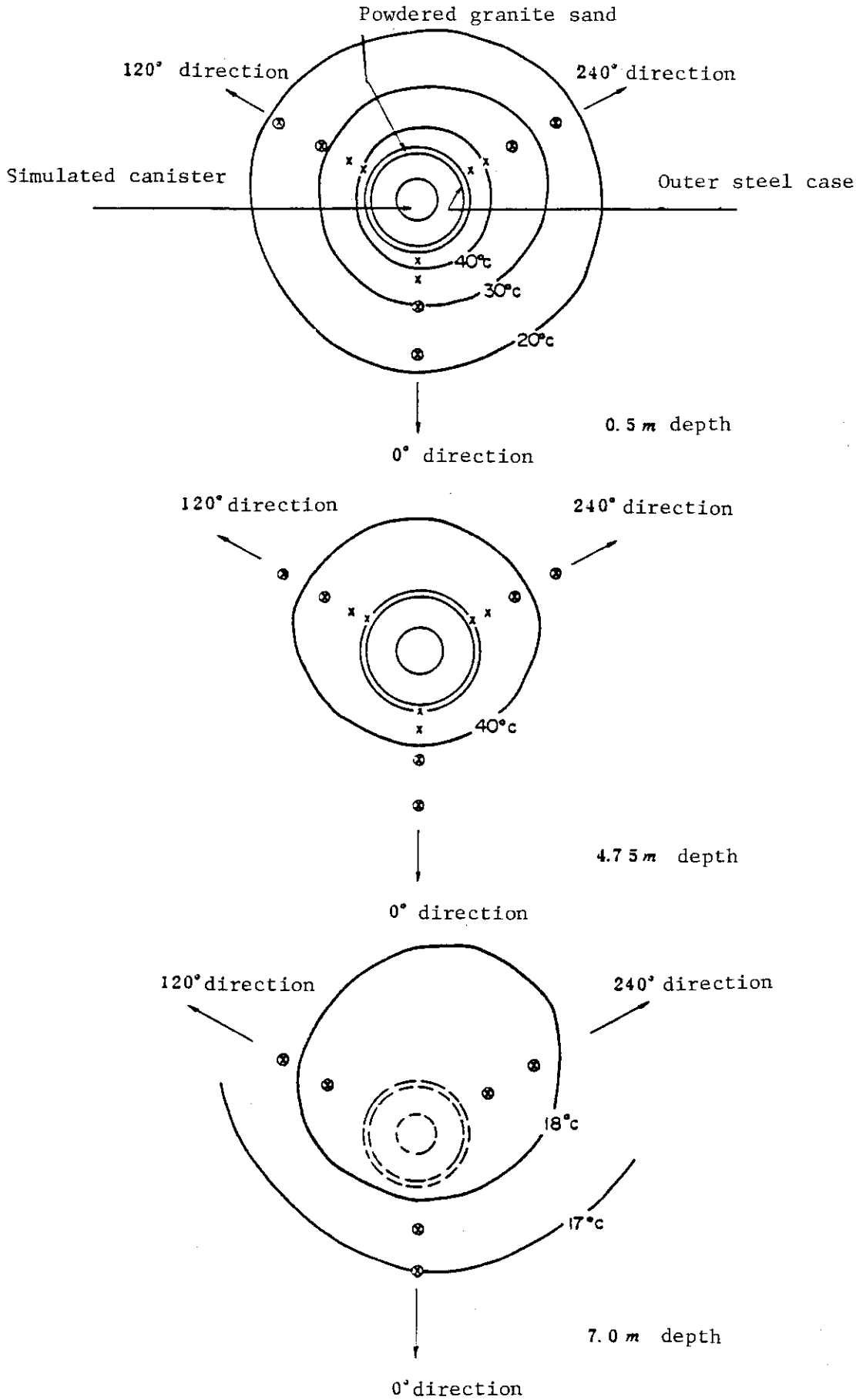

Fig. 2 Isothermal line at each depth after the heating of 1,800 hours.

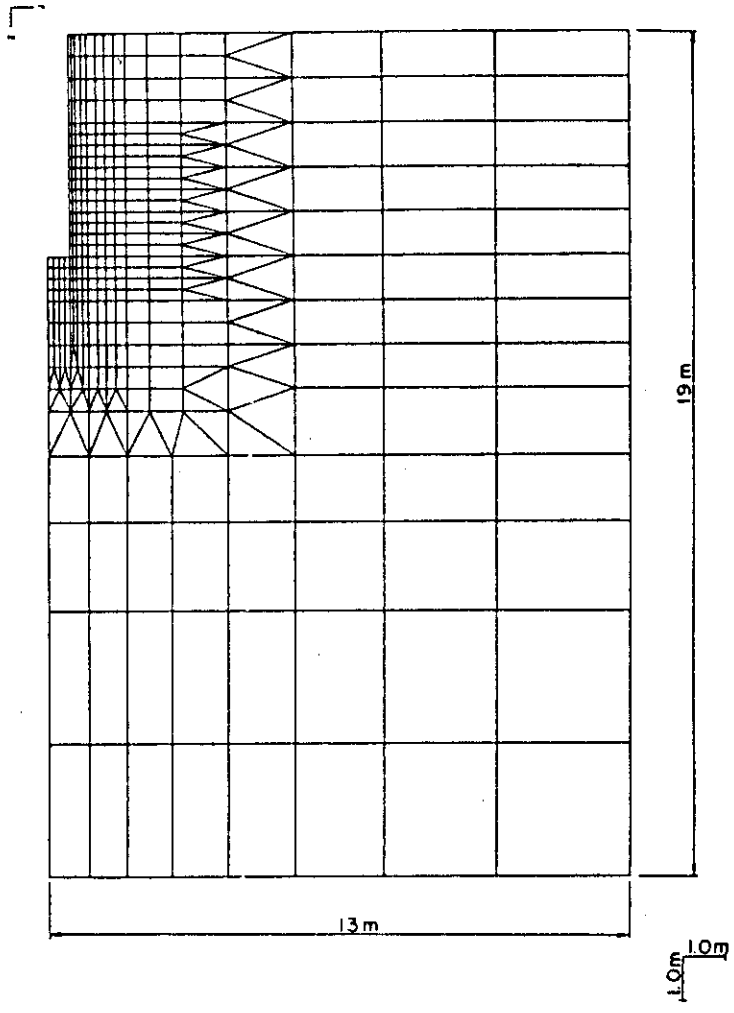

Fig. 3 Grids of finite elements

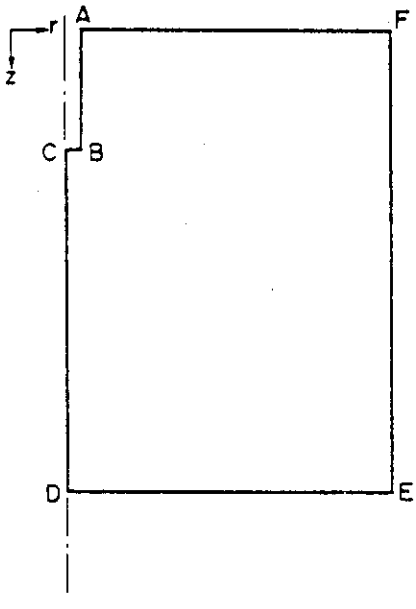

$\overline{AB}$, $\overline{BC}$: T = T(t)

$\overline{AF}$: Specified heat flux

$\overline{CD}$, $\overline{EF}$: No heat flow

$\overline{DE}$: T = const.

Fig. 4 Boundary conditions for temperature calculation

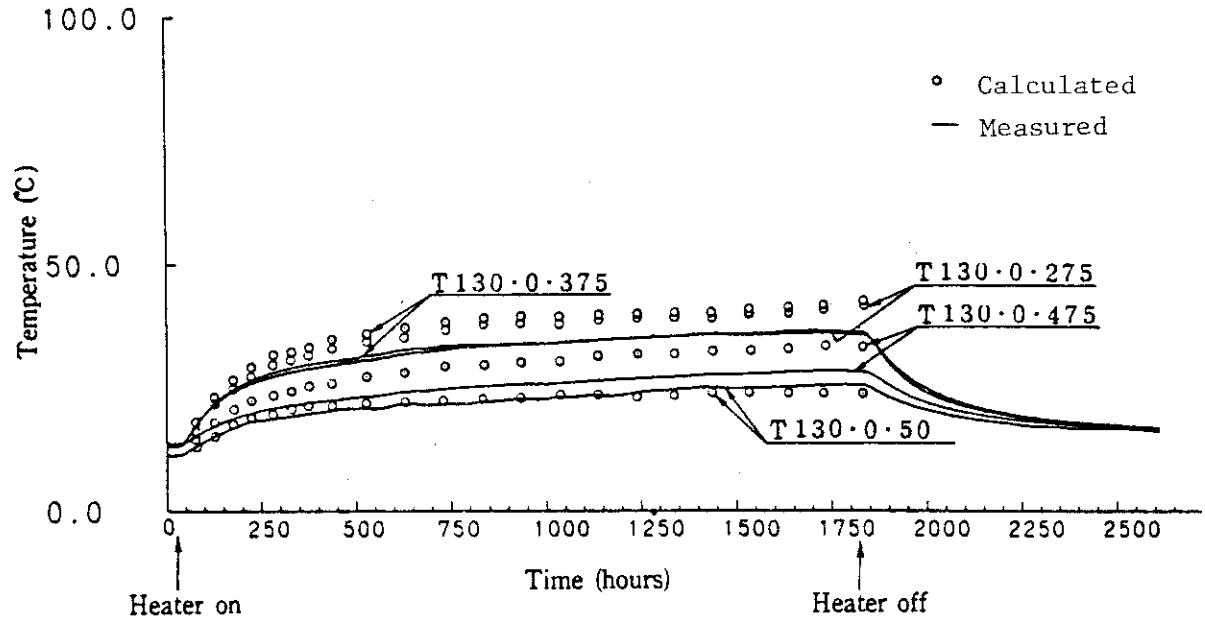

Fig. 5 Measured and calculated temperatures at the distance of 1.3 m in the direction of 0°

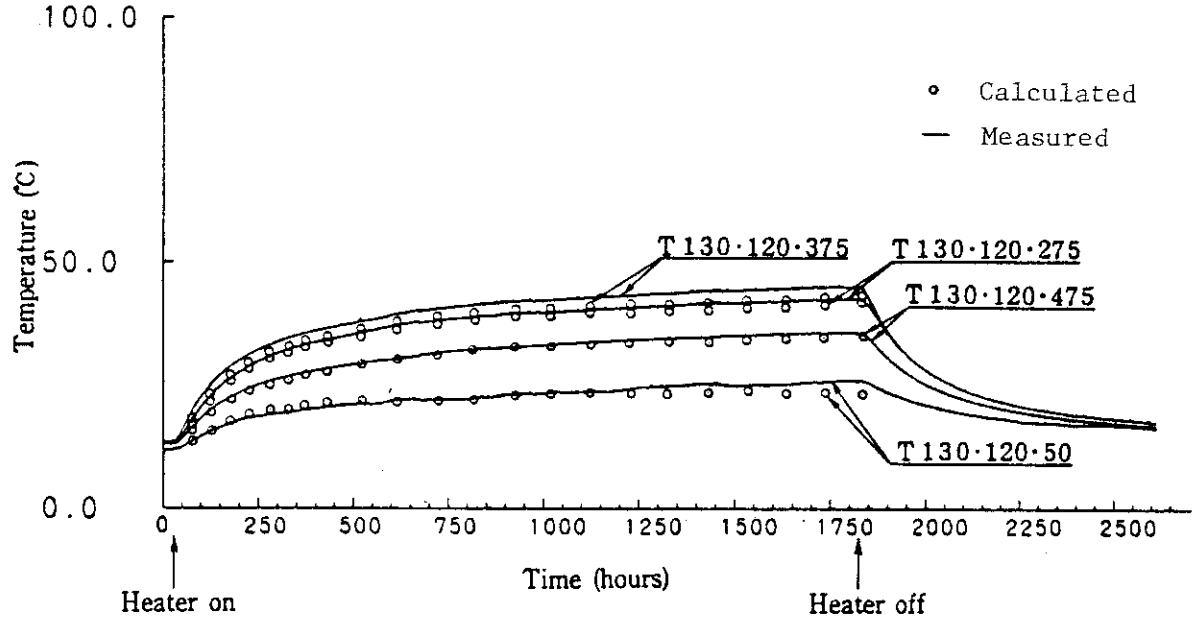

Fig. 6 Measured and caluclated temperatures at the distance of 1.3 m in the direction of 120°

(2) Migration test

A.Nakagoshi

Introduction

It is a very important part of the safety analysis of the problems associated with the storage of nuclear waste to know transport mechanisms of nuclides in crystalline rock as one of candidate bedrock for repository. It is recognized that substances dissolved in groundwater are transported in fractures and in rock matrix with water flow and dispersion. The transport of water-soluble substances will be affected by chemical and physical processes such as diffusion into the matrix, ion exchange, precipitation and filtration effect.

One of feasibilities for studies of these mechanisms is a tracer method. In this test, in order to develope the experimental techniques for the investigation of the water flow and nuclide dispersion in the fractured granite, Br^- solution was used as non-sorbing tracer.

Experimental

Conceptual layout of this test which was based on the fracture map of room and borehole investigations of the injection hole is shown in Fig.1. From about 5m above the ceiling of room, Br^- solution was injected into a fracture zone which crosses the experimental room vertically, and discharged water emerging into the upper part of the room was collected. The distribution of discharge rate of natural groundwater is shown in Fig.2.

As a preliminary test, in order to validate experimental techniques Fluorescein-Na was injected. The experimental method of main test was based on the achievements of the preliminary test. Layout and equipments of this main test were same as the preliminary test. A tracer used was KBr dissolved in the groundwater. Injection concentration (C_0) of the tracer was 8900 ppm. The tracer was injected into the injection hole, section of 46.8 - 50.0 m, at the rate of about 20 l/day for 500 hours. Total volume of tracer injected was 410.07 liters. The discharged water emerging into the each section was individually collected at regular intervals for 958.5 hours since injection had been started. A tracer in samples of collected water was detected in the laboratory by a ion-selective electrode.

Results and discussions

At each section, breakthrough curves for C/C_0 and the ratio of discharged water were obtained. The distribution of C/C_0 after 100, 300 and 500 hours are shown in Fig.3. From these results, it was clarified that a tracer was mainly transported in the fracture zone. And that a tracer was dispersing to rock matrix near the fracture zone.

At sections along the fracture zone, it was observed that the amounts of discharged water was increased by injecting the tracer. One of some interests is that no tracer could be detected at far sections from the fracture zone which had large amount of discharged water.

These results mean that channels of this area's fracture

network are simple. So the single fracture model[1] is adopted to analize the Br^- migration.

By a trial and error method, parameters of this model are obtained for three pairs of breakthrough curves, 1R1-1R2, 3R1-3R2, 4R1-4R2. Parameters obtained are listed in Table1. And experimental and calcurated breakthrough curves for 3R1-3R2 are indicated in Fig.4. These parameters are close to the results of other experiments in similar conditions[2]. This single fracture model is good to be adopted to this experimental results.

Effective diffusion coefficients are varied widely, and it will be explained by effects of flow in micro-fissures. Because, if there are no flow in matrix, these values will be smaller than molecular diffusion coefficient, 10^{-9} m^2/sec[3].

REFERENCES

(1)D.H.TANG, E.O.FRIND and E.A.SUDICKY, "CONTAMINANT TRANSPORT IN FRACTURED POROUS MEDIA: ANALITICAL SOLUTION FOR A SINGLE FRACTURE",Water Resources Research, Vol.17, No.3, 555-564,(1981)

(2)E.GUSTAFSSON and C.E.KLOCKARS, "STUDIES ON GROUNDWATER TRANSPORT IN FRACTURED CRYSTALLINE ROCK UNDER CONTROLLED CONDITIONS USING NONRADIOACTIVE TRACERS",KBS TECNISK RAPPORT 81-07,(1981)

(3)M.M.WADDEN and T.J.KATSUBE, "RADIONUCLIDE DIFFUSION RATES IN IGNEOUS CRYSTALLINE ROCKS" CHEMICAL GEOLOGY, 36,191-214,(1981)

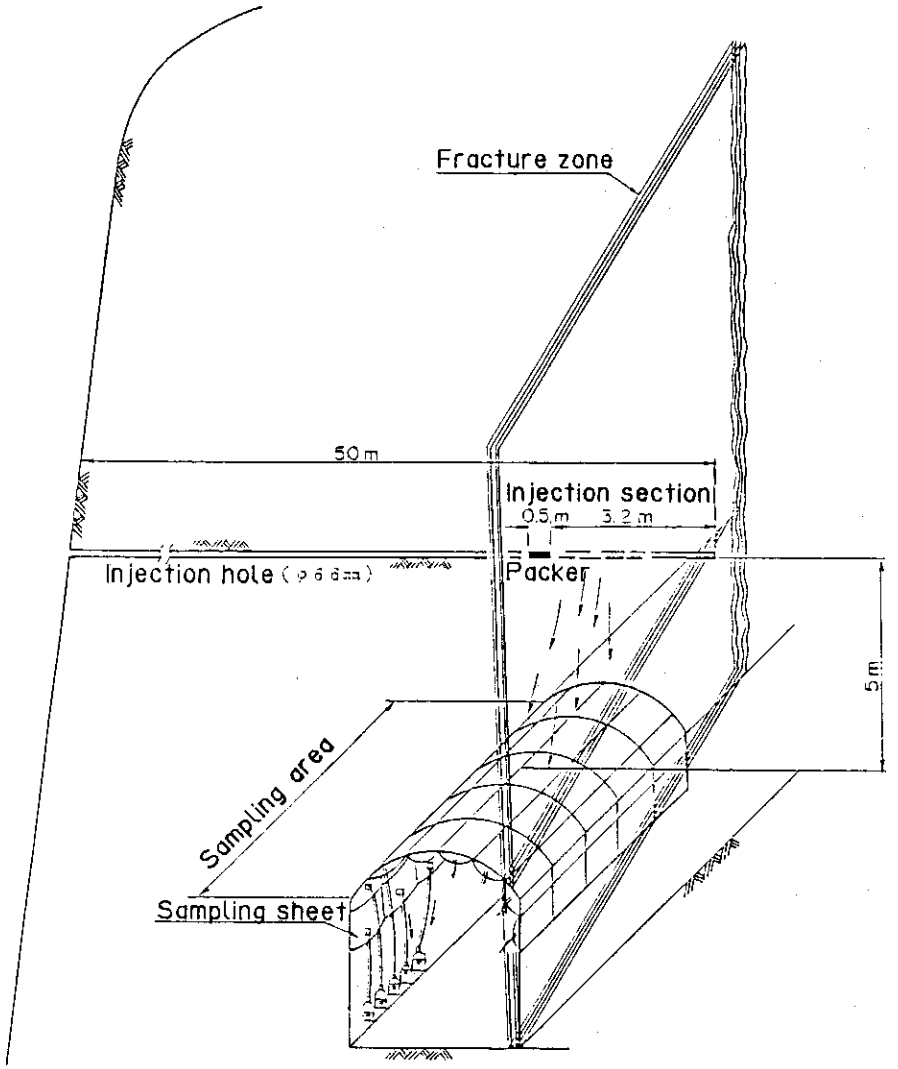

Fig.1 Conceptual layout of migration test

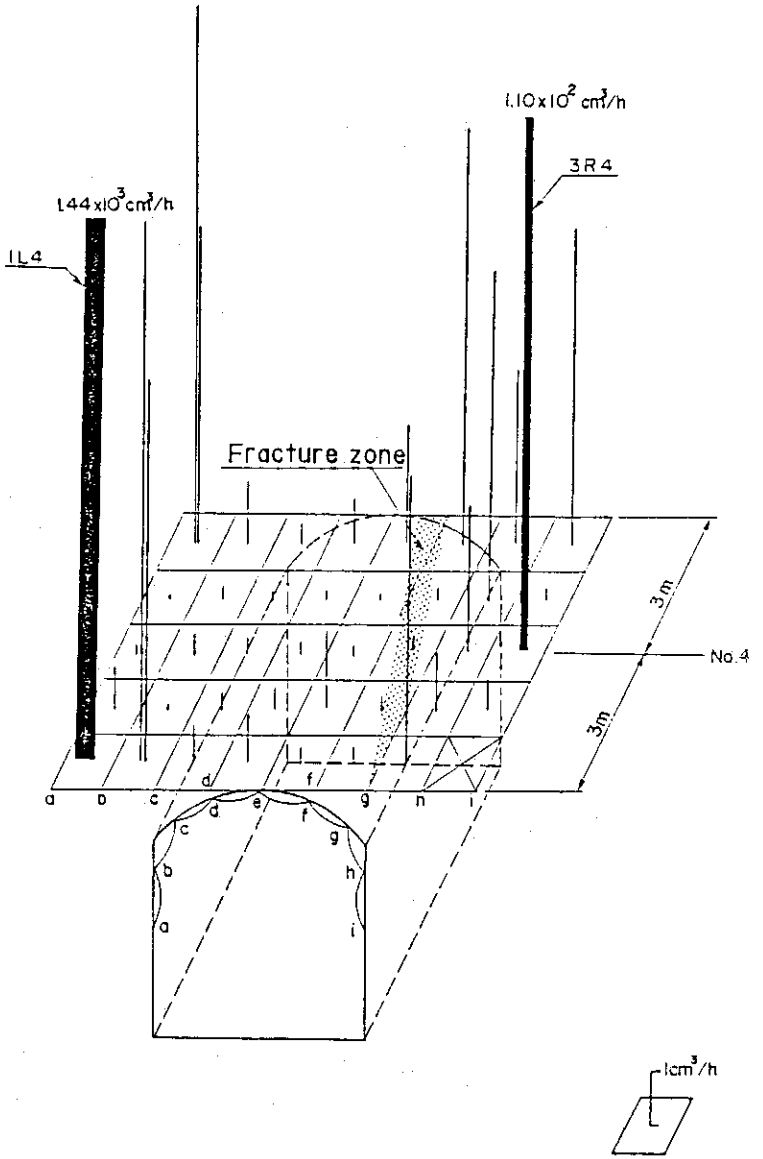

Fig.2 Distribution of discharged water emerging into the room

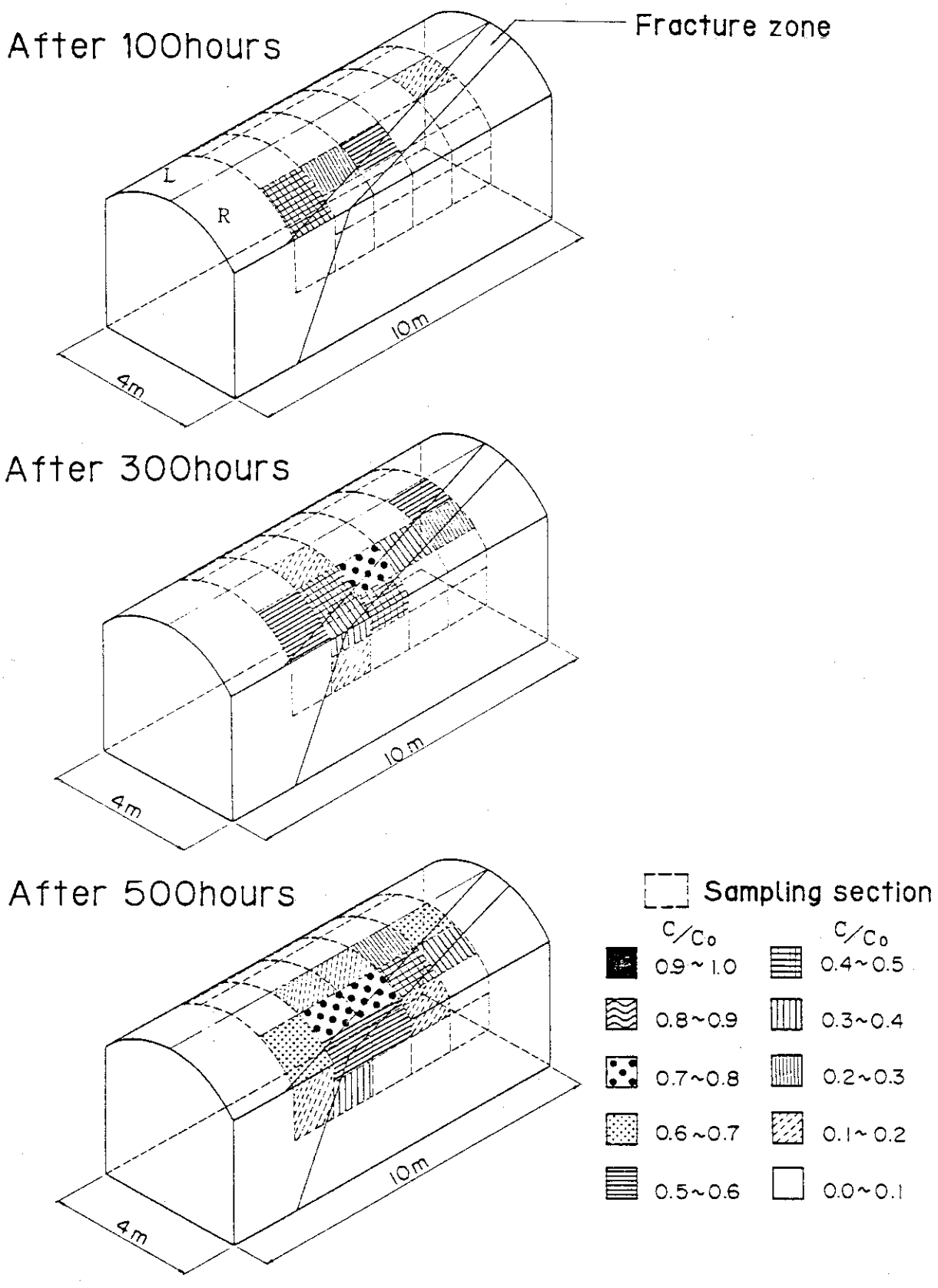

Fig.3 Distribution of C/Co after 100,300,500hours

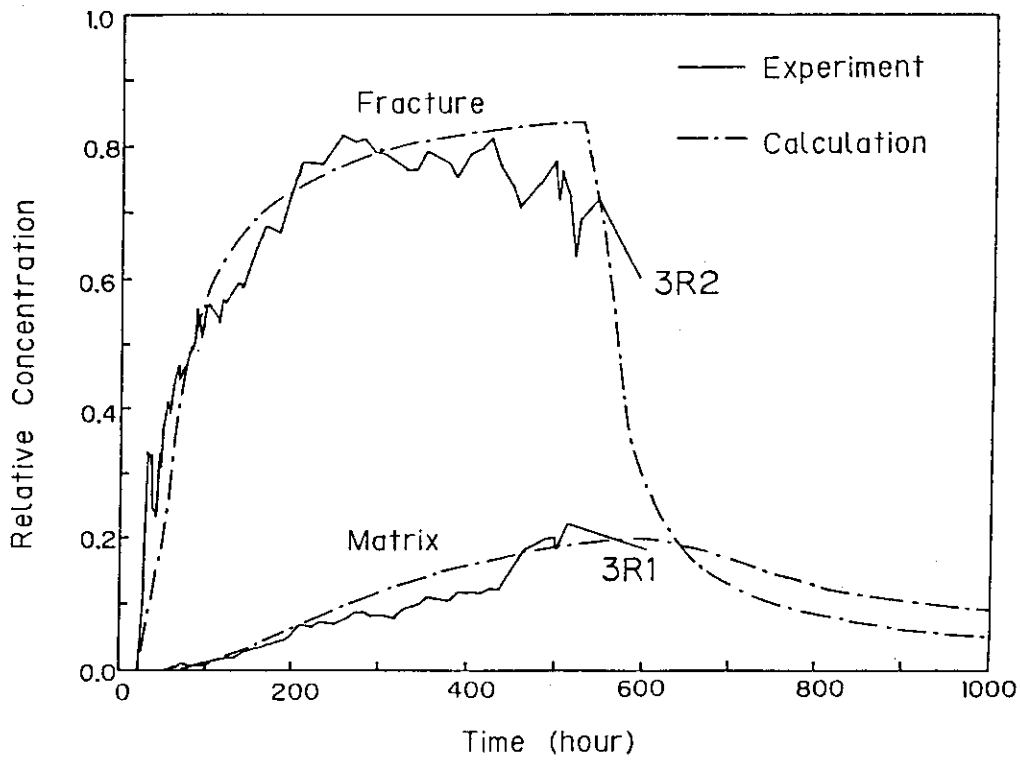

Fig. 4 Time dependent concentration profiles of Br

Table 1 Adopted parameters for the single fracture model

Parameters	Unit	1R1-1R2	3R1-3R2	4R1-4R2
Velocity in the fracture	m/h	0.10	0.12	0.10
Hydrodynamic dispersion coefficient of the fracture	m^2/h	0.05	0.06	0.05
Effective diffusion coefficient of the matrix	m^2/h	0.1 E-3	0.2 E-3	1.0 E-3
Fracture width	m	0.0010	0.0010	0.0007
Dispersivity in the direction of the fracture axis	m	0.5		

(3) In-situ Corrosion Test

S.Muraoka

Introduction

In the safety assessment of geological disposal of high level waste , performance of the canister material must be evaluated. This study is aimed at studying the corrosion resistance of candidate alloys of metallic container material in the real field. In this study stress corrosion cracking test is carried out for ten types of alloys. The experiment started from the end of 1984. The test will be performed over two years.

Experimental

The materials tested are Stainless Steels (Type 304, Type 304L,Type 304EL, Type 309S), Nickel base alloys (Inconel 600, Inconel 625, Incoloy 825, Hastelloy C), Ti and Ticode. In order to simulate the thermal history of the canister during high level waste vitrification and welding, sensitized heat treatment was carried out.

Chemical composition and heat treatment of the specimens are listed in Table 1. Stress was applied by bending two coupon specimens along their longitudinal direction into a double U-bend type. Two types of double U bend specimen with the dimensions shown in Fig.1 were tested. All the specimens are installed in the borehole drilled in the wall of granite rock. The hole is always filled with ground water naturally. The test has been

performed at 25 °C and at 75 °C. The occurrence of crack in the specimen has been observed and propagation rate has been estimated periodically by surface and section observation. The change of pH and Eh was also measured.

Results

Type 304L ss, Hastelloy C and Inconel 625 cracked at 75 °C within one year in in-situ test as well as laboratory test with deionized water. In the test at room temperature Type 304L ss and Inconel 625 showed the susceptibility to stress corrosion cracking. The other specimens did not crack in a year. The cracked specimens were only V-notched ones as shown in Table 2.

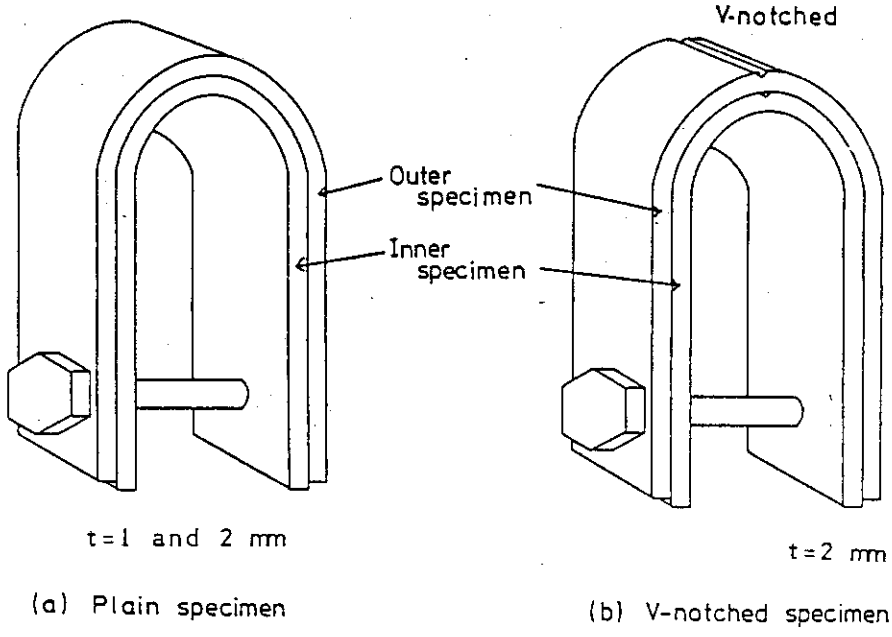

Fig.1 Schematic diagram of double U-bend type specimen

Table 1 Chemical composition and heat treatment

Alloy	Element (%)										Heat treatment
	C	Si	Mn	P	S	Ni	Cr	Fe	Mo	その他	
SUS 304 ss	0.075	0.52	0.95	0.010	0.024	9.2	18.22	bal.	—	—	700°Cx100min→A.C. →500°Cx24h→A.C.
SUS 304L ss	0.035	0.46	0.96	0.032	0.004	8.52	18.11	bal.	—	—	
SUS 304EL ss	0.015	0.59	1.50	0.034	0.003	10.20	18.16	bal.	—	—	
SUS 309S ss	0.14	0.56	1.53	0.023	<0.005	14.30	23.76	bal.	—	—	1050°Cx30min→W.C. →700°Cx100min→A.C. →500°Cx24h→A.C.
Incoloy 825	0.003	0.34	0.68	0.020	0.002	40.66	22.41	bal.	3.00	Cu;2.0 Ti;0.8 Ai;0.10 Al;0.16	1100°Cx30min→W.C. →700°Cx100min→A.C. →500°Cx24h→A.C.
Inconel 600	0.050	0.33	0.50	0.004	0.001	bal.	15.37	6～10	—	Cu;0.5max	
Inconel 625	0.05	0.25	0.25	0.007	0.008	61.0	21.5	3.89	9.00	Nb;3.65 Ti;0.2 Al;0.20	
Hastelloy C*	0.1	0.7	0.7	—	—	57	16	5	17	W;4	
Ticode 12*	0.012	—	—	—	—	0.84	—	0.09	0.34	Ti;98.9	700°Cx100min→A.C. →500°Cx24h→A.C.
Ti	0.045 Fe, 0.069 O, 0.0026 H, 0.0045 Ni, 99.88 Ti										

Note

A.C. : Air Cooling
W.C. : Water Cooling
* : Nominal value

Table 2 Result of stree corrosioncracking test

Alloy	Specimen	Test at 75°C	Test at 20°C
SUS 304	A - P *	0 / 3 **	0 / 3
SUS 304L	B - P	0 / 3	0 / 3
	B - N *	3 / 3	0 / 3
SUS 304EL	C - P	0 / 1	0 / 1
	C - N	0 / 3	0 / 2
Ticode	D - P	0 / 3	0 / 3
Incoloy 825	E - P	0 / 3	0 / 3
	E - N	0 / 3	0 / 3
Inconel 600	F - P	0 / 3	0 / 3
	F - N	0 / 3	0 / 3
SUS 309S	G - P	0 / 3	0 / 3
Hastelloy C	H - P	0 / 3	0 / 3
	H - N	3 / 3	3 / 3
Inconel 625	I - P	0 / 3	0 / 3
	I - N	3 / 3	3 / 3
Ti	T - P	0 / 3	0 / 3

P* : plain specimen

N* : V-notched specimen

** : number of cracked specimen/number of total specimen

2.3 Model for safety assessment

(1) Coupling model of heat and groundwater flow

K. Kimura

Introduction

The heat generated from a repository of high level waste can induce regional groundwater flows which last for thousands of years after burial. The coupling computer code of heat and groundwater flow 2D-SEEP was developed to quantify this problem. 2D-SEEP finite element code can handle 2-dimensional saturated-unsaturated steady and transient groundwater flow and also heat flow of conduction and convection. The flow arised from temperature field is assumed to be given by buoyancy effect from the Boussinesq approximation. The elements used in this code are the isoparametric and complex elements, and 2D-SEEP can treat the complicated geologic media.

HYDROCOIN level-1 study was performed using 2D-SEEP code, and good agreements with analytical solutions and initial attempt were obtained in case 1, 2 and 4.

Numerical model

The two dependent variables to be determined in 2D-SEEP code are the pressure head h_p and the temperature T. The two coupled partial equations being solved are

$$C \frac{\partial h_p}{\partial t} + \mathrm{div}\ \bar{u} = Q_f \qquad (1)$$

and

$$\frac{\partial}{\partial t}[(\rho c)_a T] + \mathrm{div}(\rho c)_f \vec{u} T = \mathrm{div}[K_T \cdot \nabla T] + Q_T \qquad (2)$$

where the Darcy velocity is given by

$$\vec{u} = -k(\nabla h_p + \frac{\rho_f}{\rho_o} \nabla h_e) \qquad (3)$$

C ; specific moisture capacity

Q_f ; nodal flux of fluid

$(\rho c)_a$; average heat capacity of the rock and fluid

ρ_f ; fluid density $\rho_f = \rho_0(1-\beta T)$

c_f ; fluid specific heat

K_T ; thermal conductivity of rock

Q_T ; heat source strength

k ; hydraulic conductivity

h_e ; elevation head

These equations are discretized in space using the Galerkin and Bubnov-Galerkin method, and discretized in time by Crank-Nicholson method. The non-linear equations are solved by a kind of successive subsititution method.

Calculated results

We calculated the three cases (case 1, 2 and 4) of HYDROCOIN level-1 study to verify 2D-SEEP code, and got good agreements with

the examples of initial attempt. Calculated results of case 4 are shown as the representatives of this study. The finite element grid we used is shown in Fig. 1. The profiles of time dependent pressure rise at z=125m and 250m are shown in Fig. 2, and the distribution of pressure rise at fixed time t=50, 100, 500 and 1000 years are shown in Fig. 3.

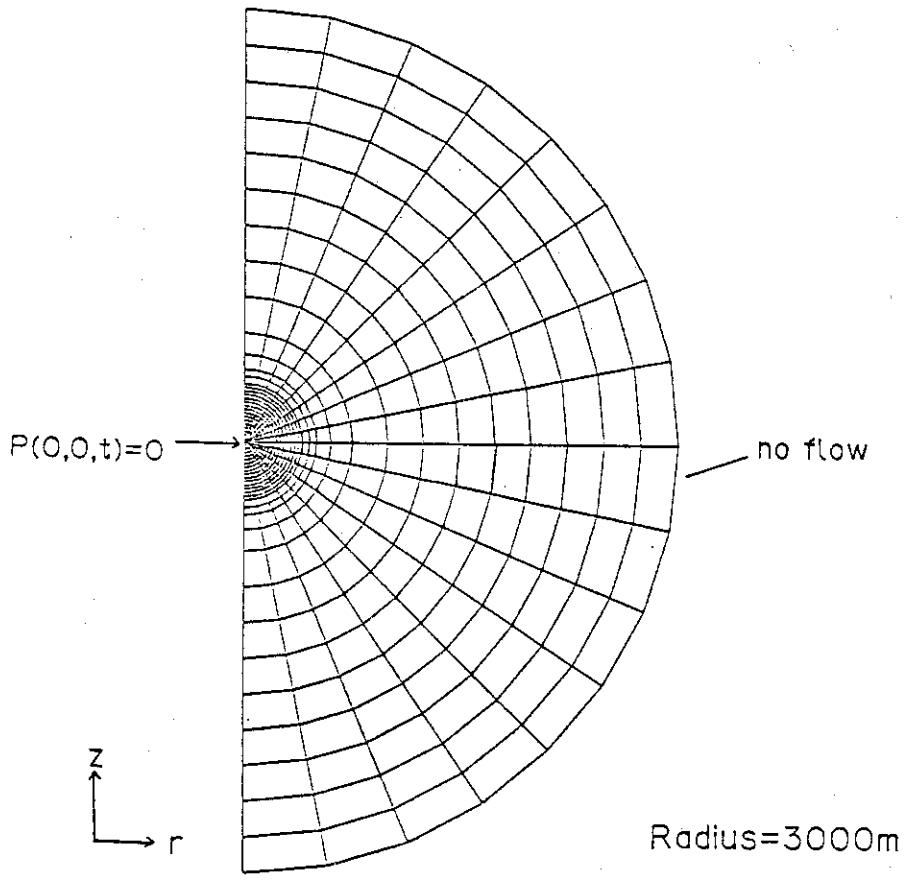

Fig. 1 The finite element grid of CASE-4

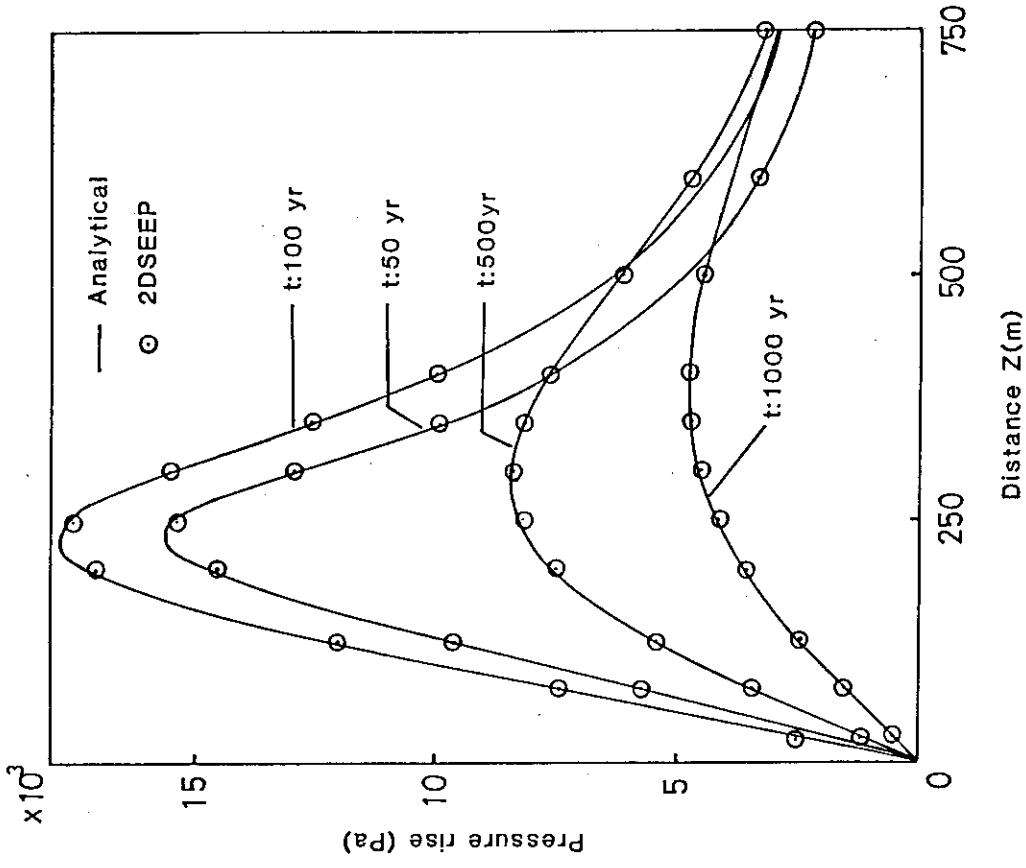

Fig. 3 The distributions of pressure rise at fixed time t=50, 100, 500 and 1000 year

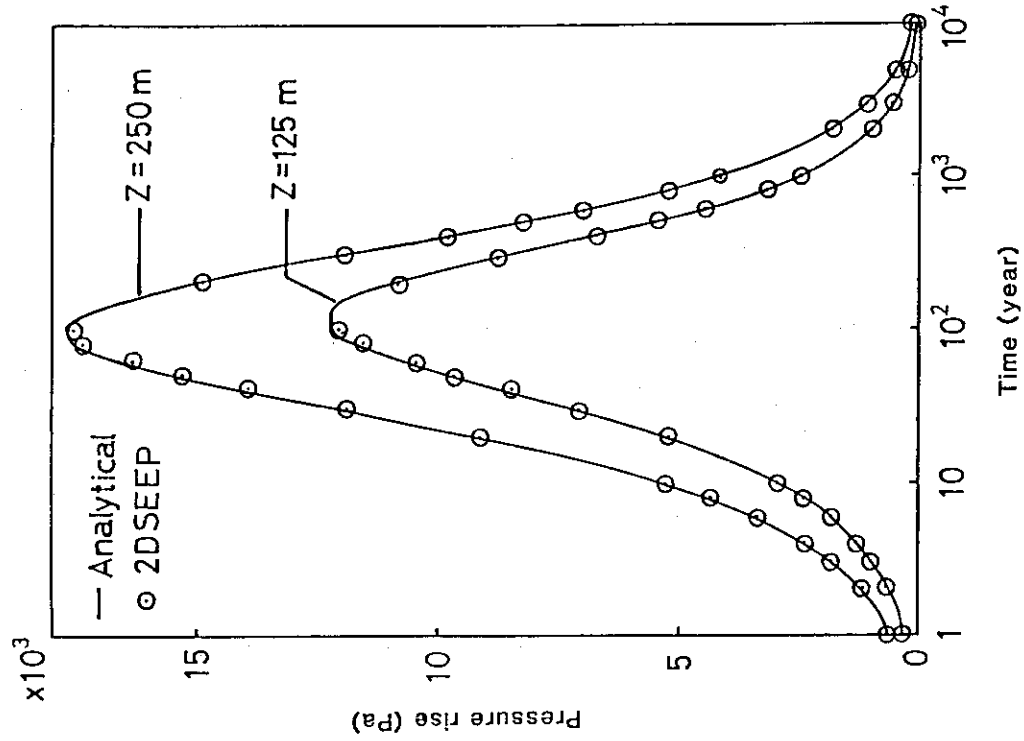

Fig. 2 The profiles of time dependent pressure rise at z=125 m and z=250 m

2.4 NATURAL ANALOGUE

S. NAKASHIMA

Application of natural phenomena to the safety evaluation of waste disposal has been paid much attention recently in Japan. Among many research programs involved in this "natural analogue", our main interest is the following:

1)Study of microphases in minerals and rocks, which are supposed to play an important role in radionuclide migration and fixation. The characterization of microinclusions in minerals, crystal defects, metamict minerals, crystal boundaries etc. by means of microanalytical devices.

2)Developpement of ultrasensitive trace element analytical techniques for some important radionuclides such as ^{129}I, ^{99}Tc, ^{237}Np and ^{239}Pu.

3)Role of colloids and amorphous phases in radionuclide transport and fixation.

4)Fixation and transport of radionuclides by natural organic matter such as coaly substances and porphyrins.

(1) Study of Red Altered Feldspars.

- Application of Microphase Determination Technique in Rocks. -

S. NAKASHIMA

Occurence of red feldspars are common in alteration zones of feldspar-bearing rocks, especially granitic rocks. The origin of red color of these altered feldspars has been considered to be the presence of iron, but its chemical form in feldspars has not yet been well established. Iron can be present in the crystal structure, as iron-bearing microcrystals such as hematite (ISSHIKI,1958) or as iron staining on the grain boundaries and cleavage plains (DEER et al,1966).

Scanning elecron microscopy combined with energy dispersive X-ray analyzer (SEM-EDX) was applied to characterize the microphases in a red feldspar from altered granite. Red feldspars are observed only in alteration zones along fractures. Among alkali feldspars of this altered zone , white feldspars are also recognized together with red feldspars. SEM-EDX analyses of these alkali feldspars indicate that potassium rich feldspars do not show red color. Inside the red feldspars studied here, no iron-bearing minerals are identified. The red alkali feldspar has a heterogeneity in its chemical compositions: K-rich part and Na-rich part. The Na-rich parts seem to correspond to the red parts. This heterogeneity can also be observed in the ten-micron order. Further magnifications of the view reveal the presence of Ca-rich part in the order of several microns inside the Na-rich

parts. Iron is finally found in a part of these Ca-rich parts.

We do not know if iron is present as ferrous or ferric iron cations in the crystal structure or as aggregates of microcrystals, but it is quite interresting that iron is present only in Ca-rich parts inside Na-rich phases of alkali feldspars. HOFMEISTER and ROSSMAN (1984) rerported the substitution of Fe^{2+} for Ca (not Na) in plagioclase. The iron present in Anorthite molecule of alkali feldspars in our study can be then supposed to be ferrous iron. Optical and resonance spectra of the minerals can provide further informations on the valence states and the coordinations of iron in red feldspars.

A tentative explanation of the red color in altered feldspars studied here is the presence of iron cations which replace calcium in Anorthite molecule of alkali feldspars. These irons can be supplied by groundwaters during alteration which possibly causes also the replacement of potassium by sodium.

These results suggest the applications of microphase characterization techniques to the study of trace element migration and fixation in minerals and rocks, especially around uranium ore bodies, as a natural analogue to the radioactive waste disposal.

DEER W.A.,HOWIE R.A. and ZUSSMAN J.(1966) An introduction to the rock forming minerals. Longman,London.

HOFMEISTER A.M. and ROSSMAN G.R.(1984) Determination of Fe^{3+} and Fe^{2+} concentrations in feldspar by optical absorption and EPR spectroscopy. Phys.Chem.Minerals,11,213-224.

ISSHIKI N.(1958) Notes on rock-forming minerals (3) Red coloration of anorthite from Hachijo-jima. J.Geol.Soc.Japan,64,644-647.

2.5 Subseabed Disposal

K. SHIMOOKA

Based on the Japanese policy for research and development of high-level radioactive waste (HLW) management, the JAERI has initiated studies on the feasibility of subseabed disporsal of HLW. We are now conducting the fundamental studies in this field participating in the international co-operative programs supported by the OECD/NEA.

· Main part of the activities of the last year was the participation in the ESOPE (in French: Etude des Sediments Oceaniques par Penetration = Study of oceanic sediments by penetration) cruise. Experiments in Japan at laboratories are underway on the long core samples of 30 m taken out from the Great Meteor East section of the Madeira Abysasal Plain (GME) and the Southern Nares Abussal Plain (NAP) sites during the cruise to perform following measurements.

1) Diffusion of Tc in the sediments. (HLW Management Laboratory in JAERI)
2) Measurement of the sediment characteristics, particle size, element composition and distribution coefficient for Tc, Np, Am and Pu. (Environmental Research Laboratory II in JAERI)
3) Measurement of U/Th decay series and amino acid (Tokyo University)
4) Remnant magnetization (Kobe University)

(1) Diffusion of Technetium in Deep-sea Sediments and Bentonite.

S. NAKASHIMA

INTRODUCTION

An estimate of radionuclide migration rate in deep-sea sediments is an important aim of the safety evaluation of the seabed disposal of high level wastes. Diffusion of radionuclides in pore water is believed to be a major process of transport in deep-sea sediments. Technetium is considered to be one of the most mobile hazardous long-lived radioisotopes originated from nuclear wastes and migrate as pertechnetate anion (TcO_4^-) in water under oxic conditions, while it is believed to be precipitated as oxides of lower oxidation states such as TcO_2 under anoxic conditions (ALLARD et al.,1979).

Several series of measurements of diffusion coefficients of pertechnetate anion were made on selected samples of the deep-sea sediments taken during OECD/NEA's ESOPE expedition, together with a Na-bentonite sample.

EXPERIMENTAL

Some properties of materials used are listed in Table 1. The diffusion experiments were carried out in the presence of air at room temperature, according mainly to the description given by SCHREINER et al.(1982): the diffusing source was set up by putting a filter paper wet with 100 μl of the source solution ($^{95m}TcO_4^-$, 1μCi/100μl, pH=5) onto one end of the cylindrical sediments. After 17 to 124 hours, the

sediments were cut into 3 mm disks and γ-ray activity was measured on each disk.

The diffusion coefficeints were determined by using two different solutions (exponential and error functions) of Fick's second law. The values calculated by two different ways are in good agreement and both methods can be considered to be valid in our experimental conditions (Table 1). The easier method (exponential solution) can be then taken to determine apparent diffusion coefficients D_{app} (Table 1).

RESULTS AND DISCUSSION

Linear correlations between D_{app} values and several physical parameters of these sediments (water weight fraction W, water volume fraction V and porosity n) have been noticed on a logarithmic scale (Fig.1). The D_{app} values at zero points estimated by these lines are near from the diffusion coefficients of ions in water (D_o; 1-2 x10^{-9} m^2/s). The slopes of these lines are smaller in deep-sea sediemnts than in Na-bentonite. This fact suggests that the diffusion coefficeints in deep-sea sediments are larger than those in Bentonite for the same water contents and porosity.

The grain size distributions of the samples determined by a Coulter Counter TA-II show that the deep-sea sediments are richer in comparatively large grains than Bentonite. The diffusion of ions in comparatively fine-grained sediments (Bentonite, in this study) should be hindered more by larger numbers of fine particles, in the same length of the diffusion path, than in coarse-grained sediments (deep-sea sediments, in this study). The tortuosity of fine-grained

sediemnts appears to be larger and so that the apparent diffusion coefficient becomes smaller. This fact can explain at least a part of the difference in D_{app} values of the two sediments for the same water content or porosity.

The empirical correlations determined in this study for two different sediments (Fig.1) are quite useful to estimate diffusion coefficeints of non-sorbing radionuclides in sediments, knowing some of their physical properties such as water contents, porosity, grain size distribution and tortuosity.

The D_{app} value determined on a deep-sea sediment sample containing black parts (G-5) appears to be nearly one order lower than is expected by its water content (Table 1 and Fig.1). Technetium appears to be fixed by the black spots in this sample (Fig.2). The characterization of these black parts is then necessary in order to explain the technetium retardation process in this sample.

REFERENCES

ALLARD B.,KIGATSI H. and TORSTENFELT B.(1979) Technetium reduction and sorption in granitic bedrock. Radiochem.Radioanal.Letters,37,223-230.

SCHREINER F.,FRIED S. and FRIEDMAN A.M.(1982) Measurement of radionuclide diffusion in ocean floor sediment and clay. Nucl.Technol.,59,429-438.

Table 1. Diffusion data of TcO_4^- in sediments.

No.	*Water content W	V	Porosity n	**Diffusion coefficients D_{exp} (x 10^{-10} m^2/s)	D_{erfc}	D_{app}	***Tortuosity τ	Diffusion time (hours)
Bentonite								
NK-4	0.296	0.567	0.438	0.80	0.73	0.80	4.0	120
NK-5	0.407	0.681	0.587	1.5	1.5	1.5	2.8	124
NK-8	0.433	0.694	0.621	2.0	2.2	2.0	2.4	49
NK-6	0.492	0.748	0.678	2.5	2.4	2.5	2.2	124
NK-9	0.553	0.802	0.730	2.7	2.9	2.7	2.1	24
Deep-sea sediments								
G-1	0.582	0.855	0.773	7.4	6.9	7.4	1.3	17
G-2	0.620	0.868	0.804	8.1	7.8	8.1	1.2	17
G-3	0.587	0.867	0.775	8.3	7.7	8.3	1.2	18
G-4	0.472	0.775	0.680	7.0	6.7	7.0	1.3	17
G-5	0.622	0.968	0.787	1.2	1.3	1.2	3.0	18
G-6	0.535	0.820	0.737	7.8	7.3	7.8	1.3	18
G-7	0.545	0.845	0.740	7.8	7.7	7.8	1.2	20
G-8	0.471	0.732	0.697	5.9	5.3	5.9	1.4	18

* W:water weight fraction, V:water volume fraction, n:porosity,

**D_{exp}, D_{erfc}:diffusion coefficients determined by exponential and error function solutions, D_{app}: apparent diffusion coefficients (=D_{exp}).

**The tortuosity values are determined by the equation $D_{app}=D_o/\tau^2$.
The diffusion coefficient in water D_o is assumed to be $1.2\times10^{-9}m^2/s$.

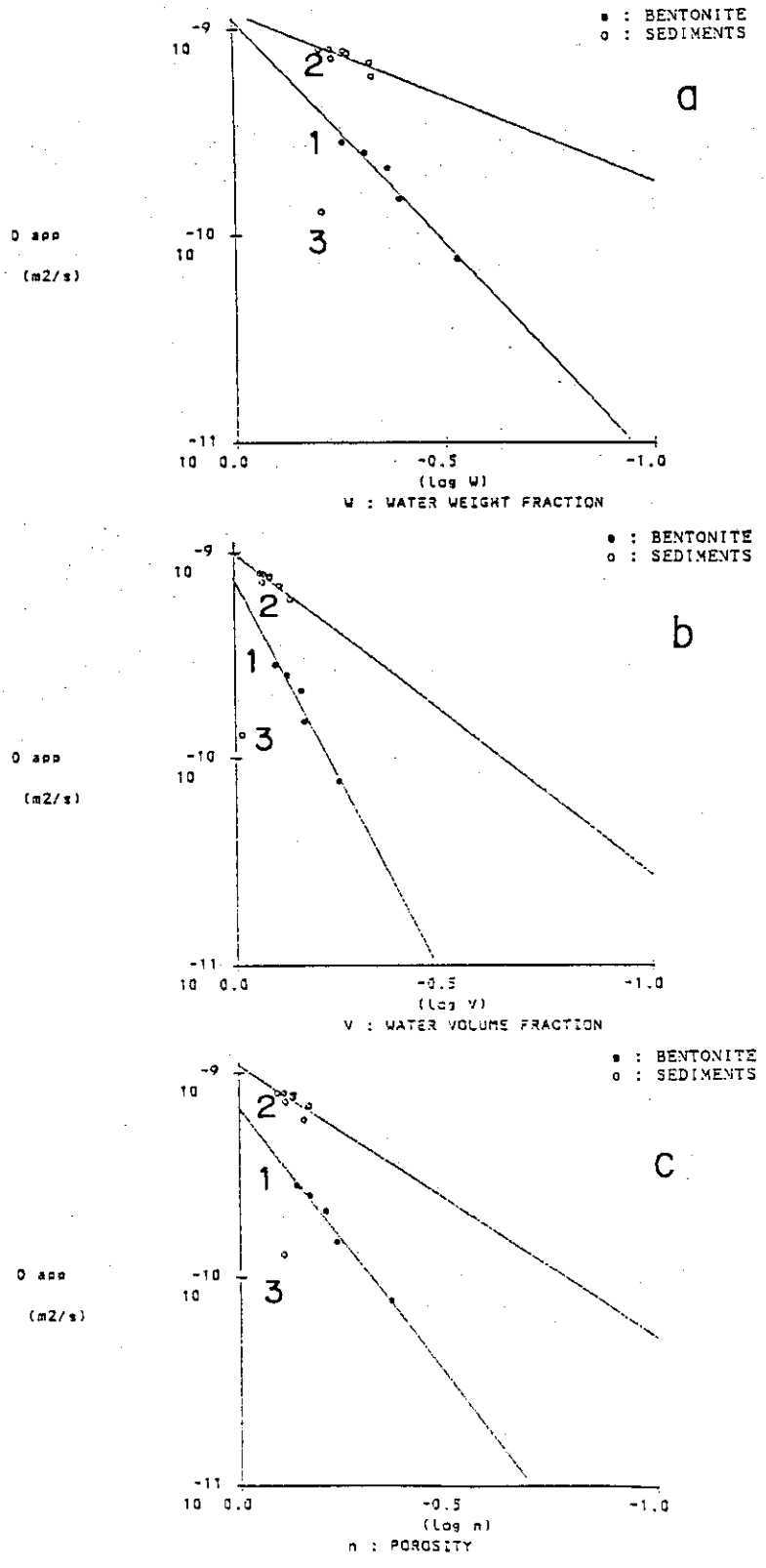

Fig.1. Correlations between the apparent diffusion coefficients D_{app} and the physical properties of sediments (W:water weight fraction, V:water volume fraction and n:porosity). o:Data on Bentonite samples fitted by line 1, o:Data on deep-sea sediments fitted by line 2, points 3:Data on G-5 sample containing black parts.

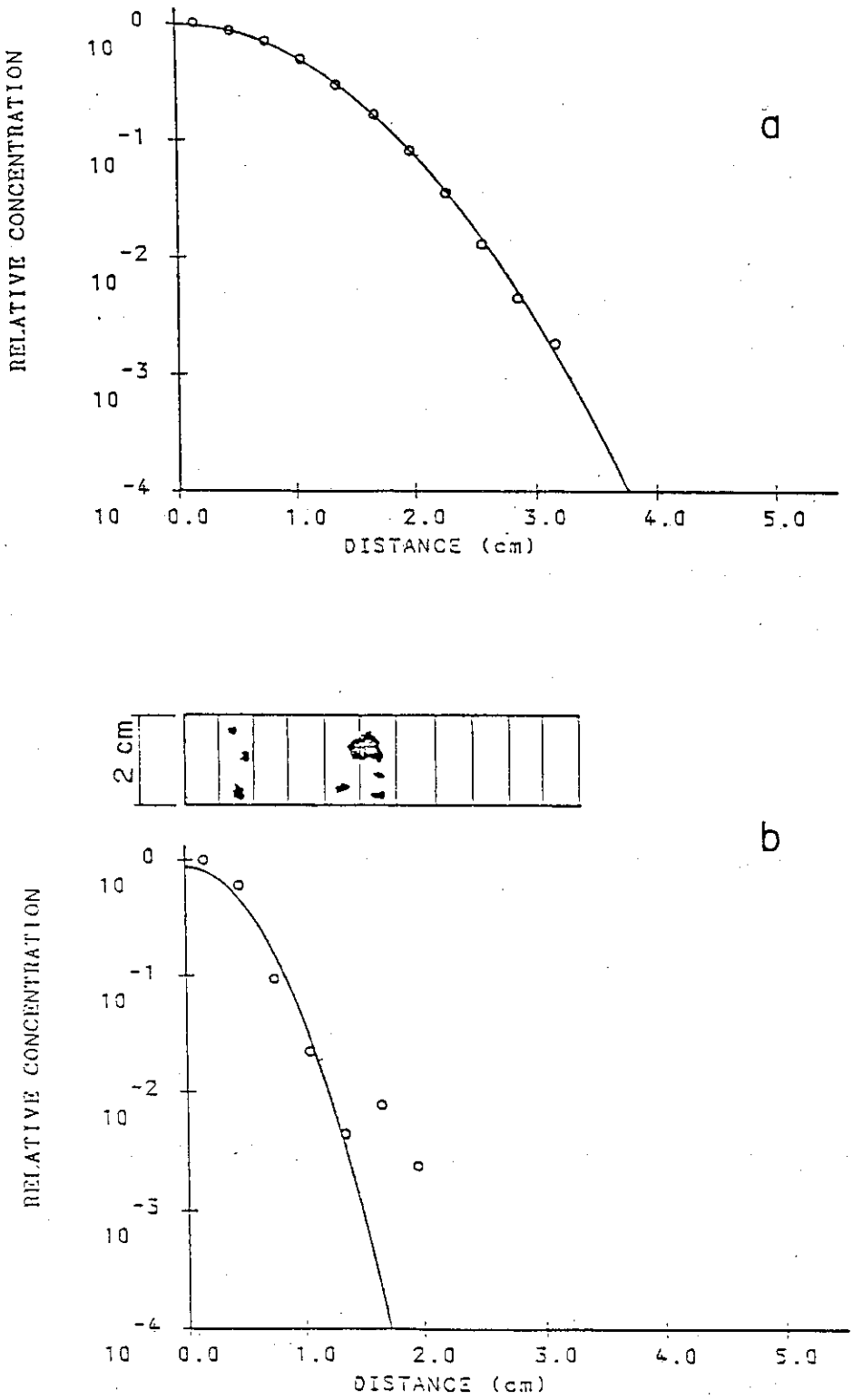

Fig.2 Diffusion profiles of pertechnetate anion in the deep-sea sediments. a)the G-3 sample, b)the G-5 sample with a schematic figure of the sample containing the black spots. Retardation of pertechnetate is observed on the G-5 sample.

(2) Pertechnetate retardation in deep sea sediment

H.KITA

INTRODUCTION

Pertechnetate diffusion experiments were conducted on some deep-sea sediment samples and a significant retardation of its diffusion in a sample(G-5) containing some black spots was recognized (2.5.(1)). Reduction is considered to be a main retardation mechanisum of this non-sorbing element. Ferrous iron containing minerals and organic matter are the possible reducing agents in rocks and sediments (ALLARD et al.,1979). The black materials found in the deep-sea sediments are expected to contain some such reducing agents. In order to characterize the possible pertechnetate reducing capacity in the black materials, several analyses were conducted on them together with host deep-sea sediments.

EXPERIMENTAL

8 samples were selected from the core 10 of GME site. The description of the deep-sea sediment samples and measured diffusion coefficients of pertechnetate anion in these samples (NAKASHIMA et al.,1986) are listed in Table 1.

These samples were analysed by X-Ray Diffractometry (XRD) and Differencial Thermal Analysis (DTA). Visible absorption spectra of

acetone extracts from the deep-sea sediment samples were recorded. The black part in G-5 sample after the dissolution of carbonates was also analyzed by XRD and DTA.

RESULTS AND DISCUSSION

The mineral compositions of the deep-sea sediments were analyzed by XRD (Table 1). They are mainly composed of calcite ($CaCO_3$), and its weight per cent in dry sediments is around 55 (courtesy of Dr.R.CRANSTON). Other minor minerals are quartz and feldspars.

The DTA data on these sediments show that only the G-5 and G-8 samples have significant exothermic peaks around 300 C (Fig.1). These peaks can be attributed to organic phases including algae and bacteria (MITCHEL and BIRNIE,1970).

The visible absorption spectra of acetone extracts of the sediments (Fig.2) indicate a presence of pigments having porphyrin structures (ORR and GRAY,1957;HODGSON and BAKER,1967;ISHIWATARI,1969) only for the G-5 and G-8 samples, which are green sediments.

The black parts of the G-5 sample after dissolution of carbonates contain pyrite, quartz with minor feldspars, mica and clay (Table 1). The DTA data confirms that pyrite is a main constituent in these black parts (Fig.1).

In these black parts, pyrite is supposed to be accumulated locally by complex processes including reduction. The black spots containing pyrite were previously found to retard pertechnetate diffusion (see 2.5.(1)). In order to verify possible reducing agents

for pertechnetate, pyrite and biotite were put in pertechnetate solution. Pyrite is a main constituent of the black parts and biotite is an example of ferrous iron containing minerals. These mineral phases are found to have no fixation capacity of pertechnetate at least within the same experimental duration as the diffusion experiments (several days).

Since no mineral phases have significant influence on technetium fixation, the active reducing capacity can be attributed to some types of organic matter including certain bacteria and hydroxyl groups bearing geopolymers. The further characterizations of the organic phases will be then necessary in order to elucidate effective radionuclide immobilizing organics and their reducing capacity in deep-sea environments.

REFERENCES

ALLARD B., KIGATSI H. and TORSTENFELT B. (1979) Technetium reduction and sorption in granitic bedrock. Radiochem. Radional. Letters, 37, 223-230.

CRANSTON R. (1986) Personal communication.

HODGSON G.W. and BAKER B.L. (1967) Spectra of selected geochemically significant porphyrins and chlorins. Chem. Geol., 2, 187-198.

ISHIWATARI R. (1969) Fluorescence-microscopic observations of the natural state of chlorophyll pigments in recent sediments. Earth Science (Chikyu Kagaku), 23, 194-198.

MITCHELL B.D. and BIRNIE A.C. (1970) Biological materials. in

Differencial Thermal Analysis Vol.1 (ed. R.C.MACKENZIE), Academic Press, London. p.673-704.

NAKASHIMA S., KITA H., SHIMOOKA K. and NAKAMURA H. (1986) Diffusion of technetium in deep-sea sediments and bentonite (in prep.)

ORR W.L. and GRAY J.R. (1957) Determination of chlorophyll derivatives in marine sediments. Deep-Sea Res., 4, 263-271.

Table 1. Description of deep-sea sediemnts from Core 10, GME site, (Great Meteor East), ESOPE expedition, Madeira Abyssal Plain, North Atlantic Ocean (31 16.70N, 25 23.33W, depth about 5400 m).

No.	Depth (cm)	Color	Minerals*	Quartz* (wt %)	TcO_4^- D_{app}** ($\times 10^{-10} m^2/s$)
G-1	0- 5	cream	Cal,Qz	1.7	7.4
G-2	160- 165	cream	Cal,Qz	1.6	8.1
G-3	300- 305	cream	Cal,Qz,Fd	1.9	8.3
G-4	692- 697	cream	Cal,Qz	3.6	7.0
G-5	1394-1399	grayish green+black	Cal,Qz	3.1	1.2
G-6	1595-1599	cream	Cal,Qz,Fd	1.6	7.8
G-7	2398-2402	cream	Cal,Qz,Fd	1.5	7.8
G-8	3344-3351	greenish gray	Cal,Qz,Fd	5.9	5.9
G-5 black parts			Cal,Qz		
G-5 black parts after dissolution of carbonates			Qz,Fd,Py,M,K		

* Data analyzed by X-ray diffractometry. Cal:calcite,Qz:quartz,Fd:feldspar,Py: pyrite,M:mica,K:kaolinite.

** Data determined by diffusion measurements (NAKASHIMA et al.,1986)

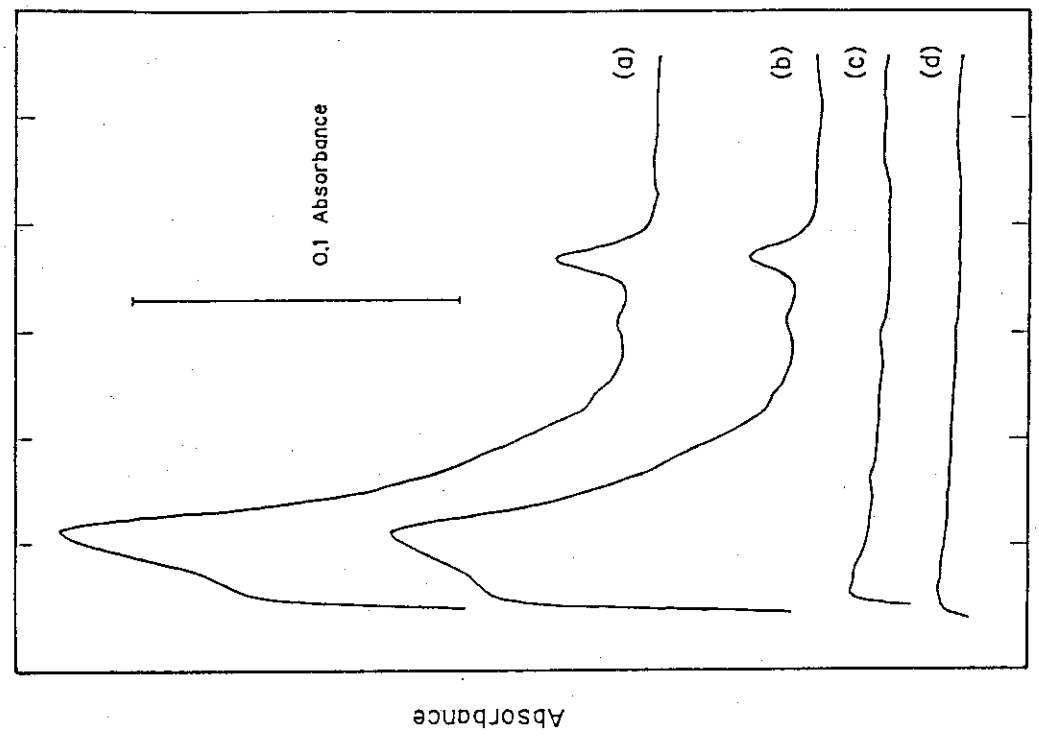

Fig.2 Visible absorption spectra of acetone extracts from the deep-sea sediments. a)the G-5 sample, b)the G-3 sample, c)the G-6 sample representing the calcareous sediments, d)acetone.

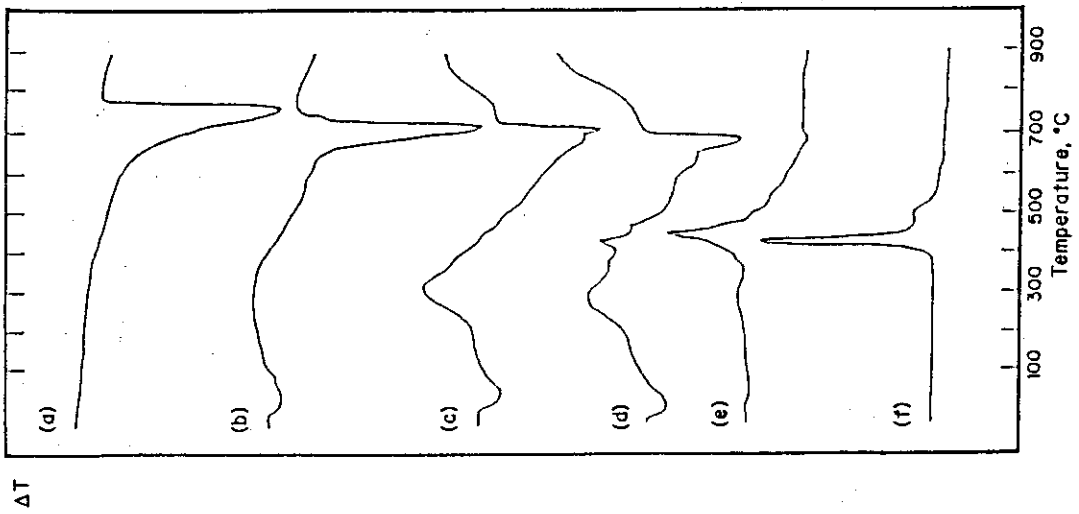

Fig.1 DTA curves for the deep-sea sediments. a)$CaCO_3$ pure chemical, b)the G-6 sample representing the calcareous sediments, c)the G-3 sample, d)the G-5 sample, e)the black part of the G-5 sample, f)a pyrite sample.The temperature increase rate is 10°C/min.

3. Safety examination of vitrified forms in the hot cells of WASTEF

S.TASHIRO

The Waste Safety Testing Facility (WASTEF) has continued safety tests on performance and durability of materials for the long-term isolation of high level radioactive wastes since it started the hot operation in November 1982.

In this fiscal year, tests on leachability of plutonium by a MCC-1-like method, migration rate of transuranium elements in rocks immersed with a vitrified form, volatilizing behaviour of the waste conponents in connection with safety assessment in the handling and storage time and leaching methods in co-operation with the Power Reactor and Nuclear Fuel Development Corporation have been continued at WASTEF. Tests on adhesive property of leached radioactive substances in ground water on granite rock granule in a column and alpha radiation stability of vitrified forms under beta and gamma irradiation have newly started.

The following briefly describes main results obtained in the year other than the above subjects.

3.1 Radioactivity balance in the Vitrification apparatus after operations

T.TSUBOI and S.KIKKAWA

Radioactivity balances in the vitrification apparatus installed in WASTEF were measured after operations using Cs-134 and Ru-106, in order to know residual radioactivity in the apparatus and removal ability of the off-gas treatment system.

Vitrification was performed with the apparatus of which flow-sheet is shown in Fig.1. Heating for the vitrification was carried out at a temperature of 1200 ℃ and in a period of two hours as shown in Fig.2. Added radioactivity was 853 mCi for Cs-134 and 112 mCi for Ru-106 respectively, and one liter glass product was obtained for each. After each operation, radioactivity of the product, upper part and the lower part of melting pot,and each components of the off-gas line was measured. Radioactivity of the products was measured by gamma scanning apparatus and calculated by measurment of sampled glass specimen. Radioactivity in the apparatus was measured at several points around the apparatus by a gamma survey meter with ionization chamber and calculated specific residual radioactivity in the components by WADOSE*.

The results are shown in Table 1 and 2. In the case of cesium 68% of the added radioactivity incorporated in the glass product, the 30% was left in the melting pot and the 1.6% went away to the off-gas line. It could be estimated that the 25% of the amount left in the pot was adhered to the upper part after volatilization and the 5% was left in the pot as glass residue. This means that the upper part of the melter acted as a cold trap and then removed most of volatilized cesium was trapped at the colder upper part of the melting pot.

---

* WADOSE is a evaluation code which has been developed to calculate the intensity of radioactive sources recided in each vessel or line of the vitrification apparatus.(cf. J.Morita et al.;JAERI-M 86-001)

In the case of ruthenium the 59% of the added radioactivity was in the glass product and the 5.1% went off to the off-gas line. The most effective component in the off-gas line was spray scrubber for cesium (DF=53), and Ru-Absorber for ruthenium (DF=10). In the both cases no significant radioactivity could be detected in gas streams after the off-gas line.

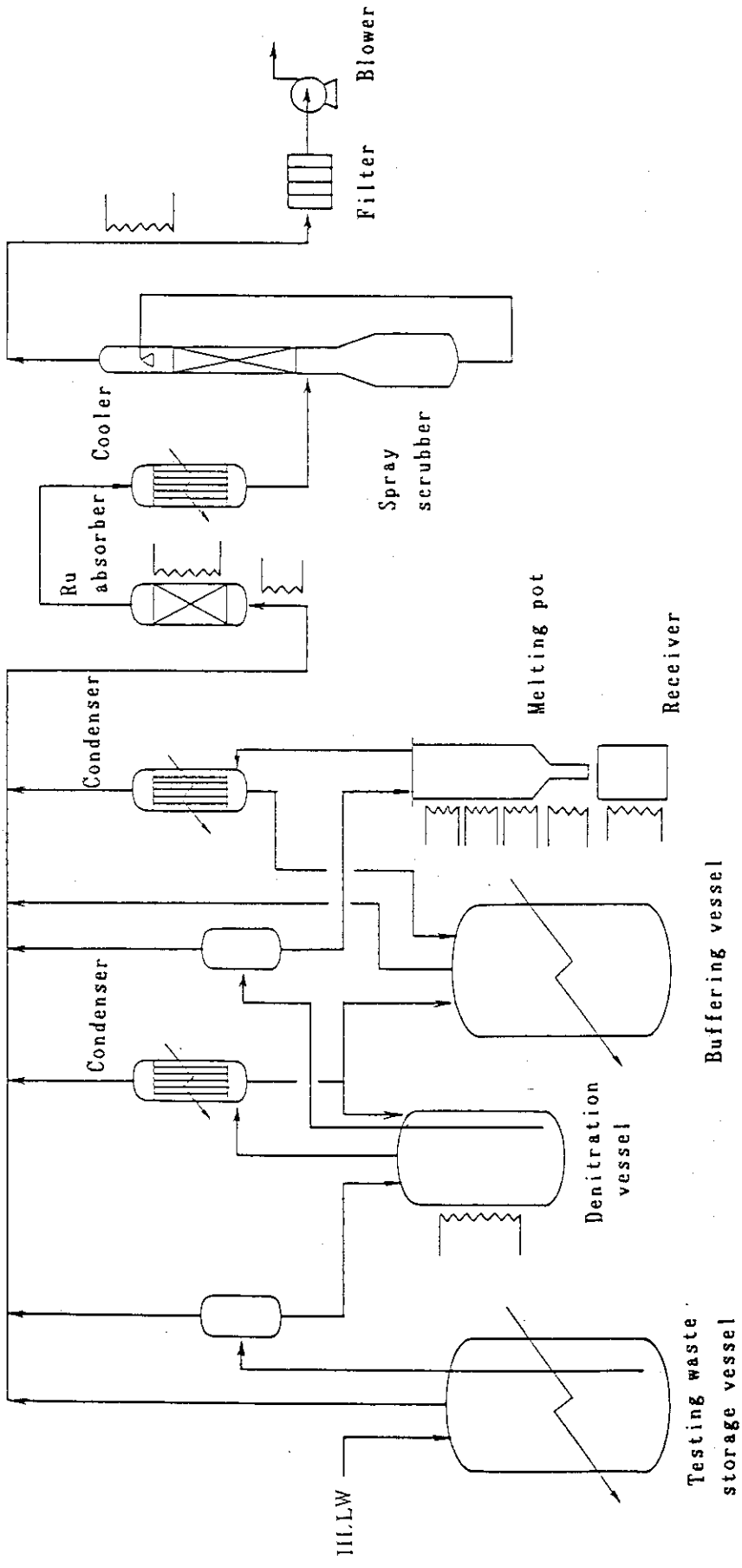

Fig. 1 Process Flow of the Vitrification Apparatus

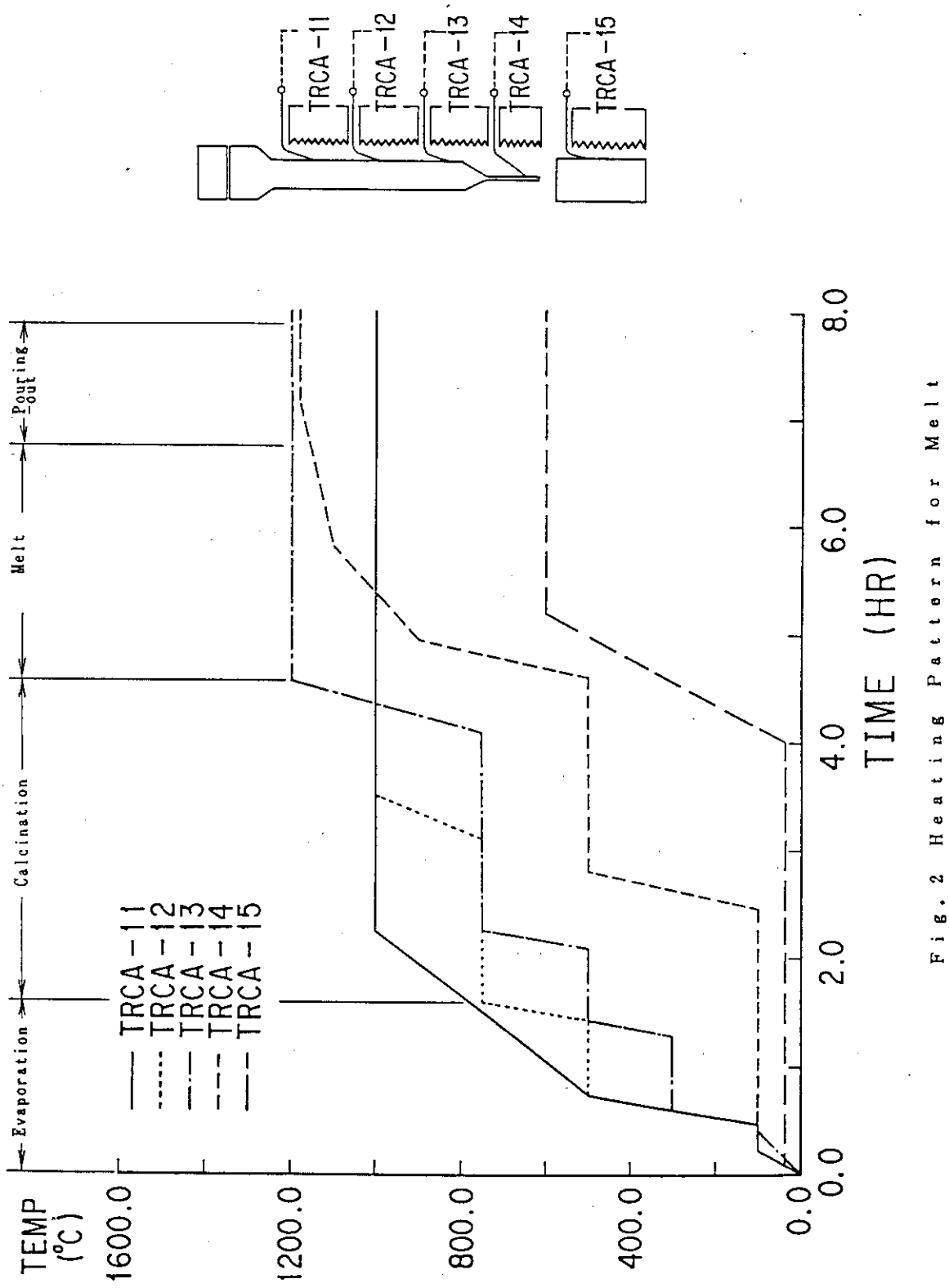

Fig. 2 Heating Pattern for Melt

Table 1 Radioactivity balance of ^{134}Cs and ^{106}Ru

		^{134}Cs		^{106}Ru	
		Activity (mCi)	Ratio to the added (%)	Activity (mCi)	Ratio to the added (%)
Glass products		580.0	68.0	66.2	59.1
Melting pot	Upper	213.8	25.1	21.5	19.2
	Lower	45.3	5.3	18.5	16.6
Off-gas line		14.3	1.6	5.8	5.1
Total		853.3	100	112.0	100

Table 2 Details in the off-gas line

	^{134}Cs			^{106}Ru		
	Activity (mCi)	Ratio in the off-gas line (%)	DF*1	Activity (mCi)	Ratio to the off-gas line (%)	DF*1
Pipe line *2	2.9	20.3	—	1.2	20.7	—
Condenser	0.9	6.3	1	0.8	13.8	1
Ru absorber	—	—	—	3.4	58.6	10
Cooler	neg.	—	—	neg.	—	—
Spray scrubber	10.3	72.0	53	0.3	5.2	4
Filter	0.2	1.4	∞	0.1	1.7	∞
Total	14.3	100		5.8	100	

*1 Decontamination factor *2 The line between the pot and the condenser

3.2 Alpha autoradiography of vitrified forms

T.SAGAWA and S.TASHIRO

A technique for alpha autoradiography of vitrified forms has been developed to know locations of alpha-decay nuclides in vitrified forms and those on handling apparatus, and to carry out safety examinations on vitrified high level wastes with alpha nuclides more preciously. The technique was applied to detect homogeneity of Cm-244 and Pu-238 in the specimen for an accelerated alpha radiation stability test first.

The foundamental technique was arranged to specimen with very high radioactivity from a method for weak radioactivity as shown in Fig. 1. The specimen for alpha autoradiography were prepared from glass forms by slicing and polishing. A sheet of cellulose nitrate film rapped with polyethylene based film of 30 μm thick(5.5 mg/cm^2) was exposed to the specimen. Exposing period depends on radioactive density on the specimen surface. For the specimen which contained 120 GBq/cm^3 the film was exposed about 15 seconds. Exposed films were etched in a aqueous solution of NaOH, KOH and $KMnO_4$ at a temperature of 35 °C and in a period of 15 minutes, washed in water, dried in air and then observed in the form and distribution of alpha trucks with a microscopy. Fig. 1 shows schematically the experimental procedure of the alpha autoradiography.

The homogeneity of alpha nuclides in the specimen used for accelerated alpha radiation stability test performed in WASTEF has been proved by an application of the technique. Two photos in Fig. 2 show the alpha tracks on the etched film. The left photo covers the full surface of a specimen and the white image indicates alpha tracks. The right also shows those in black images under a microscopic magnification. It is clear that there has been no coaggregated particle of plutonium larger than 2×10^{-12} Ci(1×10^{-13} .g),which can be calculated with the exposing period and the specific activity. Regarding the macro scale

homogeneity alpha tracks were counted in a unit area of various surface parts of specimen. The results are summarized in Table 1. Nine parts for the counting were set at crossed positions on the specimen surface. Position number 3 is at the center position and position 1, 5, 6 and 9 are at the outer. Mean values of the specimen A, B and C are 1.42, 1.30 and 1.26×10^5 tracks/mm^2 and the standard deviations are 0.08, 0.06 and 0.06 respectively. This means that the fluctuation of track density is within 6% of the mean value, thus it has been proved that plutonium was homogeneous in the specimen enough to be used for the test.

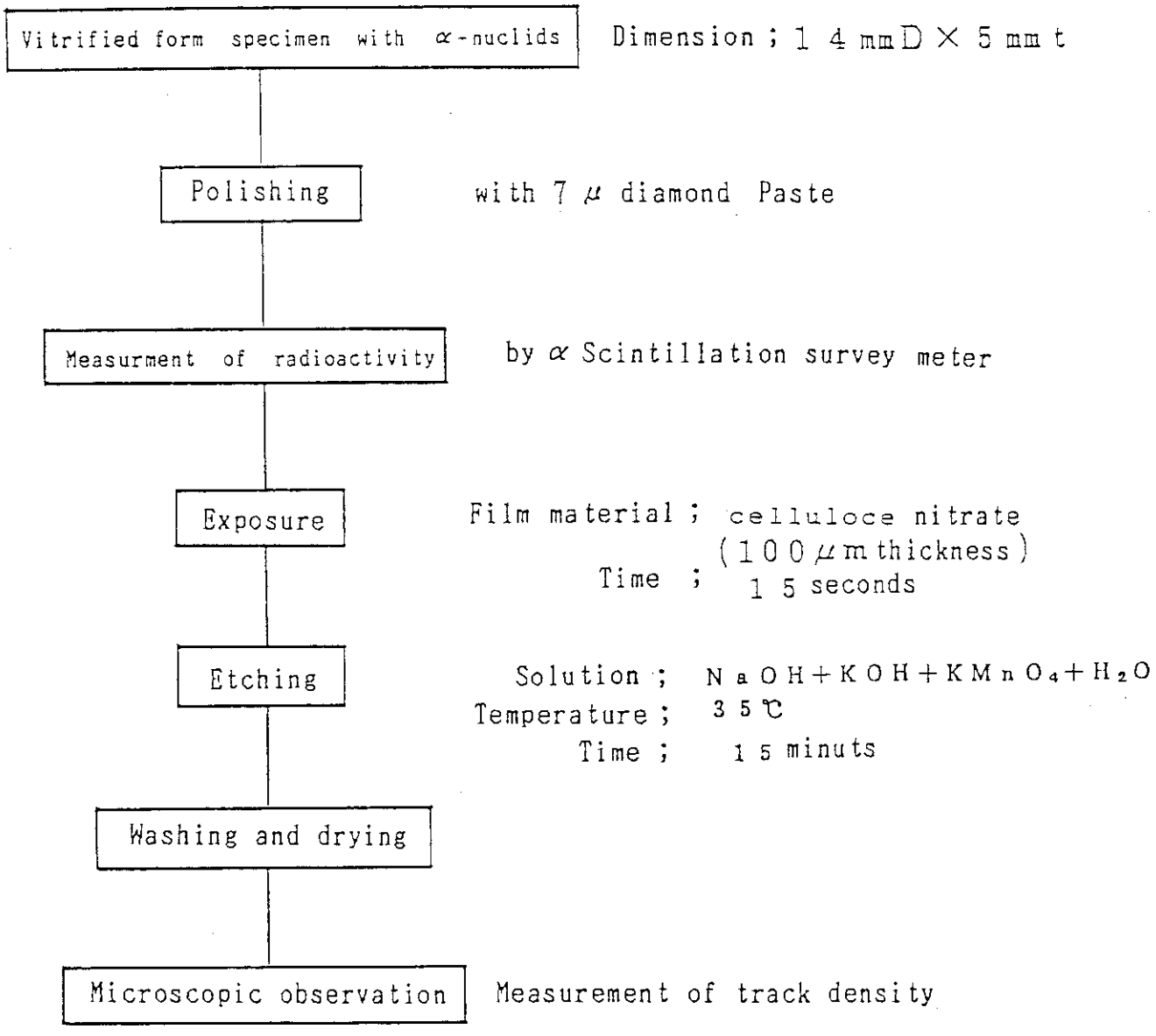

Fig 1. Experimental Procedure of α-autoradiography

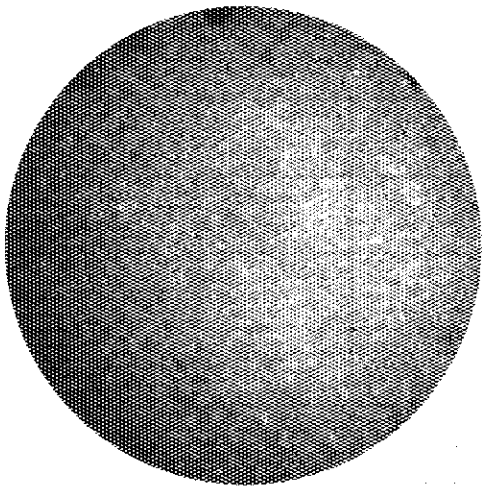

α-Autoradiograph (×4.5)

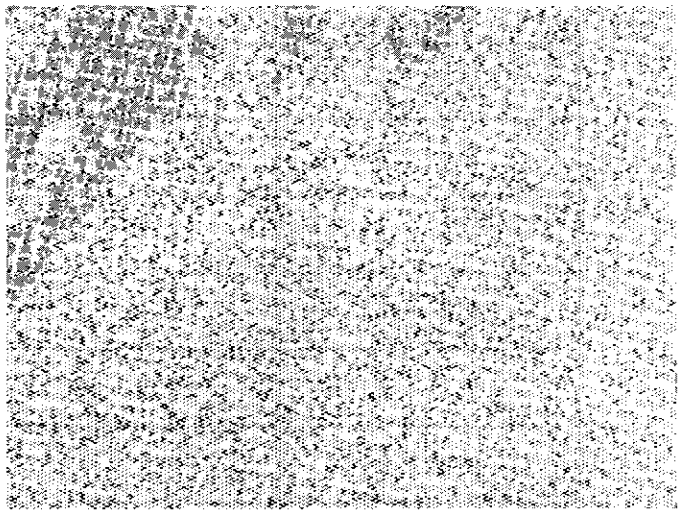

α-Autoradiograph (×400)

Fig 2. α- Autoradiograph of ^{244}Cm doped glass sample

Table 1. Alpha tracks on the various surface parts of three specimen for accelerated alpha radioation stability test

Position	Track density ($\times 10^5$/mm^2)		
	Specimen A	Specimen B	Specimen C
1	1.49	1.30	1.24
2	1.45	1.25	1.22
3	1.42	1.30	1.28
4	1.31	1.31	1.19
5	1.41	1.33	1.33
6	1.46	1.33	1.26
7	1.39	1.18	1.29
8	1.57	1.29	1.32
9	1.32	1.40	1.17

3.3 Adhesive behaviour of TRU elements leached out from vitrified forms on various surfaces

K.NUKAGA and S.TASHIRO

Adhesive property of radioactive substances leached out from vitrified forms has been investigated on various materials for leaching apparatus as a preliminary study to select a suirable material for the leaching flask and to make leaching data more accurate. Furthermore, understanding of adhesive behaviour of radioactive substances leached out will help analysis of migration behaviour in disposal circumstances.

Main scheme of the experimental method is shown in Fig. 1. Vitrified forms with Cs-137, Ce-144, Pu-238 and Cm-244 were used as radioactive source and Teflon, fused silica and gold were tested as materials for leaching apparatus. Three pieces of each test material were immersed with a vitrified source in 100 ml water in a glass flask and boiled for 7 days. This contamination procedure was applied to three vitrified sources of Cs-137;0.4 Ci and Ce-144;0.8 Ci in 1.76 g, Pu-238;0.56 Ci in 3.35 g, and Pu-238;0.34 Ci and Cm-244;2.28 Ci in 2.00 g respectively. After contamination radioactivity of the leachate and both sides of test pieces were measured with a suitable method for the radiations. Alpha autoradiography was also applied to alpha contaminated pieces. Then, all contaminated pieces were decontaminated by immersion in 0.2 N HNO_3 solution, and the radioactivity measurement was repeated.

The results on the contamination and its decontamination are summerized in Table 1. The values are a mean of three pieces and the values in parentheses indicate the standard deviation. Regarding the contaminability of three materials by the radioactive substances, the results show in general that teflon has the highest and quartz has the lowest. The contaminability of teflon by plutonium is higher about 50 times than that of fused silica. Residual amounts on fused silica after the decontamination were also

smallest among the three matarials. As the radioactivity in leaching solutions was 3.34 μCi for Pu-238 source, 159 μCi for Pu-238 and Cm-244 source, and 0.847 μCi for Cs-137 and Ce-144, the ratio of the radioactivity in leachate to the adhesive radioactivity on the apparatus wall is in maximum 5.2 in combination of teflon and Pu-238 source and in minimum 0.050 in combination of fused silica and Pu and Cm source when the immersed area is 50 cm^2.

Regarding adhesive property of leached radioactive substances, plutonium showed a specific decontaminability that is much less than the others. It would attribute to its coagulated contamination on the surface, as shown in Fig 2. A further study has been continued for detailed discussions concerning this subject.

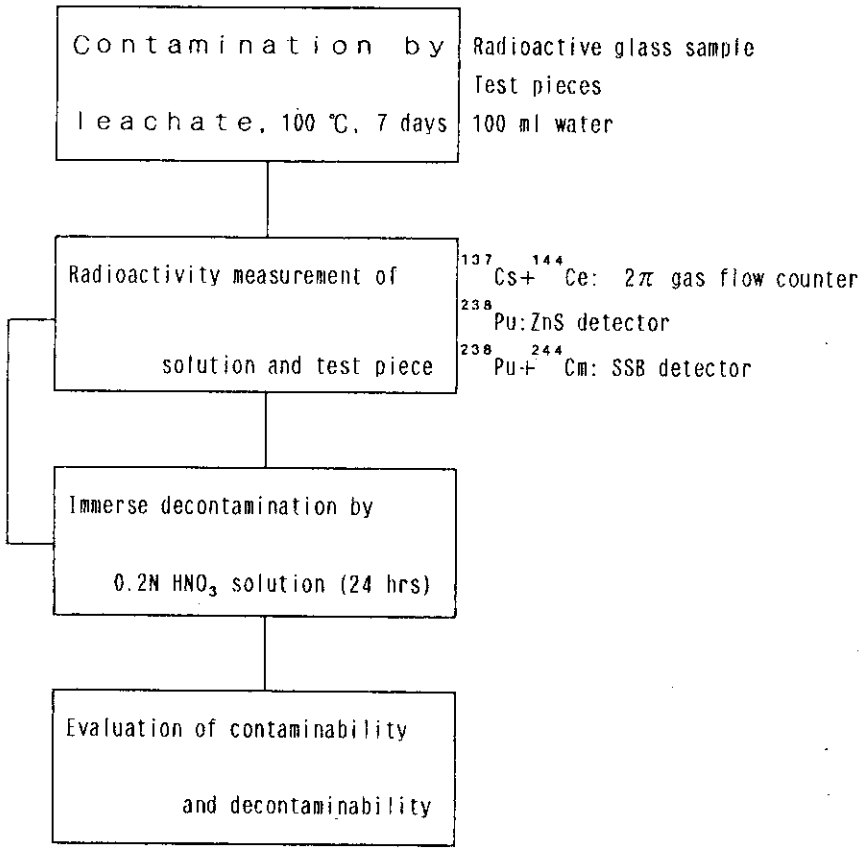

Fig. 1 Experimental procedure

Table 1 Contaminated and residual amount from various sources on different material surfaces ($\mu Ci/cm^2$)

Material / Nuclide	Teflon		Fused silica		Gold	
	Contaminated	Residual	Contaminated	Residual	Contaminated	Residual
^{238}Pu	$3.5(\pm 0.48) \times 10^{-1}$	$5.5(\pm 2.0) \times 10^{-2}$	$6.6(\pm 3.4) \times 10^{-3}$	$4.6(\pm 1.3) \times 10^{-3}$	$1.9(\pm 1.2) \times 10^{-2}$	$1.1(\pm 0.44) \times 10^{-2}$
$^{238}Pu + ^{244}Cm$	$3.0(\pm 0.38)$	$1.0(\pm 0.40) \times 10^{-1}$	$1.6(\pm 1.8) \times 10^{-1}$	$7.8(\pm 5.3) \times 10^{-3}$	$9.1(\pm 5.8) \times 10^{-1}$	$1.3(\pm 0.32) \times 10^{-1}$
$^{137}Cs + ^{144}Ce$	$1.2(\pm 0.039) \times 10^{-2}$	$6.9(\pm 0.86) \times 10^{-4}$	$1.1(\pm 0.24) \times 10^{-3}$	$1.4(\pm 0.82) \times 10^{-5}$	$1.6(\pm 0.17) \times 10^{-3}$	$1.7(\pm 1.1) \times 10^{-4}$

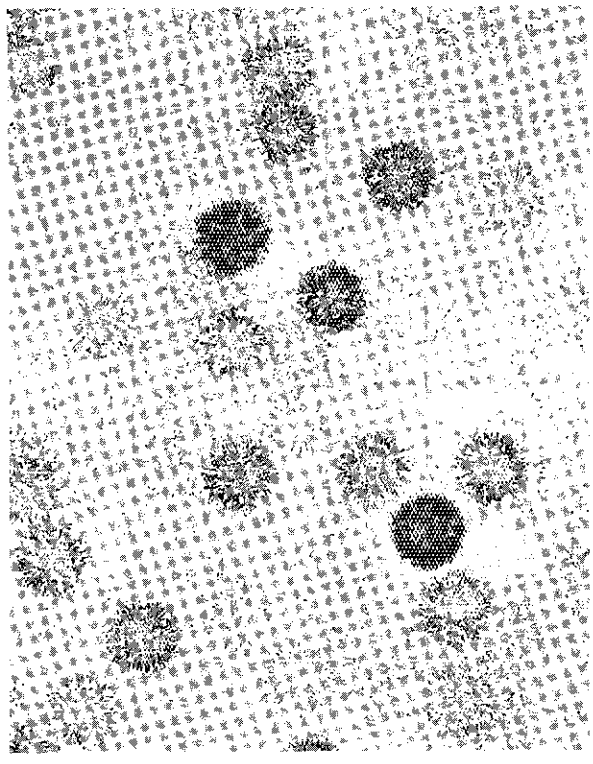

Fig.2 Alpha autoradiograph of contaminated fused silica surface by leachate from vitrified source of Pu and Cm

3.4 Accelerated alpha radiation stability test; results of 10,000 years simulation

S.TASHIRO

An accelerated alpha radiation stability test started in connection with characterization tests of re turnable wastes from oversea reprocessing and finished at 10,000 year simulation.

The test method is schematically shown in Fig. 1. Added alpha nuclides replaced transuranium elements and 90 % of rare-earth elements in a simulated waste. Melt was carried out in platinum crucible of 14 mm in diameter so that each specimen has a platinum ring in the outside circumference during the test. Four or five specimens were taken out at random from storage pits for each time duration includding zero time test. Helium generation was measured by a mass spectrometer for both of the released from and the remained in the glass matrix. The former was analyzed from helium in an atmosphere of enclosed neon gas, and the latter was detected with gas from a heated specimen. Stored energy was measured by a DSC analyzer. Leachability was examined by Soxhlet type leaching apparatus.

Results on He generation, density and leachability are shown in Fig. 2. More than 99 % of generated helium was retained by glass matrix, and the most came out to the atomosphere at temperature of above 500 °C. Density of the specimens decreased slightly with the elapse of time and then the decrement of 1.1 % was observed at 10,000 years equivalent. Regarding leachability some various values were observed at the test initiation but a flat curve obtained consequently through 10,000 years equivalent. Microscopic observation also could not find any alternation in the micro structure. Those results seem to promise that alpha radiation will have no influence on the confinement ability of vitrified forms to high-level wastes.

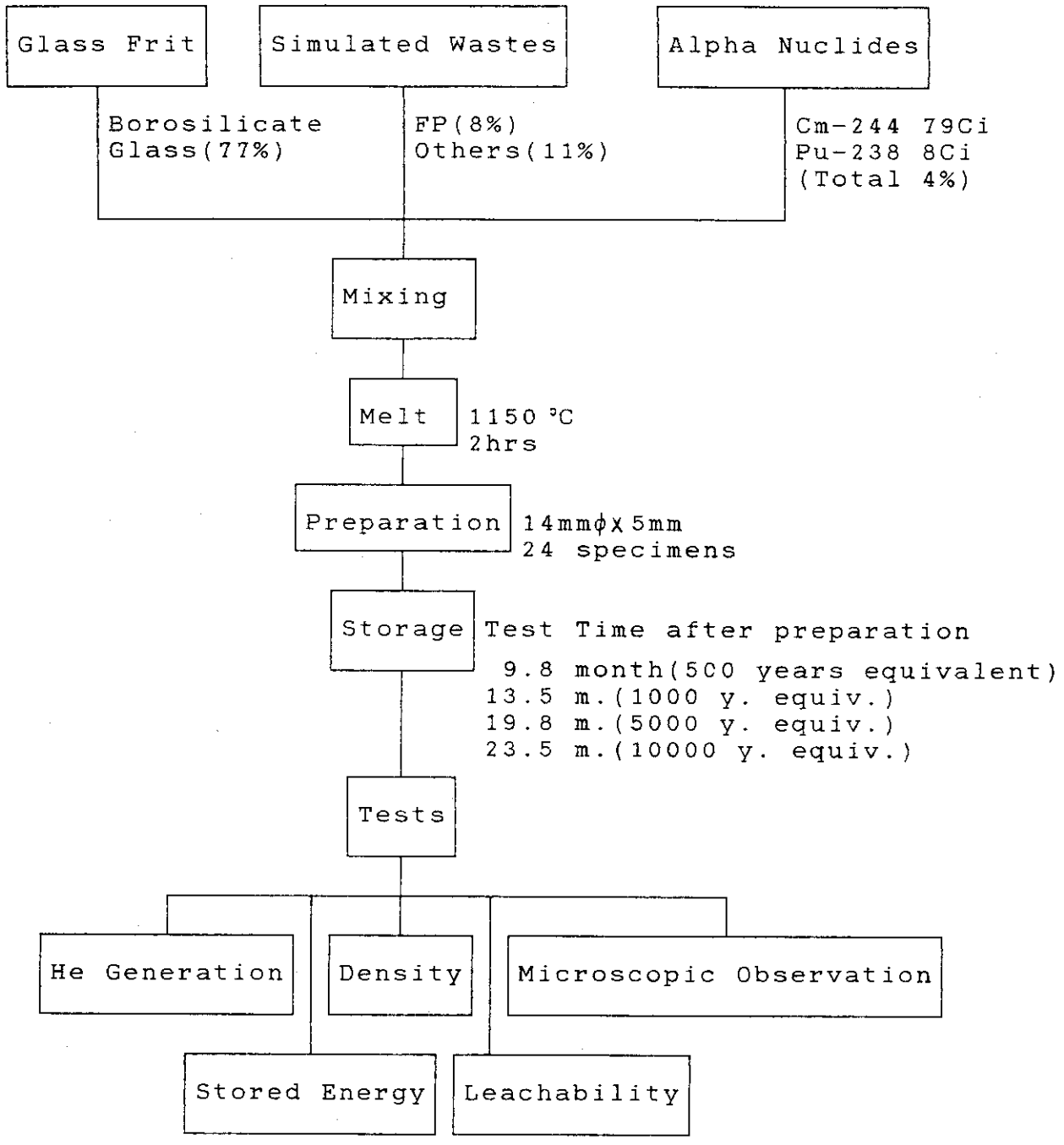

Fig.1 Block diagram of the test method for accelarated alpha radiation stability of vitrified forms

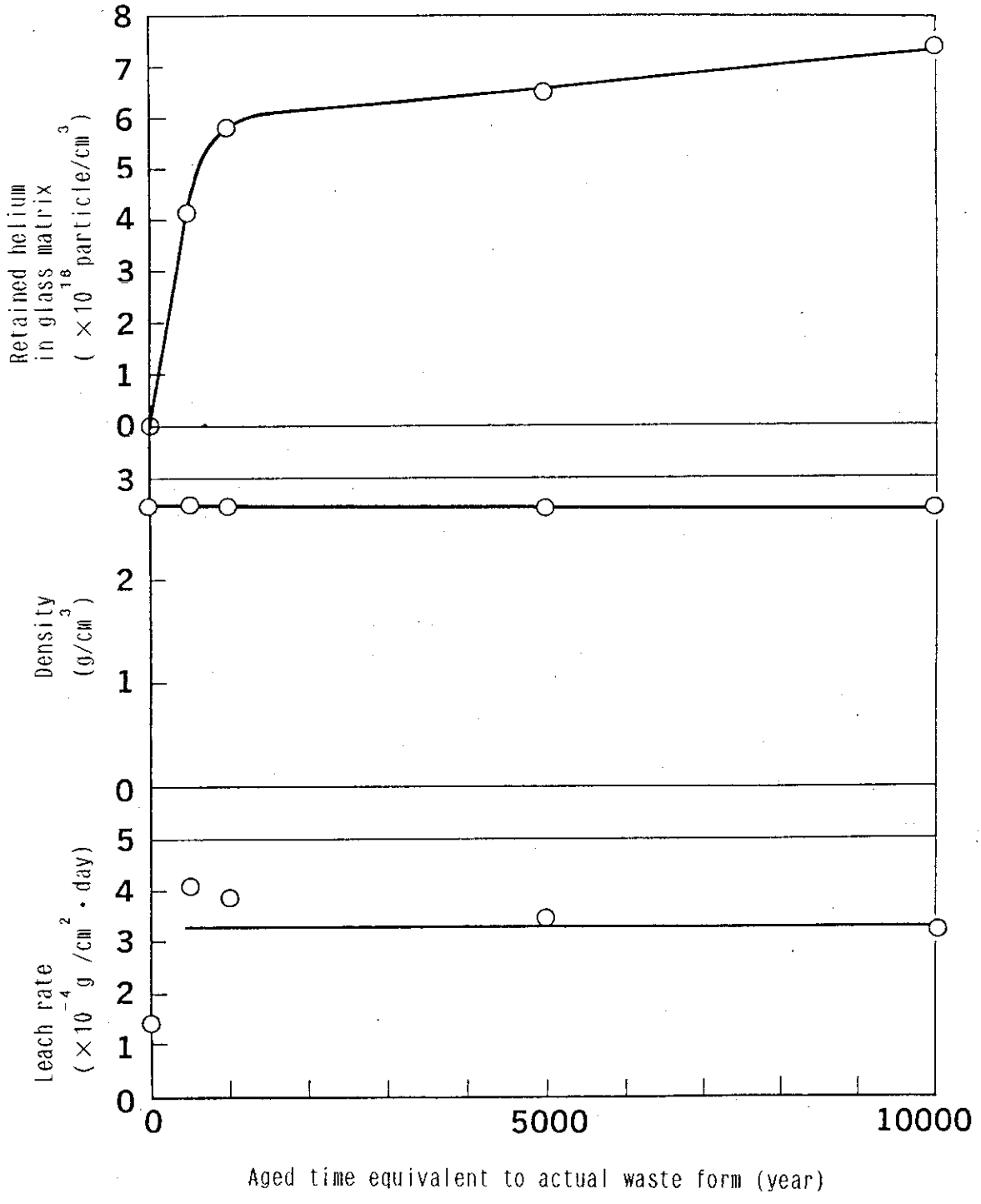

Fig.2 Results of accelerated alpha radiation stability test for vitrified forms

3.5 Nuclide Diffusion in a Granite Matrix

K. SHIMOOKA

A concept of multibarrier system is suggested for a geological disporsal system. A number of barriers such as waste forms, canister and buffer materials would delay the release and transport of radionuclides from the repository. The major barrier preventing the radionuclides from reaching the biosphere would be host-rock itself. Material released from the repository can be transported by the groundwater flow in the host-rock. The most important pathways would be the network of open fractures where the groundwater can flow. During the radionuclides migrate with groundwater, those nuclides may be retarded by dispersion, diffusion and chemical interaction between nuclides and rock.

In order to study the nuclide migration behavior in the rock, diffusion experiment is carried out.

Experimental

Granite block (5 cm in diameter and 5 cm in height) which has 3 small holes (1 cm in diameter) surrounded a center hole (2 cm in diameter) was prepared for the diffusion experiment of Pu and Cm. Three holes were arranged to set the diffusion distance from the center hole, approximately 2, 4 and 6 cm respectively. The block was saturated with distilled water before the diffusion experiment. In the center hole, a disk of vitrified Pu and Cm was immersed in distilled water to make the concentration of Pu and Cm constant, and distilled water was kept in 3 other holes. The granite block itself was also put in the distilled water in a plastic case with lid and kept at a room temperature. Solutions were sampled after 20 days, 4 months and 8 months from each hole and baked on the stainless steel for radioactive assay. Activities of Pu and Cm were measured by the surface barrier semi-conductor detector.

Result

Apparent diffusivities (D) for Pu and Cm in the granite block were calculated with the following equation

$$C / C_0 = \mathrm{erfc}\ X / 2\sqrt{Dt}$$

where C_0 is the concentration of Pu and Cm in the center hole at time = 0 and C is the concentration of each nuclide in the sampling hole at distance X from the center hole.

In Figure 1 and 2, the measured activities in the sampling holes as a function of distance are shown. The diffusivity of Pu and Cm in the granite was estimated to be approximately an order of 10^{-11} - 10^{-12} m^2/s.

The expeirment is underway and will be continued untill the end of this year.

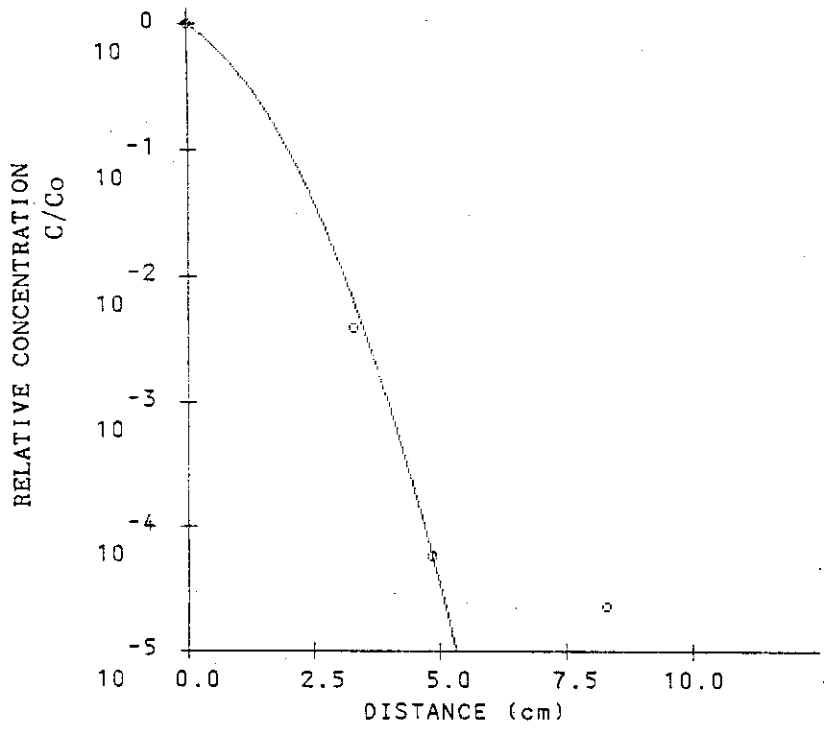

Fig. 1 Pu diffusion in granite after 20 days

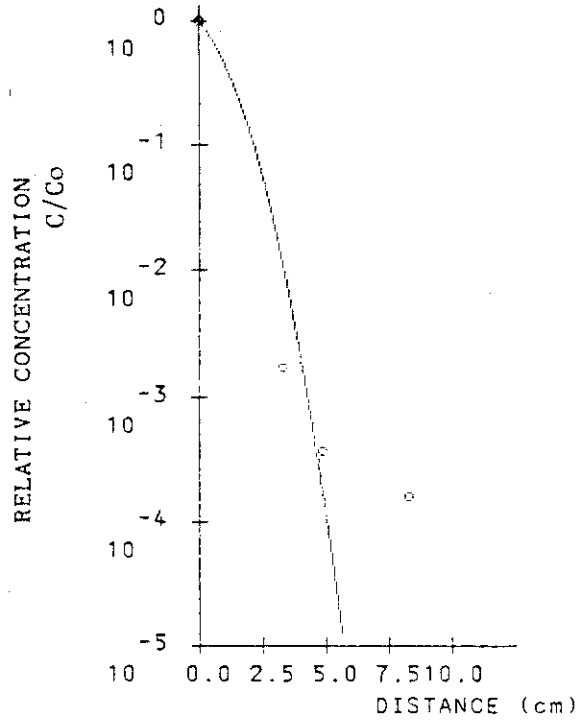

Fig. 2 Cm diffusion in granite after 20 days